



Tânia Sofia Ribeiro Simões

Licenciado em Ciências da Engenharia Civil

Moisture buffering capacity of earth mortar plasters and hemp concrete

Effect of temperature and thickness

Dissertação para obtenção do Grau de Mestre em
Engenharia Civil - Perfil de Construção

Orientador: Antonin Fabbri, Researcher, Ecole Nationale des Travaux Publics de
l'Etat

Co-orientador: M^a Paulina Faria Rodrigues, Professora Associada, Faculdade de
Ciências e Tecnologia da Universidade Nova de Lisboa

Júri:

Presidente: Doutora M^a Graça Oliveira Neves
Arguente: Doutor Fernando M. A. Henriques
Vogal: Doutor Antonin Fabbri

Copyright” Tânia Sofia Ribeiro Simões, FCT/UNL e UNL

A Faculdade de Ciências e Tecnologia e a Universidade Nova de Lisboa têm o direito, perpétuo e sem limites geográficos, de arquivar e publicar esta dissertação através de exemplares impressos reproduzidos em papel ou de forma digital, ou por qualquer outro meio conhecido ou que venha a ser inventado, e de a divulgar através de repositórios científicos e de admitir a sua cópia e distribuição com objetivos educacionais ou de investigação, não comerciais, desde que seja dado crédito ao autor e editor.

Acknowledgements

First of all I would like to thank Professor Paulina Faria, because this adventure only started with your vote of confidence and invitation. In addition, for your background support, regardless of distance, I never felt alone on the scientifically level.

I would also like to express my gratitude to Antonin Fabbri, who did the proposal of internship, and without this, it would not have been possible to live this rewarding experience, both on human and scientific point of view. I also thank for all scientific knowledge and good humour every day.

A great support came from Fionn Mcgregor. Therefore, I would like to thank for the unconditional aid always when I needed and for the fellowship and sympathy in good and not so good moments.

I am grateful to the fantastic people (PhD, Post-Doc and laboratory auxiliaries), who I have met at ENTPE during my dissertation and with who I learned a lot, personally and professionally, during these six months far from my country.

This dissertation was developed within the IBIS project and BIOTERRA project with the collaboration of the "Direction Territoriale Centre-Est" of the CEREMA where the earth mortar plaster samples were made, thus thanks to all.

As the distance is not a barrier for the friendship, I would like to thank my friends: Magda Ferreira and Cláudio Jorge, for affection, motivation, and constant interest in my wellbeing in all of these years.

I am grateful to my parents, sister, brother-in-law and nephews as without them I would not have been able to find the daily motivation during the time of my studies.

Finally yet importantly, I would like to thank my boyfriend, Ricardo, for the push and support to taking up this challenge, which until now was the biggest of my life story.

Abstract

Earth mortar plasters and hemp concrete are hygroscopic materials since they have the ability to uptake and release water vapour. These materials can be used for a passive control of relative humidity (RH) inside buildings, with the benefits of improving the health and comfort of the occupants, as well as reducing the energy consumption of buildings. The quantification of this passive control potential for buildings material has been extensively studied by the scientific community since the last decade. These studies notably lead to the Nordtest project (Rode et al. 2005) where the concept of Moisture Buffering Value (MBV) was developed, as well as a test protocol in order to quantify this characteristic of the material.

The main objective of this dissertation is to study the impact of temperature and thickness of a coating material on its passive regulation potential of indoor air RH. For that purpose, two types of hygroscopic coatings materials are studied: earth mortar plasters and hemp concretes. The influence of the thickness is analysed through dynamic MBV test ("Moisture Buffering Value" test) at 23°C on three formulations of each material (earth and hemp concrete) at three different thicknesses. The influence of temperature is performed only for hemp concrete formulations on static (sorption curves) and dynamic (MBV tests) tests at 23°C and 40°C.

The analysis of the results, made using the support of theoretical models, allows underlining that the thickness involved in the daily passive control of RH remains most of the time limited (only the first centimetre of the earth plasters and 5cm for hemp concretes). However, some surface irregularities may have a strong impact on this active thickness. The other main result of this dissertation is the strong impact of temperature on both static and dynamic hygroscopic characteristics of the material. Indeed, the increase of temperature at a constant RH tends to significantly reduce the water content of the material. But, on the other side, due to higher vapour pressure at saturation and water vapour diffusion coefficient, the dynamic sorption-desorption properties increased with temperature by approximately 65%.

Keywords: Earth mortar plasters; Hemp concrete; Hygrothermal capacity; Moisture Buffering; Penetration depth; Temperature

Resumo

Argamassas de rebocos de terra e betão de cânhamo são materiais higroscópicos, uma vez que possuem a capacidade de adsorver e desadsorver vapor de água. Podendo estes materiais ser utilizados como reguladores passivos da humidade relativa (HR) no interior dos edifícios, tendo como benefícios a melhoria da saúde e do conforto dos ocupantes, bem como a redução do consumo de energia dos edifícios. A quantificação deste potencial como regulador passivo de HR tem sido amplamente estudado pela comunidade científica desde a última década. Estes estudos nomeadamente levaram ao projeto Nordtest (Rode et al. 2005) em que o conceito de *Moisture Buffering Value (MBV)* foi desenvolvido, bem como um protocolo de teste de modo a quantificar esta característica do material.

O objetivo principal da presente dissertação é o estudo do impacto da temperatura e da espessura de um material de revestimento no seu potencial como regulador passivo da HR do ar interior. Para o efeito, dois tipos de materiais de revestimento higroscópicos são usados: argamassas de terra e betão de cânhamo. A influência da espessura é analisada através do teste dinâmico de MBV (teste de *Moisture Buffering Value*) a 23°C em três formulações de cada material (terra e betão de cânhamo) em três espessuras diferentes. A influência da temperatura é testada apenas para formulações de betão de cânhamo utilizando ensaios estático (curvas de adsorção) e dinâmico (teste de MBV) a 23°C e 40°C.

A análise dos resultados, feita com o auxílio de modelos teóricos, permite destacar que a espessura envolvida na regulação passiva da HR se mantém a maior parte do tempo limitada (apenas ao primeiro centímetro na argamassas de reboco de terra e a 5cm no betão de cânhamo). No entanto, algumas irregularidades da superfície podem ter um forte impacto sobre a espessura ativa. O outro resultado principal desta dissertação é o forte impacto da temperatura nas características higroscópicas estáticas e dinâmicas do material. De facto, o aumento de temperatura a dada HR constante tende a reduzir significativamente o teor de água do material. Mas, por outro lado, devido à pressão de vapor mais elevada em saturação e coeficiente de difusão de vapor de água, as propriedades de adsorção-desadsorção dinâmicas aumentam com a temperatura, aproximadamente, 65%.

Termos chave: Argamassas de reboco de terra; Betão de cânhamo; Capacidade higroscópica; *Moisture Buffering*; Espessura de penetração; Temperatura

Notations and symbols

A	Exposed surface area (m ²)
a	Thermal diffusivity (m ² /s)
b _m	Moisture effusivity (kg/(m ² Pa s ^{1/2}))
b _T	Thermal effusivity (J/(s ^{1/2} K m ²))
d	Thickness (m)
d _a	Thickness of the air layer(m)
D _w	Moisture diffusivity (m ² /s)
EMC	Equilibrium moisture content
G	Water vapour flow rate through specimen (kg/s)
g _v	Water vapour diffusion flux density (kg/(m ² s))
MBV	Moisture buffering value (g/(m ² %RH))
m	Mass of wet material (g)
m ₀	Mass of dry material (g)
M _w	Molar mass of water (kg/mol)
P _a -P _w	Matric suction (Pa)
p _v	Partial pressure of air (Pa)
p _{v,sat}	Saturation water vapour partial pressure (Pa)
R	Perfect gas constant (J/mol/K)
RH	Relative humidity (%)
r _p	Radium of the spherical interface (m)
s _d	Equivalent air layer thickness (m)
S _r	Saturation ratio
T	Temperature (K)
t _p	Period (s)
u	Water content (kg/kg)
w	Water content (kg/m ³)
W	Water vapour permeance with respect to partial vapour pressure (kg/(m ² s Pa))
β	Apparent vapour transfer coefficient at the sample surface
γ	Surface tension of the liquid-air interface (N/m)
δ _a	Water vapour permeability of air (kg/(Pa m s))
δ _p	Water vapour permeability (kg/(Pa m s))
Δp _v	Vapour pressure gradient (Pa)
θ	Wetting angle of the pore surface (°)

λ	Thermal conductivity (W/(m °C))
μ	Vapour resistance factor (-)
ξ	Moisture capacity (kg/m ³)
ρC_p	Volumetric thermal capacity (J/(K m ³))
ρ_d	Apparent density of dried material (kg/m ³)
ρ_w	Water density (kg/m ³)
ϕ	Porosity (-)
φ	Relative humidity (-)
Ω	Volume of the material (m ³)

Contents

Acknowledgements	III
Abstract	I
Resumo	III
Notations and symbols	V
Contents	VII
List of Figures	XI
List of Tables	XV
1. Introduction	1
1.1. Context	1
1.2. Objective and methodology.....	2
1.3. Dissertation content	2
2. General characterization of studied materials	5
2.1. Earth (soil).....	5
2.2. Hemp and hemp concrete	6
2.3. The use of eco-materials in buildings.....	7
2.4. Plasters and insulation system	8
2.5. Hygroscopic coating materials for buildings.....	9
3. Theoretical background	13
3.1. Definition of hygroscopic material as porous medium.....	13
3.1.1. Definition of the different phases - solid, liquid and gas.....	13
3.1.2. Type of pores.....	14
3.2. Sorption in pores and RH	15
3.2.1. Water content and matric suction	15
3.2.2. Liquid water and water vapour equilibrium	17
3.2.3. Definition of the saturation domains	20
3.2.4. Differences between sorption and desorption	22
3.3. Mass transfer in porous media.....	24
3.3.1. Equation of water mass conservation	24
3.3.2. Moisture buffer value (MBV).....	25
3.3.3. Analytical solution to estimate the MBV	28
3.3.4. Moisture penetration depth.....	29

4. Materials and methods.....	33
4.1. Materials.....	33
4.1.1. Hemp concrete.....	33
4.1.2. Earth mortar plasters.....	35
4.2. Test procedure: Standard characterization	37
4.2.1. Sorption isotherms.....	37
4.2.2. Water vapour permeability	39
4.3. Test procedure: Dynamic test - Moisture buffering test.....	42
5. Standard characterisation	45
5.1. Density.....	45
5.2. Sorption isotherms.....	46
5.3. Water vapour permeability	51
6. Impact of thickness on hygroscopic capacity: Results and Discussion	61
6.1. On moisture buffering values	61
6.1.1. Results on earth mortar plasters.....	61
6.1.2. Results on hemp concrete	64
6.2. On penetration depth practical and theoretical	67
7. Influence of temperature on hygroscopic capacity: Results and Analysis	73
7.1. On sorption isotherms.....	73
7.2. On moisture buffering values	78
7.3. Discussion	80
8. Conclusion.....	87
8.1. Concluding remarks.....	87
8.2. Future work	89
References	91
Appendix	97
A. Proof of the Kelvin's law.....	97
B. Materials information	98
B.1. Technical sheet of PF70.....	98
B.2. Technical sheet of Calco.....	99
B.3. Drying of earth mortar plasters	100
C. Sorption Isotherms	100
C.1. Hemp concrete at 23°C.....	100

C.2. Earth mortar plasters	102
C.3. Hemp concrete at 40°C	104
D. Diffusion test	106
D.1. β correction.....	106
D.2. Variation of mass in the diffusion test for hemp concrete- 1st phase.....	107
E. MBV.....	109
E.1. Earth mortar plasters	109
E.2. Hemp concrete at 40°C.....	110
F. Practical penetration depth	111

List of Figures

Figure 2.1- Microtomography slices of a (a) hemp shiv and (b) hemp concrete (Dubois et al. 2014).....	7
Figure 2.2- Relationship between RH and germination (left) and growth (right) of fungi (Tegernsee, K. 2001 referred by Correia 2013)	10
Figure 2.3- Evaporation effect (ANAH 2004).....	11
Figure 3.1- Schematic representation of the porous material morphology	13
Figure 3.2- Schematic cross-section of a porous material (Rouquerolt et al. 1994).....	15
Figure 3.3- Water molecule (H ₂ O) (Straube 2006).....	16
Figure 3.4- Contact angle in Hydrophilic and Hydrophobic materials	16
Figure 3.5- Variation of p_v , sat with temperature. The solid line represents the values calculated using eq. 8, and the squares are the values extracted from the data base of the CRC Handbook (Lide 2001)	18
Figure 3.6- Psychrometric chart (BSI 1989)	19
Figure 3.7- The six types of sorption isotherms (Sing et al. 1985)	20
Figure 3.8- Regimes of moisture storage in a hygroscopic porous material (Straube 2006)	21
Figure 3.9- Hysteresis loop between the sorption and desorption curves	23
Figure 3.10- Ink-bottle effect (left (a) and (b)) and raindrop effect (right) (Albers 2014).....	24
Figure 3.11- Determination of MBV _{practical} from dynamic measurements. Definition of 3 cycles inside the ellipse, moisture uptake and the changes of RH that promote the cycles. (Rode et al. 2005).....	26
Figure 3.12- The penetration depth (Rode et al. 2005)	31
Figure 4.1- Mould used for earth mortar plaster samples with 50x50x4cm ³	36
Figure 4.2- Samples setup for sorption isotherms test (Left- Earth mortar plaster F0; Right- Hemp concrete NL).....	37
Figure 4.3- Sorption isotherms setup (Left- procedure at 40°C and Right- procedure at 23°C).....	38
Figure 4.4- Example of setup for diffusion on water vapour permeability test (F5).....	39
Figure 4.5- Three possible stages during the diffusion test.....	40
Figure 4.6- Example of samples for Moisture buffering test (Left- Hemp concrete Calco; Right- Earth mortar plaster F3)	42
Figure 4.7- Moisture buffering test setup	43
Figure 4.8- Earth plaster MBV test results when hemp concrete are in the same time in the climatic chamber. The unusual behaviours are highlighted with the red circles.....	44
Figure 5.1- Sorption isotherms for hemp concrete at 23°C.....	46

Figure 5.2- Sorption and desorption from 75% and 85%RH level for Calco.....	47
Figure 5.3- Sorption and desorption from 75% and 85%RH level for PF70	48
Figure 5.4- Sorption and desorption from 75% and 85%RH level for NL.....	48
Figure 5.5- Sorption curve for each type of earth mortar plasters.....	49
Figure 5.6- Sorption and desorption from 97%RH level for each type of earth mortar plasters.....	49
Figure 5.7- Sorption and desorption from 85%RH level for each type of earth mortar plasters.....	50
Figure 5.8- Comparison between earth mortar plasters and hemp concrete formulations using mass by volume	51
Figure 5.9- Variation of mass during the water vapour permeability test of earth mortar plaster F0 (the second number in the reference of the sample is the thickness).....	52
Figure 5.10- Variation of mass during the water vapour permeability test of earth mortar plaster F3 (the second number in the reference of the sample is the thickness).....	52
Figure 5.11- Variation of mass during the water vapour permeability test of earth mortar plaster F5 (the second number in the reference of the sample is the thickness).....	53
Figure 5.12- Layout of the processes during the test.....	55
Figure 5.13- Comparison between the obtained values of water vapour resistance factor (μ) for Earth mortar plaster (with and without correction).....	56
Figure 5.14- Comparison between the obtained values of water vapour resistance factor (μ) for hemp concrete (with and without correction).....	58
Figure 5.15- Transport of water vapour in the wet and dry cup test methods	59
Figure 6.1- Moisture buffering test for F0 with 1, 2 and 4cm.....	61
Figure 6.2- Moisture buffering test for F3 with 1, 2 and 4cm.....	62
Figure 6.3- Moisture buffering test for F5 with 1, 2 and 4cm.....	62
Figure 6.4- Moisture buffering test for all earth mortar plasters formulations, average values for different thicknesses	63
Figure 6.5- MBVpractical for earth mortar plasters with different thicknesses	63
Figure 6.6- Moisture buffering test for NL with 5, 10 and 15cm at 23°C.....	65
Figure 6.7- Moisture buffering test for PF70 with 5, 10 and 15cm at 23°C.....	65
Figure 6.8- Moisture buffering test for Calco with 5, 10 and 15cm at several temperatures	66
Figure 6.9- Prepared sample of NL in the climatic chamber.....	68
Figure 6.10- Real penetration depth for NL at 23°C	68
Figure 6.11- Real penetration depth for PF70 at 23°C	69
Figure 6.12- Real penetration depth for Calco at 23°C	69
Figure 6.13- Hemp concrete adsorption for long time at 40°C and 75%RH.....	71
Figure 7.1- Temperature influence in the sorption curve of Calco.....	74

Figure 7.2- Temperature influence in the sorption curve of PF70	74
Figure 7.3- Temperature influence in the sorption curve of NL.....	74
Figure 7.4- Practical and theoretical sorption isotherms for Calco	76
Figure 7.5- Practical and theoretical sorption isotherms for PF70	76
Figure 7.6- Practical and theoretical sorption isotherms for NL	76
Figure 7.7- Results of sorption curves for juvenile wood at 15°C and 3°C by Esteban et al. (2015) and implementation of the theoretical model at 35°C	77
Figure 7.8- Average value from the moisture buffering test for NL at 40°C and 23°C	79
Figure 7.9- Average value from the moisture buffering test for PF70 at 40°C and 23°C	79
Figure 7.10- Comparison between moisture buffering value of NL and PF70 at 23 and 40°C	80
Figure 7.11- Monitored RH and temperature at 23°C	82
Figure 7.12- Monitored RH and temperature at 40°C	82
Figure 7.13- Correlation between measured and calculated MBV with different moisture capacities and corrections of water vapour permeability at 23°C (MC-Moisture Capacity; sorp- sorption curve; des- desorption curve)	84
Figure 7.14- Moisture effusivity using ISO and β corrections (23°C and 40°C) and moisture effusivity value calculated from MBV at 23°C and 40°C for hemp concrete with 5cm of thickness	85
Figure B.1- Drying curves for all samples of earth mortar plasters	100
Figure D.1- Layout of the processes during the test.....	106
Figure D.2- Variation of mass during the first phase of the penetration depth of PF70.....	107
Figure D.3- Variation of mass during the first phase of the penetration depth of NL.....	108
Figure D.4- Variation of mass during the first phase of the penetration depth of Calco.....	108
Figure E.1- Moisture buffering test for NL with 5, 10 and 15cm at 40°C	110
Figure E.2- Moisture buffering test for PF70 with 5, 10 and 15cm at 40°C	110
Figure E.3- Moisture buffering test for Calco with 5, 10 and 15cm at 40°C	111
Figure F.1- Real penetration depth for NL at 40°C	111
Figure F.2- Real penetration depth for PF70 at 40°C	112
Figure F.3- Real penetration depth for Calco at 40°C	112

List of Tables

Table 3.1- Practical MBV classes (Rode et al. 2005).....	27
Table 3.2- Results from the Round Robin test (Rode et al. 2005)	27
Table 4.1- Mixtures proportions of studied hemp concrete, wet density, samples and curing.....	34
Table 4.2- Formulation of mortar F0.....	35
Table 4.3- Formulation of mortar F3.....	35
Table 4.4- Formulation of mortar F5. The value in brackets corresponds to the initial formulation that must be changed due to the occurrence of cracks during the drying period.....	35
Table 4.5- Clay, fibre and water content of earth mortar plasters	36
Table 4.6- Substances for salt solution for each RH	38
Table 5.1- Dry density (ρ_d) of hemp concrete materials in function of their hemp/binder mass ratio and comparison with literature.....	45
Table 5.2- Dry density of earth mortar plasters and comparison with literature.....	45
Table 5.3- Hysteresis values for two different RH levels (97% and 85%) for earth mortar plasters	50
Table 5.4- Moisture capacity for all formulations.....	51
Table 5.5- Average values of water vapour permeability and water vapour resistance factor for each formulation of earth mortar plaster.....	53
Table 5.6- Results of water vapour diffusion-equivalent air layer thickness for earth mortar plasters	54
Table 5.7- Average values of water vapour permeability and water vapour resistance factor for each formulation of earth mortar plaster with ISO correction.....	54
Table 5.8- Average values of water vapour permeability and water vapour resistance factor for each formulation of earth mortar plaster with β correction	55
Table 5.9- Average values of water vapour permeability and water vapour resistance factor for each formulation of hemp concrete	57
Table 5.10- Average values of water vapour permeability and water vapour resistance factor for each formulation of hemp concrete with ISO correction.....	57
Table 5.11- Average values of water vapour permeability and water vapour resistance factor for each formulation of hemp concrete with β correction	57
Table 5.12- Results of dry cup for Calco and PF70 (Chabriac 2014, personal communication).....	58
Table 6.1- MBV _{ideal} for all earth mortar plasters formulations with different corrections and compared with the value of MBV _{practical}	64
Table 6.2- MBV for hemp concrete at 40°C and 23°C with different thicknesses	66

Table 6.3- MBV _{ideal} for all hemp concrete formulations with different corrections and compared with the value of MBV _{practical}	67
Table 6.4- Penetration depth for hemp concrete using the different approximation of water vapour permeability with the average moisture capacity	70
Table 6.5- Penetration depth for hemp concrete using the different approximation of water vapour permeability with the moisture capacity in desorption.....	70
Table 6.6- Penetration depth for earth mortar plasters using the different approximation of water vapour permeability.....	72
Table 7.1- Thicknesses of the Hemp concrete samples used on MBV test.....	78
Table 7.2- Moisture capacity using only sorption curves for hemp concrete at 23°C and 40°C	81
Table 7.3- MBV _{ideal} for NL and PF70 with different corrections of water vapour permeability and compared to the value of MBV _{practical}	83
Table C.1- EMC for sorption and desorption curve from 97%	103
Table C.2- EMC for sorption and desorption from 85% processes for earth mortar plasters	103
Table E.1- General information of earth mortar plasters samples.....	109

1. Introduction

1.1.Context

A big challenge of the 21th century is to minimize the impact of the building sector on the global climate change. Indeed, the stabilization of atmospheric greenhouse gas concentrations requires the reduction of emissions and thus of energy consumption. According to Dixit et al. (2010) the building sector is responsible for approximately 40% of global greenhouse gas generation. In the last fifteen years, especially in Europe and USA (Melià et al. 2014), there has been an upsurge of interest in use of locally sourced, non-processed building materials (with low embodied energy), such as unfired earth. This type of constructions could have a big impact to reduce the energy consumption of the building (Choudhury & Misra 2013) and therefore be beneficial to attenuate climate changes. Other advantages of earth as a building material are its abundance, its low cost and the fact that it is reusable (Gomes et al. 2013).

Raw earth and bio-based materials have a very low environmental impact, both in the production and disposal phases. Regarding the use of bio-based material, the reduction on the carbon footprint is explained by the low industrial process needed and the carbon stored during the growth phase of the plant. Furthermore these materials are widely available in most regions and, for example, earth constructions are often built with local soil and therefore there is no pollution associated to its transportation (Sassoni et al. 2014 ; Dubois 2014). Considering that bio-based materials refers to crop by-products and are abundant available agro-wastes, this type of construction offers a solution for solving the problem of their disposal (Dubois 2014).

The earth and bio-materials under study can easily absorb water vapour in excess, or release it when it is scarce; in this way they work as passive humidity regulators (Melià et al. 2014). These hygroscopic properties can provide high benefits in both, comfort and health, for inhabitants (Lima & Faria 2015). This capacity as passive humidity regulation can reduce the energy consumption of the building in use because it does not depend on an energy input (Mcgregor 2014). But depending on regional climates and indoor conditions, the material may be exposed to high relative humidity (RH) for a long time, which can lead to growth of fungi.

The use of crop by-products is an opportunity for developing local rural economy.

Economic aspects of earth materials depend on several factors such as labour costs, stabilization process, durability and repair needs. The material itself has a very low impact on the final costs. However, and according to Sanya (2007), this provides a very important way to create decentralized job.

This dissertation was developed under the IBIS project and BIOTERRA project. The focus material of IBIS project is hemp concrete while the BIOTERRA project proposes to study earth mortar plasters. All the experimental tests were realized at *Ecole Nationale des Travaux Publics de l'Etat* (ENTPE). The earth plasters were made in collaboration with the "Direction Territoriale Centre-Est" of the CEREMA. The hemp concrete samples were done at ENTPE and one formulation was done with a collaboration of PAREX group.

The hemp concrete samples were done 1 year before the beginning of the experimental work of the present dissertation.

The passive regulation of the RH inside the building was the major focus in this dissertation. On the experimental stage, the characterization and quantification of the impact of different thicknesses on the samples of earth mortar plasters and hemp concrete were done. In addition, the hemp concrete formulations tests were made at several temperatures..

1.2. Objective and methodology

The main objective of this dissertation is to study the impact of temperature and thickness of a coating material on its passive regulation potential of indoor air RH. For that purpose, two types of hygroscopic coating materials are studied: earth mortar plasters and hemp concretes. These two particular materials have been chosen because they are, in the author's view, representative of the commonly used hygroscopic coating materials.

The influence of the thickness is estimated from comparison of the Nordtest's Moisture Buffering Value (Rode et al. 2005) of samples of different thicknesses at 23°C. Three formulations of earth plasters (F0, F3 and F5) and three formulations of hemp concrete (PF70, Calco and NL). The earth samples of 1cm, 2cm and 4cm thick have been realised during the first stage of the experimental work of the dissertation (in Marsh 2015). The hemp concrete samples of 5cm, 10cm and 15cm thick have been realised at the ENTPE more than 6 month before the start of the experimental work.

For practical reasons, the influence of temperature is only made on the hemp concrete samples on the basis of the evolution of the sorption curve and of the Nordtest's Moisture Buffering Value between 23°C and 40°C.

It is worth mentioning that the Northtest RH conditions (i.e. high relative humidity of 75% and low humidity of 33%) are representative of the average indoor RH daily variations in Northern European Countries. In consequence, this dissertation's results on the moisture buffering potential of the tested materials should not be generalized to all countries, whatever their climate.

1.3. Dissertation content

This dissertation is divided in eight chapters, including this first introductory chapter. The second chapter is dedicated to the a literature review on hygroscopic insulation systems and plasters as hemp concrete and earth mortar, their applications, advantages and capacities. This literature review continues in the Chapter 3 that focus on description and characterisation of the porous specific nature of these materials, and its consequences on the vapour and liquid water mass transfers.

Thereafter, the Chapter 4 describes the composition of each formulation of hemp concrete and earth mortar plaster, as well as the way they are prepared. The experimental protocols of the characterisation tests (sorption-desorption isotherms, vapour diffusion coefficient, MBV) are also presented in detail in this chapter in reference to the normative documents. The standard characterization of all studied formulations at 23°C (density, sorption curves, vapour diffusion coefficient) is given in Chapter 5 while the impact of thickness and temperature are respectively reported in Chapter 6 and Chapter 7. Finally, conclusions of this dissertation and suggestions for future works are presented in Chapter 8.

2. General characterization of studied materials

2.1. Earth (soil)

This material is the product of the deterioration of rocks (chemical and mechanical processes, for example). Fragmented minerals from the original rock, minerals formed by chemical decay processes (e.g., clays), new minerals formed by contact with water and substances dissolved in it, and organic molecules formed by biological processes (e.g. humus) are the possible composition of the soil. Soils can be divided into horizontal layers called “horizons” because of their variable composition. The top horizon is most often rich in organic matter (humus) and typically not suitable for earth construction. It is commonly recommended to use soils free of humus and plant matter in earthen constructions (Maniatidis & Walker 2003). The “subsoil” horizon usually has the most appropriate composition for construction purposes (Mcgregor 2014). The subsoil is composed of three phases, the solid phase is composed of mineral particles with a large variation in size and nature, the liquid phase is composed of water and the last is the gas phase composed of air, as can be seen below in Figure 3.1. In this document soil material refers to the subsoil.

According to Mcgregor (2014), for example, in Europe the classification of particle sizes is divided into gravels (> 2mm), sand (between 2 mm and 0,063mm), silt (between 0,063mm and 0,002mm) and clay (<0,002mm). Different size intervals are used in other classifications in other countries, but the name of the soil fraction does not change (Gomes et al. 2014)

In the clay materials the main components are the finer fractions, silts and clays. Both become sticky and plastic when they are wet. For this reason, silt and clay bind the grains of the coarser fractions of the soil and allow its use as a building material. In opposition, the coarse fraction, gravel and sand, have no cohesive force by themselves, but they constitute the aggregates in earth constructions.

To be used as a building material it is necessary to select a soil rich in clay material (clay and silt) to be plastic when wet and hard when dry, but an excess of clay in the mixture must be avoided because it would cause shrinkage and cracking during the drying of building elements. According with Torraca (2009) the ideal composition of the earth for construction is clay and silt within the range of values between 20% to 30% and sand/gravels between 70% to 80%.

However, the earth construction uses local soils, and it may be necessary to use additions of material in the mixture to improve the final properties of the hardened material. Vegetal fibres such as straw, sisal fibres, timber and hay chopped, are used to improve the thermal performance, bending and tensile strength (Torraca 2009; Maniatidis & Walker 2003). But one disadvantage of the use of fibres is that compressive strength of soil decreases when the straw content increases over a certain amount (Minke, 2000, cited by Maniatidis & Walker 2003).

Cow dung is sometimes used to improve the resistance to water; when an excess of water occurs this material prevents the dispersion of clays. In modern earth construction the use of lime and cement induces an improvement of mechanical properties and water resistance. The mixture obtained by the

addition of up to 20% of lime or 10% of cement is called stabilized earth (Torraca 2009). Sodium silicate can also be used in quantities of around 5% to act as a binding agent to increase compressive strength in sandy and silty soils (Maniatidis & Walker 2003).

2.2.Hemp and hemp concrete

Hemp (*Cannabis sativa*) is one of the world's oldest cultivated annual crops. For decades, the cultivation of hemp vanished or was interrupted, in the most Western countries, as a result of competition with other feedstock's such as cotton and synthetic fibres and the prohibition of cultivation due to the use of cannabis as a narcotic. The crops of this material are well adapted to most regions of the world (in a wide range of climatic zones). China, Europe and Canada are the three most important hemp planting regions in the world, producing in 2011 globally 61.318 ha (Salentijn et al. 2015).

The hemp plant has a fast grow up (4 m in only 3.5 months), with low fertilization and irrigation, making it very efficient in use and material resources (Le et al. 2014; Sassoni et al. 2014). This material has received a lot of attention because, in addition to the properties described above, has good thermal isolation and good mechanical properties (Sassoni et al. 2014) and is more resistant to biological decay than other bio-based building material (Maalouf et al. 2013).

Hemp shiv (Figure 2.1) is a bio-based building material, with origin on the stalk of hemp plant, which was rediscovered in France in the beginning of the nineties and has been improved over the last 20 years.

The lime–hemp concrete, in this document called hemp concrete, is generally used in the construction as a filling in wood frames, prefabricated slabs, bricks or blocks and as mortar coating to cover masonry wall, in old or new buildings (Evrard 2006 and Collet et al. 2013). The hemp concrete consists of shives mixed with the material lime-based binder in proportions depending on the desired mechanical, acoustic and hygrothermal properties (Dubois 2014). The lightweight particles leads to an impact on the strength/density ratio, on the deformability and the matrix (formed by the binder) in the mechanical behaviour, in other words, a high quantity of this fiber leads to an impact on the mechanical properties of the material. It is the porosity between the particles that provides the low thermal conductivity. The open porosity in the surface, as is possible to see in the Figure 2.1, gives the material a good sound absorption. Finally, the same porous aspect that includes pores of varying sizes where the fibres has an imperfect arrangement strongly influences the exchange of water vapour (Le et al. 2014).

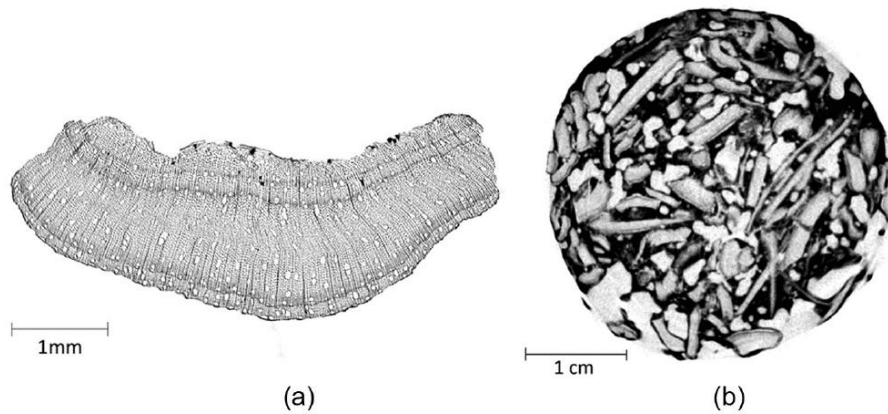


Figure 2.1- Microtomography slices of a (a) hemp shiv and (b) hemp concrete (Dubois et al. 2014)

2.3. The use of eco-materials in buildings

Earth construction techniques are dated back to the Neolithic era, over more than 9000 years (Bruno & Faria 2010). Since then, they have been used throughout the world since earth is a material widely available and easy to work (Röhlen & Ziegert 2011; Melià et al. 2014).

Adobes or "mud bricks" are part of the most used and oldest building materials. Their first use, dating back to 8000 BC, have been found in Turkestan (Minke 2006). The production of this technique consist of filling wooden moulds with earth mixed with water and, most of time, with a stabilization such as straw or dung which are then placed in the air to dry. After a first stage of drying, sometimes the bricks are turned around to finish drying. To provide a uniform drying and good mechanical proprieties it is necessary to choose an appropriate thickness.

Rammed earth foundations dating from 5000BC have been discovered in Assyria (Minke 2006). The process consists of compacting raw earth with a rammer directly on site between a temporary wooden formwork, producing monolithic walls. In Europe the steel formworks are replacing the wooden traditional ones.

The Compressed Earth Block (CEB) consists in compressing (manually or mechanically) the earth material within a mould. The fabrication water content of CEB is lower than the adobe's one, and the earth used is commonly less clayey. This process results in an earth block with similar density to rammed earth and consequently which are more resistant than adobe bricks.

Cob has been used for building since prehistoric times. This technology is a type of monolithic construction; it involves mixing earth with straw and water. The masonry wall layer is directly shaped by hand. .

For a long time earth construction was confined to the rural areas of developing countries. During the 20th century this techniques was largely substituted by cement-based techniques. The reason for the change concerns the fact that most of constructions with raw earth are more labour intensive and need periodical maintenance. However, in more recent years, a growing interest for these traditional techniques

is observed (Melià et al. 2014), as it also an increasing number of rehabilitation for modern uses of old earthen buildings (Gomes et al. 2013). The development of efficient coating and insulation systems adapted for these materials became necessary.

According with Torraca (2009) the use of cement rendering on earthen constructions is not advisable. Because, apart from the reduction in the passive moisture regulation, adding an impermeable coating can lead to irreversible damage in the wall. In this situation, accumulation of water can occur at the surface of the wall and in the material, especially at the interfaces between two different materials. This leads to a deterioration of the cohesion between the wall and the coating system.

2.4.Plasters and insulation system

Still in the perspective of sustainable development, there is a need to use raw materials (e.g. plant particles and earth) as building material. There is a significant growth in the use of natural fibres such as hemp, straw, flax and bamboo (Le et al. 2014).

The selection of an appropriate plaster system depends on the technology used in the wall and the desired surface quality. Contrary to expectation, the use of cement or hydraulic lime plasters on the external surface of earth buildings proved to be less efficient than traditional systems (Torraca 2009), they are too impermeable and overly stiff causing the deterioration of the earth wall. Lime and earth renders and plasters are compatible with earthen walls, earth mortar plasters being the traditional ones used indoors for this type of building technique, while lime or lime and earth renders are for exterior use. This compatibility is associated with the fact that earth mortar plasters are permeable to water vapour and their mechanical properties are very similar to that of earthen walls. Thereby this enable the vapour exchange between the wall and the environment and has similar deformation when compared with earth walls (Hamard et al. 2013).

Earth mortar plasters consist mainly on a mixture of sand and silt with 5% to 12% of clay, normally (Minke 2006), for increasing their adhesive and binding forces and, most of the time, with addition of vegetable fibres (Faria et al. 2015). The proportions of this type of plaster are very difficult to determine because the building materials (the earth) are not standardized. In earth mortar the binding material is the clay, whereas, in the case of hemp concrete, it is the lime that does this function.

The coating materials of external surfaces require must be resistant to bad weather. This can be reached by adding admixtures or lime (Hamard et al. 2013), or having a water-proof coating system (not advisable in earth construction) or a physic protection like a long roof overhang. However, the main requirements are low liquid water uptake, for example, when expose to the rain and capillary rising, and high permeability to the water vapour.

Indoor plastering can contribute to improve the building performance, particularly in terms of thermal comfort, health and sustainability. The contribution relative to the health of inhabitants is due to the

humidity buffer capacity, that comes from the high hygroscopicity of the clay (Lima & Faria 2014) and the hemp shives (Collet & Pretot 2014).

Hemp concrete due to be a low-density material, with a large quantity of pours can be used as an insulation system.

2.5. Hygroscopic coating materials for buildings

It is understood that hygroscopicity is the characteristic that quantify the change in water content of a material when it is exposed to an environment with moisture variations (Correia 2013). This happens due to the fact that, in a hygroscopic material, any variation of relative humidity in air leads to adsorption/desorption phenomena at the pores surface of the material. The equilibrium moisture content (EMC) is reached when the material is neither gaining nor losing water. Little is known about the hygroscopic propriety of earth mortar plasters. The hygroscopic proprieties of the materials, the permeability to airflow and their capillary transfer ability are the main parameters (Ashour et al. 2011).

According to Osanyintola & Simonson (2006) "research into dynamic moisture storage of hygroscopic building materials has renewed interest in the moisture buffering capacity of building materials and shown the potential for these materials to improve indoor humidity, thermal comfort and indoor air quality in buildings".

Very low or high RH provide some physical discomfort, since the RH has an influence on the temperature perception (Arundel et al. 1986). The characteristics of the inside air are very important for the users of the building, since the environment and air quality inside the building can influence comfort, health and productivity (Ramos 2007). Air quality is a subject particularly important since people spend the majority of their time inside buildings.

Extremely low RH levels (below 20%) may also cause eyes or skin irritations and dry the nasal mucous membranes, providing a bigger risk of respiratory infections (Arundel et al. 1986; Pires 2013). According to the research of Arundel et al. (1986) the RH range to minimize many adverse effects is between 40% and 60%.

The high RH may cause severe durability problems in the building materials. The majority of fungi species require high RH (above 75%) in order to grow and it is known that fungi cause allergies such asthma or rhinitis (Arundel et al. 1986; Gonçalves et al. 2014). In Figure 2.2 is possible to see how the RH influences the generation and growth of fungi.

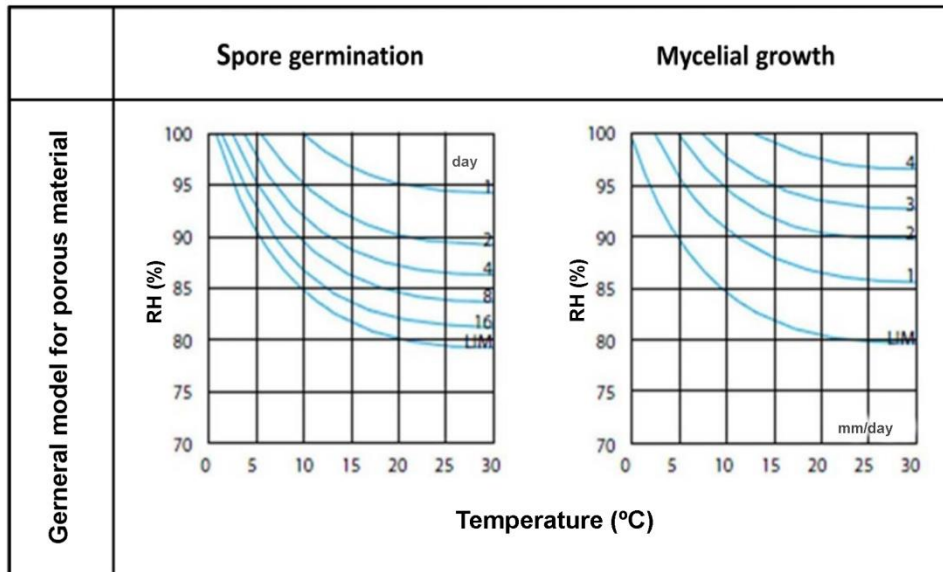


Figure 2.2- Relationship between RH and germination (left) and growth (right) of fungi (Tegersee, K. 2001 referred by Correia 2013)

During the use of the space inside the building, it can be observed that the values of moisture are increased due to the production by indoor activities, for example, coking, bathing, expiration of living beings, etc. This production varies with environment and type of activity, is considered that one average adult person produce 45g/h and 110g/h in rest and light physical activities, respectively, in a temperature of 20°C (Hens 2011).

For these reasons studies about potentially using a passive humidity regulation are important. For this, is necessary to considerate the moisture buffer capacity of the hygroscopic materials.

When moisture tolerance is taken in account, several humidity sources must be considered. These are the rain, rising damp, accidental causes, hygroscopic moisture, surface condensation and industrial condensation (Hens 2011). In the context of study, the important cause is hygroscopic moisture.

The property of temperature and humidity regulation in earth building is due to the transfer of heat and moisture. When these walls are covered by an envelope with low permeancy, a reduction of vapour transfer appears (Allinson & Hall 2010). The difference between two different types of envelope and evaporation effects in the earth walls are represented in Figure 2.3. When is considered the capillary rise or the water infiltration from the soil in the wall, it is important to take into account this vapour transfer.

Therefore, the use of coating systems with low permeancy on earthen constructions is not advisable (Torraca 2009). The liquid water has to evaporate at the surface in contact with the air to reduce the effect of the capillary rise. The stagnation of water, for a long time, at the surface of the wall and in the material, can lead to a reduction of mechanical properties and therefore problem of security.

The impact of water content can be seen in an experimental programme developed by Heath et al. (2009), on commercial mass-produced extruded unfired clay bricks. All tested samples, under the same

environmental conditions, show a similar trend where compressive strength is decreased by approximately 51%, when increasing the moisture content from 1 to 6%.

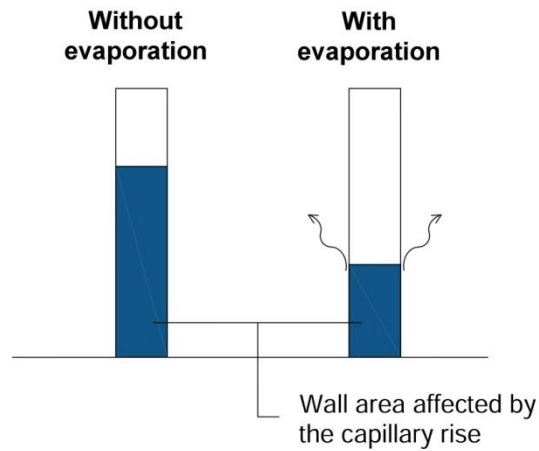


Figure 2.3- Evaporation effect (ANAH 2004)

According with McGregor (2014) the temperature does influence the process of adsorption in the material. Studies have been made by Ashour et al. (2011) for clay plasters at different temperatures, between 10°C to 40°C, to measure the EMC. Their results showed a decrease in EMC with an increase temperature, however the difference was low compared with the difference in RH. However, authors such as Künzle (1995), consider that in terms of building physics the effect of temperature on the EMC can be disregarded between 5°C to 70°C.

3. Theoretical background

3.1. Definition of hygroscopic material as porous medium

3.1.1. Definition of the different phases - solid, liquid and gas

Since the connections between the constituents of earth mortar plaster or hemp concrete are not perfect, some voids, called pores, are embedded within the solid material. Due to this property, earthen materials and hemp concretes can be considered as porous media. Consequently, these materials consist in three phases (Ramos 2007): the solid skeleton S (solid phase), the liquid water L (liquid phase) and the gas phase G which is assumed to be a mixture of perfect gases composed by dried air A and water vapour V (Figure 3.1).

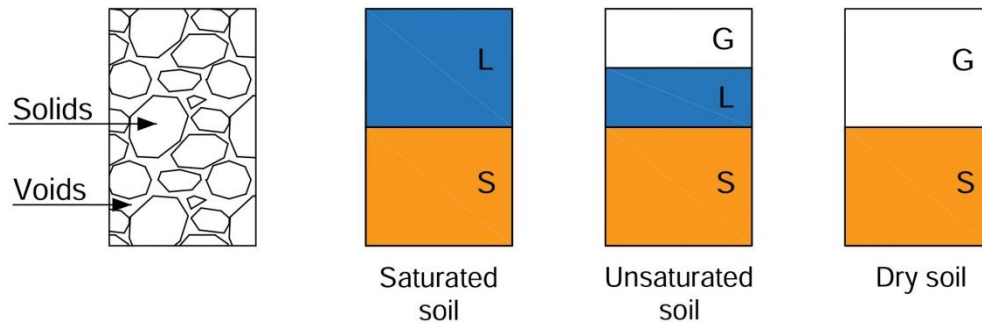


Figure 3.1- Schematic representation of the porous material morphology

In Figure 3.1 the three possible states of the porous material are represented. When all porous space is filled by air or water, the material is said to be dried or saturated, respectively. Most of the time, there will be the coexistence between liquid water and air within the porous network of the material, and it will be under the unsaturated state. Following a description, the porous material morphology can be described by eq. 1 to 3, as:

$$\Omega_s = (1 - \phi)\Omega \quad (1)$$

$$\Omega_L = \phi_L \Omega = S_r \phi \Omega \quad (2)$$

$$\Omega_G = \phi_G \Omega = (1 - S_r) \phi \Omega \quad (3)$$

where Ω is the volume of the material. The actual volumes of S, L and G are respectively denoted by Ω_s , Ω_L and Ω_G . The Lagrangian porosity of the material is noted ϕ , while ϕ_I denotes the porosity filled by the phase I=L,G. Finally, S_r is the saturation ratio, defined as the ratio between the current volume of liquid and

the current volume of the porous network. Another way to express the amount of water within the material is to use the gravimetric water content, denoted by u , which is defined accordingly with the EN ISO 12571:2000 (CEN 2000) as the ratio between the mass of wet material (m) and the mass of dried material (m_0). The main asset of this latter is to be easily measurable by the weighting of the wet and dried sample (eq. 4).

$$u = \frac{m - m_0}{m_0} \quad (4)$$

The relation between the saturation ratio and the water content is given by eq. 5:

$$S_r = u \frac{\rho_d}{\phi \rho_w} \quad (5)$$

where u is the water content in porous medium, ρ_d is the apparent density of the dried material and ρ_w is the water density.

3.1.2. Type of pores

If the definition of the pores is quite simple (i.e. pores are spaces between particles), their geometry can be highly complicated and it is sometimes quite difficult to properly represent the shape of the porous network (see for example Figure 3.2). To ease its description, the pores have been separate in two categories in function of their availability to the water: closed and connected. The closed pores (represented by (a) in Figure 3.2) are those which are totally isolated from their neighbours. This type of pores influences the density, mechanical strength and thermal conductivity, but they do not influence fluid flow and adsorption. The second category, which is the connected (or open) pores, forms a continuous channel of communication with the external surface of the body (represented by (b), (c), (d), (e) and (f) in Figure 3.2). Mathematically, open porosity is the volume of open pores per volume-unit material (Radu et al. 2012). But this binary classification is not sufficient to properly represent the variable dimensions and various shapes of the pores which are present in building materials. For that purpose, a shape-based classification, which considers cylindrical pores (c) or (f), ink-bottle shaped (b), funnel shaped or slit-shaped (d) is also commonly used (Rouquerolt et al. 1994).

Although pore network is, by definition, a joining series of interconnected pores, it may be itself isolated from the rest of the pore structure (Jaquin 2008).

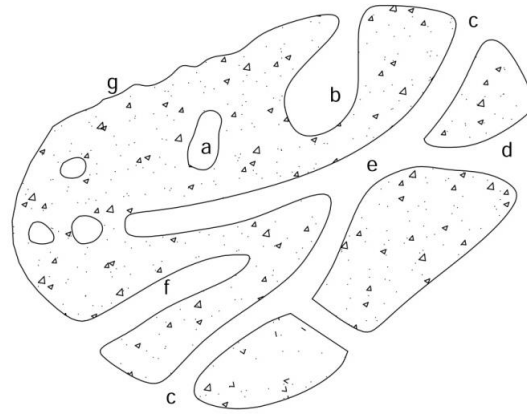


Figure 3.2- Schematic cross-section of a porous material (Rouquerolt et al. 1994)

In the following only the connected pores are considered. The closed porosity is then assumed to be included in the solid phase of the material.

3.2. Sorption in pores and RH

3.2.1. Water content and matric suction

In unsaturated porous medium, the water content is known to decrease with the increase in matric suction, which is the difference between the total pressures of the non-wetting (air) and the wetting (in-pore liquid) phases (eq. 6):

$$u = f(P_a - P_w) \quad (6)$$

where u is the gravimetric moisture content [kg/kg], P_a and P_w are the air and the liquid total pressures, respectively, while f is a decreasing function of the matric suction ($P_a - P_w$). This link between u and $P_a - P_w$ can be subjected to hysteresis (i.e. the function f changes if the material is either in drainage or in imbibition). This phenomenon will be discussed in detail in chapter 3.2.4 of this document.

The link between the water content and the matric suction can be simply explained using the Jurin's Law. Assuming a spherical interface between the liquid and the air, this latter leads to eq. 7:

$$(P_a - P_w) = \frac{2\gamma\cos(\theta)}{r_p} \quad (7)$$

where γ is the surface tension of the liquid-air interface [$\text{N}\cdot\text{m}^{-1}$], r_p is the radius of the capillary pore [m], and θ the wetting angle of the pore surface. Since the liquid is the wetting fluid and the gas the non-wetting fluid, it is commonly assumed that all the pores with a radius lower than r_p are filled by liquid water while all the pores with a radius higher than r_p are filled by air. In consequence, when the matric suction increases the amount of the pore space, r_p , invaded by water decrease.

The picture is not so simple in earth mortar plaster and hemp concrete, since the remaining water molecules are not only in a condensed form, but can also be strongly adsorbed onto the pore surfaces. To explain this phenomenon, there is a need to look at the scale of intermolecular forces or the Van Der Waals forces. To facilitate the comprehension of this intern mechanism, a molecule of water for which the centroid of the two positive charges is not coincident with the centroid of the two negative charges is represented in Figure 3.3. This spatially-unbalanced distribution of charges means that the water molecule is polar and behaves like a tiny magnet.

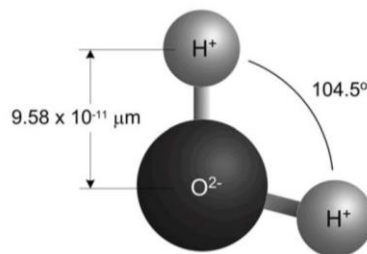


Figure 3.3- Water molecule (H_2O) (Straube 2006)

On account to this polarity of water molecules, many surfaces in contact with water vapour molecules have the tendency to capture and hold water molecules. The materials with these properties are called hydrophilic. If a drop of water is deposited on the surface of a hydrophilic material, the contact angle (θ) of the drop is always smaller than 90° (Torraca 2009). In other words, a material is hydrophilic when the water spreads on its surfaces, wetting them. For a perfectly wetting surface, $\theta = 0$.

The materials with contact angle (θ) larger than 90° are called hydrophobic, repelling the water molecules. The mentioned contact angles can be seen in the Figure 3.4.

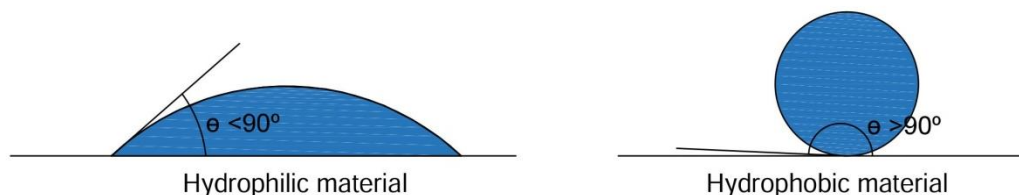


Figure 3.4- Contact angle in Hydrophilic and Hydrophobic materials

Considering that the volume of particles contain some porosity, water can be adsorbed/absorbed into the body of the particles or retained on its surface as a film of moisture. The water content can vary

between 0 and u_{sat} , which corresponds to the water content at saturation (i.e. $S_r = 1$). It is important to underline that this extreme case is very difficult to obtain, because of the creation of trapped air pockets within the porous network at high saturation ratio (Lai et al. 2015).

Even if the physic of water adsorption is a bit different than in the capillary equilibrium depicted by the Jurin's law (eq. 7), the global tendency remains the same: a decrease of the water content when the matric suction increase.

3.2.2. Liquid water and water vapour equilibrium

Alternatively, the process of in-pore condensation/evaporation is governed by the equilibrium between the liquid water and the water in the gas phase. At first, consider pure water which is not confined within the porous medium. The partial pressure of vapour within the surrounding air is denoted by p_v , while the partial pressure of vapour at saturation is denoted by $p_{v,sat}$. This latter is a function of temperature and is a limit for the quantity of water that a volume of air can support. The resulting equilibrium between the liquid phase and gas phase of water can be expressed, at first order, by eq. 8:

$$p_{v,sat}(T) = p_{v,sat}(T_0) \exp \left\{ \frac{M_w}{RT} \left[\frac{L_0}{T_{ref}} (T - T_{ref}) + (C_{p,V} - C_{p,L}) \cdot \left(T \ln \left(\frac{T}{T_{ref}} \right) - (T - T_{ref}) \right) \right] \right\} \quad (8)$$

where L_0 is the latent heat of evaporation/condensation at T_{ref} and $p_a = p_w = 1$ bar (for water at $T_{ref} = 373$ K, $L_0 = 2.26 \times 10^6$ J/kg (Coussy 2004)). Finally, $C_{p,V}$ and $C_{p,L}$ are, respectively, the vapour and liquid specific heat at constant pressure. The numerical application, depicted in Figure 3.5, shows that the vapour pressure at saturation is an increasing function of the temperature.

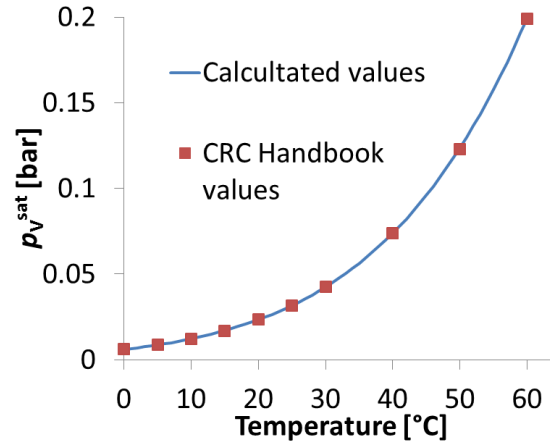


Figure 3.5- Variation of $p_{v,sat}$ with temperature. The solid line represents the values calculated using eq. 8, and the squares are the values extracted from the data base of the CRC Handbook (Lide 2001)

Let us define the RH, denoted by φ , as the ratio between the partial vapour pressure and the saturated vapour pressure (eq. 9):

$$\varphi = \frac{p_v}{p_{v,sat}} \quad (9)$$

The equilibrium between unconfined pure water and the surrounding air is reached when $\varphi = 1$ (i.e. the partial pressure of vapour is equal to the saturated vapour pressure, $p_{v,sat}$). In other words, liquid water will evaporate if the RH is lower than 1 and water vapour will condensate if the RH is higher than 1. According to the eq. 9 and taking in account the Figure 3.5, the RH changes inversely with the increase of the temperature. This tendency is represented on the psychrometric chart (Figure 3.6), which is a practical tool that gives the temperature in the abscissa, the partial vapour pressure in ordinate and a group of curves of RH. So, for the same partial pressure of vapour, an increase of temperature leads to a decrease of the RH.

When the water is confined within the porous network, its chemical potential changes, and the water can be in equilibrium with the surrounding air at a partial pressure of vapour lower than $p_{v,sat}$. Indeed, assuming that all the gaseous phases (wet air, dry air and water vapour) follow the perfect gas relation, the chemical equilibrium between the water vapour in air and the liquid in-pore water leads to the Kelvin's law, which link the matric suction to the RH (Proof in Appendix A) (eq. 10):

$$(P_a - P_w) = -\frac{\rho_w RT}{M_w} \ln\left(\frac{p_v}{p_{v,sat}}\right) = -\frac{\rho_w RT}{M_w} \ln(\varphi) \quad (10)$$

In this expression, ρ_w is the density of water [$\text{kg}\cdot\text{m}^{-3}$], M_w its molar mass [$\text{kg}\cdot\text{mol}^{-1}$], R is the perfect gas constant [$\text{J}/\text{mol}/\text{K}$], T is the absolute temperature [K]. This expression clearly underlines that, when $P_a -$

$P_w > 0$, the RH at equilibrium is between 0 and 1. The combination between the eq. 6 and the Kelvin's law (eq. 10) leads then to a relation between the water content within the material and the RH of the surrounding air (eq. 11):

$$u = f(P_a - P_w) = f\left(-\frac{\rho_w RT}{M_w} \ln(\varphi)\right) \quad (11)$$

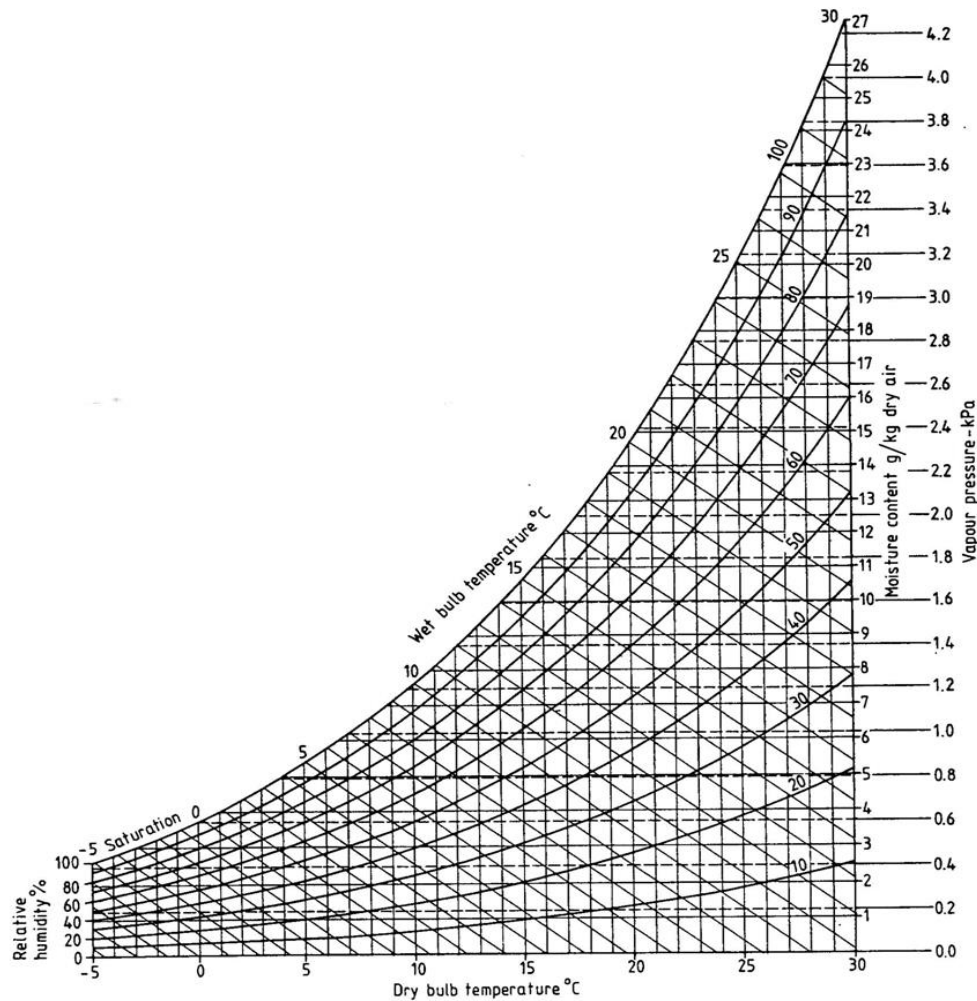


Figure 3.6- Psychrometric chart (BSI 1989)

This relation between the water content and the RH at constant temperature is called the sorption curve in case of wetting, and the desorption curve in case of drying. These curves vary as a function of the morphology of the porous network and of its affinity with water molecules. In the literature, as sketched in Figure 3.7, they can be classified in six main groups. Most of building materials present a sorption isotherm curve like a "S" with a hysteresis loop (Krus & Kiej 1998); this type of curve is referred as type IIb according to Rouquerol et al. (1999).

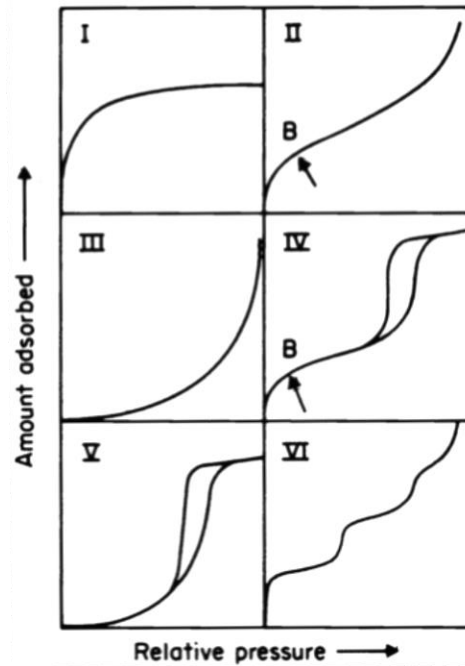


Figure 3.7- The six types of sorption isotherms (Sing et al. 1985)

From the sorption isotherms (curve of moisture storage), the specific hygroscopicity or moisture capacity (ξ) of a material is obtained by eq. 12:

$$\xi = \rho_d \left\langle \frac{du}{d\varphi} \right\rangle \quad (12)$$

where ρ_d is the dry density and $\left\langle \frac{du}{d\varphi} \right\rangle$ is the average slope of the sorption isotherm, analyzed within a range of RH. It is an average because the sorption isotherm is not a linear curve, therefore the slope can change.

3.2.3. Definition of the saturation domains

Hygroscopic building materials have the three domains of moisture storage represented in Figure 3.8: the domain of sorption moisture or hygroscopic regime (Regions A-C), the capillary water domain (D) and the domain of super saturation or over-saturated regime (E) (Krus & Kiej 1998; Straube 2006). The curve of sorption isotherm for these materials has a “S”-shaped profile and shows a hysteresis effect between moisture adsorption and desorption. The last phenomena is commonly viewed as the result of wetting characteristics variations between adsorption and desorption, or other phenomena created by pore space geometry (Krus & Kiej 1998).

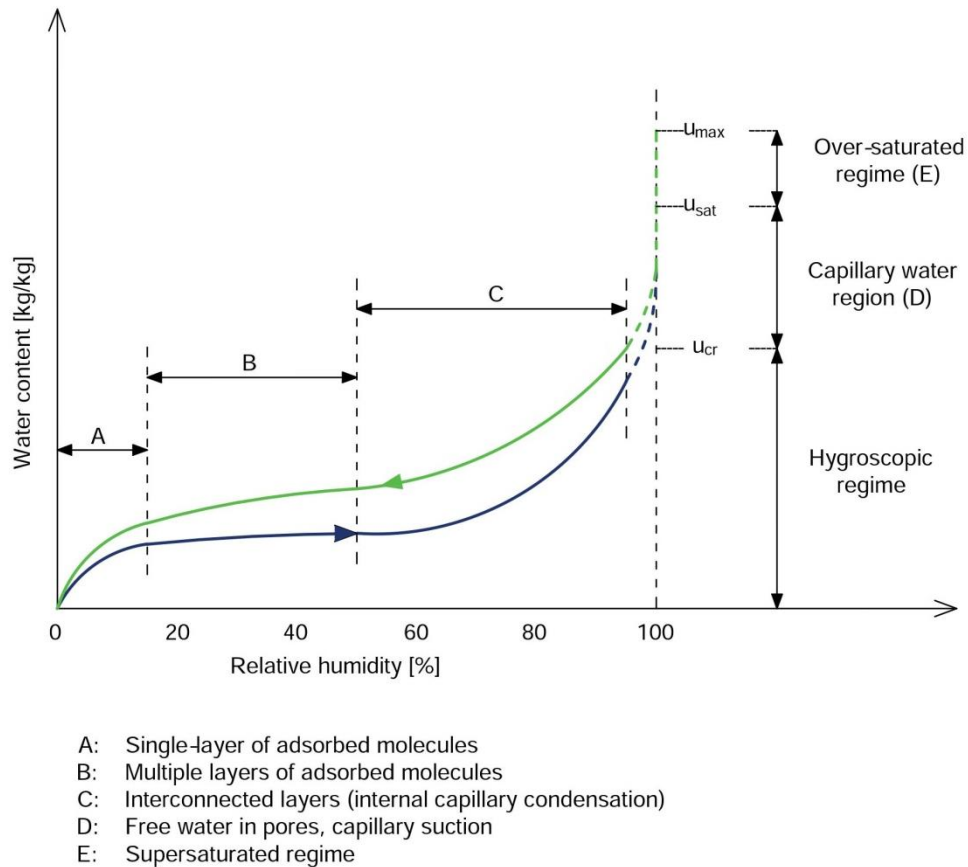


Figure 3.8- Regimes of moisture storage in a hygroscopic porous material (Straube 2006)

Sorption moisture region or hygroscopic regime

The sorption moisture region is characterized by the accumulation of water vapour adsorbed to the pore wall, until a state of equilibrium is reached. The hygroscopic regime is between 0% and 95% of RH and has three phases:

- Single-layer of adsorbed molecules - This phase happens when the values of RH are between 0% and 15% approximately (Krus & Kiej 1998) and is characterized by one layer of water molecule fixing over ground of pore. This fixing is due to the action of intermolecular forces described above in the solid-water surface.
- Multiple layers of adsorbed molecules - With increasing of RH to 50% approximately occurs the creation of multiple layers in de porous medium. This phenomenon is due to polarity of water molecule, like in single-layer, but now is a consequence of the attraction water-water and the chemical surface characteristics of the particles.
- Interconnected layers (internal capillary condensation) - In this phase the layers grow to such a size that they begin to interact and interconnect and the surface tension of water causes the formation of meniscuses within the smallest pores (Straube 2006). It is possible to observe this until 95% of RH, approximately.

Capillary water regime

At RH above 95%, the sorption curve rises very sharply. The capillary water regime is between 95% and 98%. Within this domain, it is impossible to measure with high accuracy the relation between the hygrometry and the water content. Capillary saturation is defined as the material moisture content which can be attained through natural water absorption under natural pressure without the influence of exterior forces (Krus & Kiej 1998). Both liquid water and wet air are in the porous medium and they can freely flow within the porous network.

Super saturation or over-saturated regime

For values between 98% to 100% occurred the super saturation regime. Capillary saturation can only be exceeded under pressure humidification. This is an application of vacuum (Radu et al. 2012) to remove entrapped air or forced condensation by pushing below the condensation point.

In capillary water regime and over-saturated regime, RH is over 95% and the condensation/evaporation processes becomes predominant toward the sorption/desorption processes.

3.2.4. Differences between sorption and desorption

The adsorption phenomenon should be exactly the opposite of the desorption phenomenon. However, some significant differences are commonly observed in building materials.

The first one concerns the kinetic: desorption is slower than adsorption (Henriques 2011).

The second one is the magnitude: the water content at a given RH is higher in desorption than in sorption. This phenomenon is called the sorption-desorption hysteresis loop (Figure 3.9).

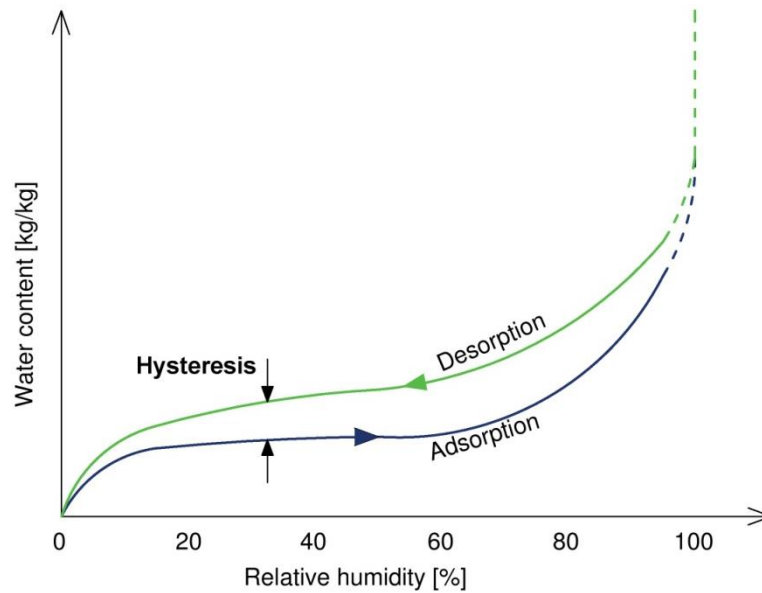


Figure 3.9- Hysteresis loop between the sorption and desorption curves

It usually appears at high RH and is related with the capillary condensation (Mcgregor 2014; Sing et al. 1985). There is not yet a consensus on its explanation, but it certainly involves the morphology and the surface roughness of pores and involves a metastable state of the adsorbate (Rouquerol et al. 1999). According with Albers (2014) this phenomena may be attributed to three causes, when water is considered in the porous medium.

The first is called "ink-bottle effect" (Figure 3.10), effect that results of the bottle shape of the pore in the transition between narrow and wide passages. During the imbibition and drainage, a meniscus with the same curvature at different locations occurs. This effect can be explained mathematically with Jurin's law (eq. 7). During imbibition, the matric suction needs to increase until it reaches values necessary to fill larger diameters in the pore. On the other side, during drainage, when the matric suction reaches the same value, the pore section with better access (high diameters) is draining but the pore is not completely dry, leaving a certain amount of water in the pore (Chabriac 2014).

The second is called the raindrop effect (Figure 3.10) and arises of a change in the contact angle between adsorption and desorption. This contact angle is lower during desorption than in adsorption and could occur due to impurities or roughness or variability of the pore wall.

The last cause for hysteresis is the consequence of the consolidation, swelling and shrinkage of the solid matrix, especially in fine porous media.

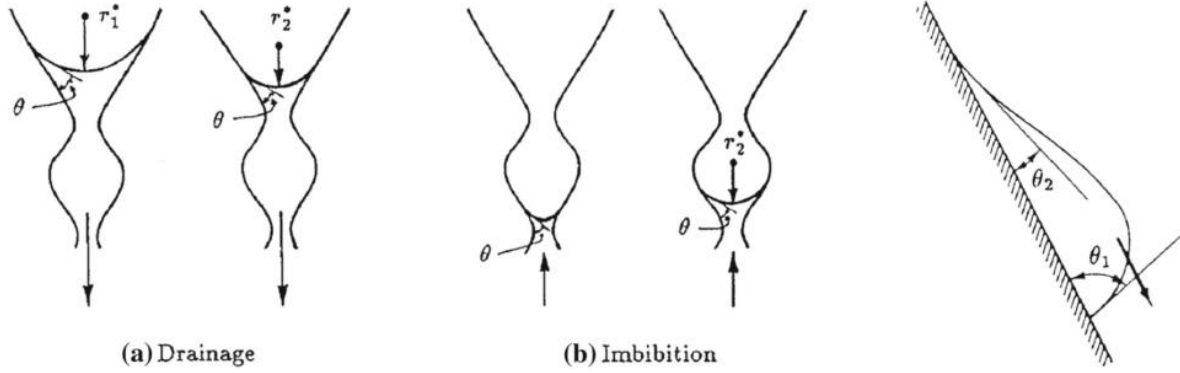


Figure 3.10- Ink-bottle effect (left (a) and (b)) and raindrop effect (right) (Albers 2014)

3.3. Mass transfer in porous media.

Remark: In the following, the vectors are represented using bold characters.

3.3.1. Equation of water mass conservation

The ideal gases have a proportional relationship between the mass fraction of a component and its portion of total pressure (Künzel 1995); the diffusion of water vapour in air can be described by the Fick's law (eq. 13):

$$\mathbf{g}_v^0 = -\delta \nabla(p_v) \quad (13)$$

where \mathbf{g}_v [kg/m².s] is the water vapour diffusion flux density vector, δ [kg/m.s.Pa] the water vapour diffusion coefficient in air, p_v [Pa] the water vapour partial pressure, and ∇ is the Nabla symbol ($\nabla(p_v) = \mathbf{grad}(p_v)$)

However, the diffusion in the porous medium is more complex since in smaller pores, the fluid interacts more frequently with the pore walls and the distance that must be covered by the vapour molecule to go through the sample becomes higher than its thickness. To take in account these interactions, it is necessary to introduce the water vapour diffusion resistance factor, which is a characteristic value of the material. In this way, the expression of diffusion of water vapour in air is given by eq. 14:

$$\mathbf{g}_v = -\frac{\delta_a}{\mu} \nabla(p_v) = -\delta_p \nabla(p_v) \quad (14)$$

where μ is the water vapour diffusion resistance factor. This value is the ratio of the diffusion coefficient of water vapour in the air and in the building material. It is considered independent of the temperature and the moisture (Künzel 1995).

At high RH, in the capillary water regime, transport of free water can occur. This transport is due to the gradient of capillary pressure and eventually due to the gravity forces in the large pores. It can be described by the Darcy's law (eq. 15):

$$\mathbf{g}_L = -D_p \cdot (\nabla p_w - \rho_w \mathbf{b}) \quad (15)$$

where \mathbf{g}_L [kg/m².s] is the liquid flux density vector, D_p [kg/m.s] is the liquid conduction coefficient and \mathbf{b} is the gravity.

Considering these two transports, and assuming that the variation of water vapour mass is negligible in comparison with the variation of liquid water mass, the overall conservation of water mass reads in the form of eq. 16:

$$\rho_d \frac{\partial u}{\partial t} = -\nabla \cdot (\mathbf{g}_v + \mathbf{g}_L) = \nabla \cdot (\delta_p \nabla(p_v)) + \nabla \cdot (D_p \cdot (\nabla p_w - \mathbf{b})) \quad (16)$$

If the mass transport is realized under isothermal conditions, the gravity is neglected, and if the liquid water permeability is assumed to be almost null (hygroscopic regime), this expression can be simplified in the form of eq. 17:

$$\rho_d \frac{\partial u}{\partial t} = \nabla \cdot (\delta_p \nabla(p_v)) \quad (17)$$

Finally assuming a 1D transfer, a constant δ_p , that $\partial u = u(\varphi)$ and taking in account the equation (9), it becomes like eq. 18:

$$\rho_d \frac{\xi}{p_{v,sat}} \frac{\partial p_v}{\partial t} = \delta_p \frac{\partial^2 p_v}{\partial x^2} \quad (18)$$

3.3.2. Moisture buffer value (MBV)

A factor that relates all the parameters explained previously is the Moisture Buffer Value (MBV), which characterises dynamic sorption.

The materials with high hygroscopicity can stabilize the humidity levels even in a very moist environment, such as in a shower room (Mcgregor 2014). The ability of materials to moderate variations in the RH is called moisture buffering. A technical report of Nordtest project (Rode et al. 2005) was published with the objective of proposing a unique value and method to obtain the MBV. This parameter can be defined at different levels:

- Room level: the MBV depends on the whole room in analyse, including exposed areas of furniture and other elements inside the room, moisture load, ventilation rate and indoor climate.

- System level: the capacity of MBV depends on the air velocity, area, and thickness of the sample. This value is the practical MBV ($MBV_{practical}$)
- Material level: at this level are analysed the proprieties of the materials and their influence on the MBV.

The definition of MBV given in the Nordtest project is: "The Moisture Buffering Value (MBV) indicates the amount of moisture uptake or release by a material when it is exposed to repeated daily variations in RH between two given levels. When the moisture uptake from beginning to end of the exposure to high RH is divided per open surface area and per % RH variation, the result is the MBV. The unit for MBV is $g/(m^2 \cdot \% RH)$ " (Rode et al. 2007).

Using eq. 19 it is possible to calculate the MBV from the experimental test results; this is called $MBV_{practical}$.

$$MBV_{practical} = \frac{\Delta m}{A \cdot \Delta \varphi} \tag{19}$$

where Δm is the difference of mass of the material exposed to a cyclic variation of moisture levels, also called moisture uptake [g], A is the area of exposed surface [m^2] and $\Delta \varphi$ the difference between high/low RH level [%]. The boundary conditions are very important for comparison between the obtained MBV and a different material. Except the area of exposed surface, in Figure 3.11 is possible to understand the parameters referred to above.

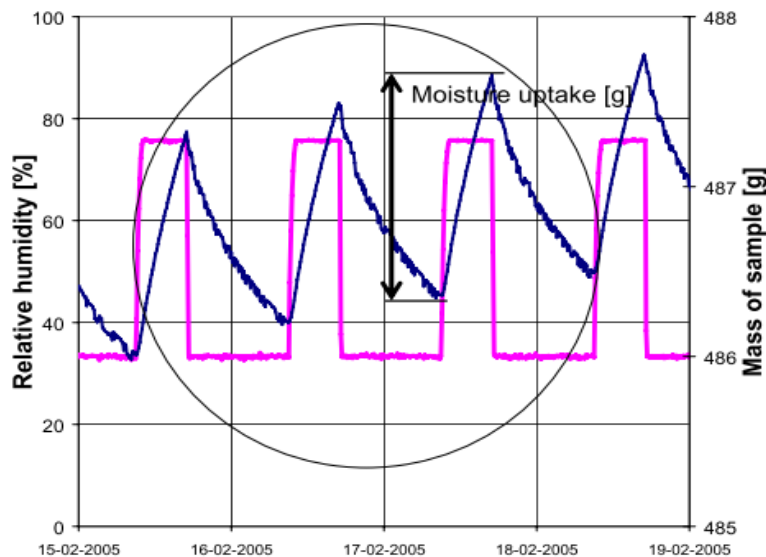


Figure 3.11- Determination of $MBV_{practical}$ from dynamic measurements. Definition of 3 cycles inside the ellipse, moisture uptake and the changes of RH that promote the cycles. (Rode et al. 2005)

The Nordtest method is the experimental test most used nowadays (Mcgregor 2014). It consists in a sequence of cycles of 8h at high RH level and 16h at low RH (Figure 3.11). For the $MBV_{\text{practical}}$, obtained by applying the eq. 19, values can be classified using five different categories. That can be seen in the Table 3.1.

Table 3.1- Practical MBV classes (Rode et al. 2005)

MBV [g/(m²·%RH)]	Classification
0-0,2	Negligible
0,2-0,5	Limited
0,5-1,0	Moderate
1,0-2,0	Good
>2,0	Excellent

This classification (Table 3.1) is valid only for the boundary conditions specified in the experimental method. In particular, the practical classes have been defined on the basis of the daily cycle of indoor relative humidity in Northern European countries, where a strong difference of temperature is common between the external and internal conditions. In the present dissertation, this classification is given for information purpose but it shall, in no case, be understood as an evaluation of the performance of these materials in warm countries like Portugal.

Round Robin test was carried out within the Nordtest project to try the testing paradigm for typical building materials. These tests were done by several universities for this test method. Table 3.2 shows the results obtained by different laboratories, DTU (Technical University of Denmark), NBI (The Norwegian Building Research Institute), VTT (Technical Research Centre of Finland), LTH (Lund University, Sweden) with different experimental setups. It is clear, in general, that there is a good agreement between the results for each laboratory, but particular attention must be paid to the experimental setup.

Table 3.2- Results from the Round Robin test (Rode et al. 2005)

		MBV_{practical} [g/(m²·%RH)]		
	Laboratory	Average	Standard deviation	%Deviation
Spruce boards	DTU	1.22	0.04	3
	NBI	1.12	0.09	8
	VTT	1.15	0.05	4
Concrete	DTU	0.42	0.11	26
	NBI	0.35	0.18	51
	LTH	0.37	0.04	10
Gypsum	NBI	0.69	0.13	19

	LTH	0.57	0.01	1
	VTT	0.65	0.02	3
Laminated wood with varnish	DTU	0.46	0.07	16
	NBI	0.39	0.06	14
	VTT	0.54	0.05	9
LW aggregate concrete with stucco	DTU	0.74	0.08	10
	NBI	0.81	0.10	12
	LTH	0.72	0.08	11
Cellular concrete	DTU	1.05	0.07	6
	LTH	0.96	0.06	6
	VTT	1.11	0.04	4
Brick	DTU	0.39	0.06	16
	LTH	0.35	0.02	5
	VTT	0.69	0.11	17
Birch panels	NBI	0.91	0.16	18
	LTH	0.61	0.05	8
	VTT	1.03	0.06	6

3.3.3. Analytical solution to estimate the MBV

The theoretical analysis of moisture buffer capacity on the material is based on the heat-mass transfer analogy. For this, in order to understand the expression of moisture effusivity, it is important to consider the thermal effusivity, doing an analogy between thermal and water mass equations. Beginning for the equation of heat balance (eq. 20), where λ is the thermal conductivity, and ρC_p is the volumetric thermal capacity. It is possible to find the thermal diffusivity (eq. 21), a , using the eq. 20, and this property is defined as the ratio between the thermal conductivity and the volumetric thermal capacity.

$$\rho C_p \frac{\partial T}{\partial t} = \lambda \frac{\partial^2 T}{\partial x^2} \quad (20)$$

$$a = \frac{\lambda}{\rho C_p} \quad (21)$$

The thermal diffusivity and thermal effusivity contain the same parameters, however they are different. Diffusion can be defined like the speed at which thermal equilibrium can be reached while thermal effusivity, sometimes called the heat penetration coefficient, is the rate at which the material can absorb

heat. Nevertheless, the thermal effusivity can be written in function of the thermal diffusivity and the volumetric thermal capacity (eq. 22):

$$b_T = \sqrt{a} \cdot \rho C_p = \sqrt{\frac{\lambda}{\rho C_p}} \cdot \rho C_p = \sqrt{\lambda \cdot \rho C_p} \quad (22)$$

Taking what was explained above in consideration, it is possible to do a parallel between thermal and moisture effusivity. For this, it can be considered the mass balance conservation of water (eq. 18).

Such as in the thermal equation in the mass balance conservation, it is possible to find the moisture diffusivity (a_m). The moisture diffusivity can be seen in the eq. 23. In addition, this parameter is related with $\frac{\xi}{p_{v,sat}}$ in order to obtain the moisture effusivity (eq. 24).

$$a_m = \frac{p_{v,sat} \cdot \delta_p}{\xi} \quad (23)$$

$$b_m = \sqrt{a_m} \cdot \frac{\xi}{p_{v,sat}} = \sqrt{\frac{\delta_p \cdot \xi}{p_{v,sat}}} \quad (24)$$

where b_m is the moisture effusivity [$\text{kg}/(\text{m}^2 \cdot \text{Pa} \cdot \text{s}^{1/2})$], δ_p is the water vapour permeability of the material [$\text{kg}/(\text{m} \cdot \text{s} \cdot \text{Pa})$], ξ is the moisture capacity of the material and $p_{v,sat}$ is the saturation vapour pressure.

To express the physical phenomenon of "a material's ability to lose or gain moisture over its surfaces, when it is brought in contact an environment at another condition" (Rode et al. 2007), a theoretical value of MBV, called MBV_{ideal} , is given in Rode et al. (2005). This theoretical model is simplified for isothermal conditions; however the temperature influences the water storage in the material that in turn affect the RH, as explained previously. According to Roels & Janssen (2006) and Peuhkuri (2003) the water vapour permeability varies according to the RH, then to assume that the water vapour permeability is constant is a limitation of this model. However, it is possible to be used for an estimation applying eq. 25, where t_p is the time of the cycle (24 hours).

$$MBV_{ideal} \approx 0.00568 \cdot p_{v,sat} \cdot b_m \cdot \sqrt{t_p} \quad (25)$$

3.3.4. Moisture penetration depth

Another information that could be interesting is the thickness of the material that is active during a daily moisture buffering cycle. This thickness, called the moisture penetration depth can be evaluated from

an analytical solution assuming that for instance a plaster can be modelled as a one dimensional semi-infinite medium, submitted at its surface by a daily sinusoidal cycle of humidity between 33% RH and 75% RH, and that the relation between the water content and the RH is linear. The asset of these assumptions is to allow an analytical expression for the RH within the sample in the form of eq. 26 (Rode et al. 2005):

$$\frac{\Delta u_x}{\Delta u_s} = \frac{\Delta \varphi_x}{\Delta \varphi_s} = e^{-x \sqrt{\frac{\pi}{D_w t_p}}} \quad (26)$$

where Δu_x is the moisture variation at a certain depth x within the material, Δu_s is a sinusoidal moisture variation on the material surface and D_w is the moisture diffusivity given by eq. 27:

$$D_w = \frac{\delta_p p_{v,sat}}{\rho_d \xi_u} \quad (27)$$

The eq. 26 and the use of the lead to the moisture profiles are presented in the Figure 3.12 at different times $(t_p, \frac{t_p}{4}, \frac{t_p}{2}, \frac{3t_p}{4})$ where $t_p = 1$ day is the time period. In this graph, the dotted curves show the maximum and minimum values of RH at different depths in the material. x_p is the point where the RH variation is equal to 1% of the outer surface variation and is therefore referred to as $d_{p,1\%}$. This point x_p can be defined as the penetration depth. The undisturbed RH (φ_{und}) is 59%, in these boundary conditions, because, although the mean value for surrounding RH is 54%, the variation of RH is, due to non-linearity, not symmetric.

Then, the analytical expression of the penetration depth can be obtained by the amplitude of moisture content variation $(\frac{\Delta u_x}{\Delta u_s})$ in eq. 26 by the value of 1%. It leads to $d_{p,1\%}$ which is equal to eq. 28:

$$d_{p,1\%} = 4.61 \sqrt{\frac{D_w t_p}{\pi}} \quad (28)$$

However, many studies found that this expression of $d_{p,1\%}$ was not consistent with experimental results. Another expression, based on a variation of $1/e \approx 37\%$, and which is in a better agreement with experimental results is then proposed. This value, denoted by $d_{1/e}$, is equal to eq. 29 (Mcgregor 2014):

$$d_{1/e} = \sqrt{\frac{D_w t_p}{\pi}} \quad (29)$$

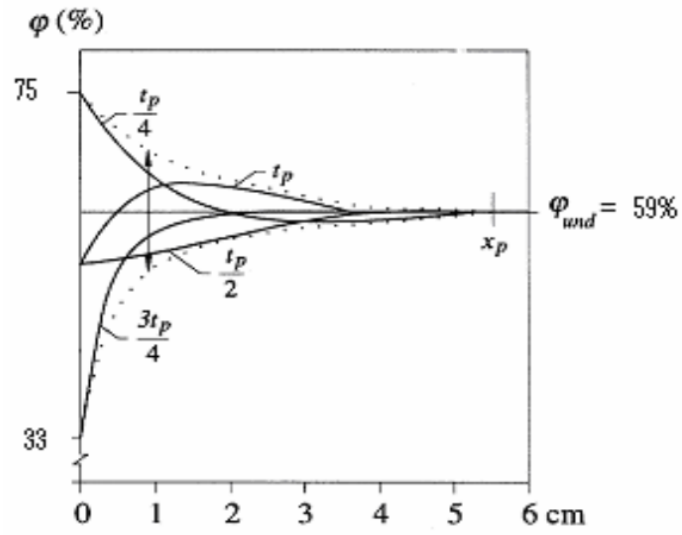


Figure 3.12- The penetration depth (Rode et al. 2005)

4. Materials and methods

This chapter describes the materials and the methods used on all experimental programs developed to assess the impact of temperature and thickness on water storage capacity, moisture buffering and penetration depth.

The aim of the experimental program to evaluate the impact of temperature is the acquisition of the dynamic characteristic at different temperatures of the material and the use of a theoretical model to verify if the practical values are in agreement. This theoretical model takes into account the equation of water vapour mass conservation (eq. 18) where it is known that $p_{v,sat}$ and p_v are temperature dependent. However, it is not known the impact of the temperature neither on the moisture capacity nor on the water vapour permeability. Therefore, tests were done in order to obtain these steady-state properties.

For the characterization of the impact of thickness, the experimental program goes through the acquisition of the dynamic characteristic of the different thicknesses samples in order to see if these values change when the thickness is different. The practical results will be compared with theoretical models based in steady state properties.

4.1. Materials

Since this work is developed under the IBIS project¹ and the BIOTERRA project², where ENTPE is a partner, the studied materials used in this experimental work can be divided in two categories: hemp concretes and earth mortar plasters. Each project is focused on a different material: the IBIS project promote the study of hemp concrete while the BIOTERRA project has the purpose of studying earth mortar plasters.

4.1.1. Hemp concrete

For hemp concrete, Table 4.1 gives the manufacturing conditions and the proportion of the mixtures of the three kinds of formulations used. In order to facilitate the manufacturing, samples of all the formulations were made in cylindrical formworks with 16cm in diameter and 32cm height.

¹ **IBIS** (Started in 2013, co-funded by ADEME). Leader: Parex Group, Partners: LGCB-ENTPE, ESITPA, C&B. Subject: Innovative bio-based insulation systems for the renovation of buildings made with local materials

² **BioTerra** (started in 2014, co-funded by ANR: French National Research Agency) Leader: LMDC, Partners: Agencement Structure, AGN Agronutrition, Carrières du Boulonnais, CTMNC, CEREMA, LGC, LGCB-ENTPE, UPS-LRSV. Subject: Control of the microbial proliferation on earth bio-based products for healthy and sustainable buildings

Table 4.1- Mixtures proportions of studied hemp concrete, wet density, samples and curing

Material	PF70	Calco	NL Parex
Binder	Lime based binder (Tradical 70)	Hydraulic lime based binder	Formulation developed by ParexGroup
Hemp/binder mass ratio (-)	0.33	0.33	0.42
Water/binder mass ratio (-)	0.81	0.88	-
Wet density after the realization (-)	0.78	0.70	-
Manufacturing	Rammed (in formwork)	Rammed (in formwork)	Sprayed (in formwork)
Curing conditions	50%RH in formwork		

The composition of each formulation is hemp shives, binder and water. Therefore, the main difference between each formulation is the binder. Attached in Appendix B.1 and B2 of this document is presented the technical sheets of these materials (except NL Parex). Where it is possible to resume the composition:

- **Tradical 70-** It is a formulated lime based binder (75%) with hydraulic binders (15%) and pozzolanas (10%).
- **Calco-** It is a formulated lime which constitution is hydraulic lime, calcareous charges, hydrophobic and rheological admixtures.
- **NL Parex-** For this binder little is known about the composition; it is a formulation developed by ParexGroup.

As a result of the project IBIS the samples of hemp concrete were made at ENTPE, except the NL formulation. The samples of PF70 were made on March 2014 and the samples of Calco were done on May in the same year. The same experimental protocol is used for their mixing. The first stage consists in mixing the dry lime with about 90% of the water during 5mins. Then, the hemp and the remaining amount of water are progressively added in the lime paste in approximately 10mins. Just after mixing, the samples are rammed into cylindrical 16cm x 32cm formworks in five stages up to a wet density of 800kg/m^3 ($\pm 30\text{kg/m}^3$).

The NL samples are directly sprayed into the cylindrical formworks using the wet spraying technique. This technique consists in three steps. The first one is the mixing of the dry lime and the water. The second one is the injection of the hemp within the lime paste. And the third one is the projection of the fresh hemp concrete with a spray lance. Thus, apart from the setting of the samples (either rammed or sprayed), the mixing procedures of the three formulations are quite similar.

4.1.2. Earth mortar plasters

For earth mortar plasters the clay is considered as the binder. There are three different formulations, each one with a type of clay as binder:

- **Kaolinite** (F0) is a clay with a low specific surface compared to other clays; yet with a high sorption capacity compared to most minerals.
- **Ascal 10** (F3) is a fine calcareous-clay material from "Carrières du Boulonnais".
- **Enduit C** (F5) is a commercial mortar proposed by "Carrière du Boulonnais"; no further is known about the composition, only that the integral fibrous material of this formulation are particles of flax.

The formulations presented in Table 4.2, Table 4.3 and Table 4.4 below were used to prepare the samples; where the values of mass are exact but the values of volume are estimated values, based on the loose bulk density of the materials. In order to speed up the manufacturing of the samples, each formulation was made in formworks (50 x 50cm²) with three different thicknesses (1cm, 2cm and 4cm).

Table 4.2- Formulation of mortar F0

F0	Sand (0, 2)	Kaolinite	Water	Straw (3-5cm)
Volume (l)	15.54	7.77	9.71	15.54
Mass (kg)	23.59	8	9.71	0.81

Table 4.3- Formulation of mortar F3

F3	Sand (0, 2)	Ascal 10	Water	Straw (1-3cm)
Volume (l)	16	-	8.51	-
Mass (kg)	24	11.06	8.51	0.78

Table 4.4- Formulation of mortar F5. The value in brackets corresponds to the initial formulation that must be changed due to the occurrence of cracks during the drying period

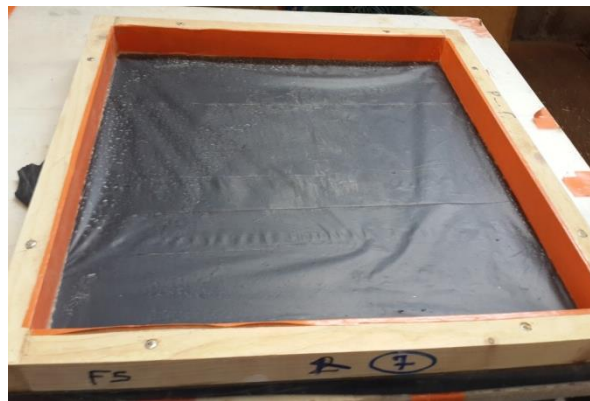
F5	Enduit C	Water
Volume (l)	-	5.70
Mass (kg)	34.4 (32)	5.70

In order to have a better perception of the proportions in each formulation in Table 4.5 is possible to see the clay, fiber and water content within the formulations in the mixture.

Table 4.5- Clay, fibre and water content of earth mortar plasters

	F0	F3	F5
Clay content (%)	19,0	24,9	-
Fibre content (%)	1,9	1,8	-
Water content (%)	23,0	19,2	14.2

The earth samples are realised within the framework of the BIOTERRA project, notably in collaboration with the "Direction Territoriale Centre-Est" of the CEREMA where the samples were made. The first procedure to be performed was the preparation of the different types of moulds. A special attention was required to the interior coating of the moulds. In order to allow free movement of the mortar and the propagation of cracks during its retraction, due to drying, a plastic was placed inside of the mould, see Figure 4.1. Three moulds of different height (1, 2 and 4cm) were prepared for each formulation.

**Figure 4.1-** Mould used for earth mortar plaster samples with 50x50x4cm³

Thereafter, the mixture was made according to the formulations presented previously with help of a hand mixer in order to obtain a homogeneous mixture.

However, during the ten first days of drying, the formulation 5 (Enduit C) showed a high quantity of cracks. Therefore the preparation of the F5 formulation had to be repeated. This repetition was done with some adjustments, increasing a quantity of dry component of this formulation from 32kg to 34.4kg for 5.7kg of water.

The drying process of the earth plasters was controlled in a conditioning room at 20°C \pm 2°C and 60% \pm 5% of RH. Periodical measurements were done in order to check the progress of drying and the time that the samples takes to reach the equilibrium with the environment to which they were exposed. The drying curves obtained are presented in Appendix B (Figure B.1).

4.2. Test procedure: Standard characterization

4.2.1. Sorption isotherms

The sorption isotherm describes the storage characteristics in the hygroscopic regime. For this determination, two tests can be made, the first called "Desiccator method" using a salt solution and the other one called "Climatic chamber method". In this case, the used procedure was the "Desiccator method". The advantage of the use of the salt solutions is that a great number of samples could be measured at the same time, but the disadvantage is the low precision and time needed for the test.

For the procedure was used the Standard EN ISO 12571 (CEN 2000). Three representative samples of each formulation with more than 10g of mass were placed in aluminium containers, in order not to lose material during the procedure, see Figure 4.2. The first step was to dry all samples in an oven at 50°C in order to start the test at dry mass. Since the samples contained organic material, the maximum temperature that could be used was 60°C, because the fibres in the material may promote degradation at higher temperatures.



Figure 4.2- Samples setup for sorption isotherms test (Left- Earth mortar plaster F0; Right- Hemp concrete NL)

The samples were placed in six different levels of RH (23, 43, 59, 75, 85 and 97%) and each level was maintained in an isolated box with a saturated salt solution. For this test, two dimensions of boxes were used (Figure 4.3): little and big boxes for the test at $40\pm 2^\circ\text{C}$ and $23\pm 2^\circ\text{C}$, respectively. It was necessary, due to their dimension, the installation of a fixe ventilation system in the big boxes in order to mixing the environmental air in the box. Each salt solution was made with a different salt in order to obtain the hygrometric conditions, see Table 4.6. These salt solutions were prepared following Annex B in EN ISO 12571 (CEN 2000). A portable sensor (Rotronic HygroLog HL-NT) was used for constant control of the RH and the temperature in the boxes.

This test was made at two different temperatures: $23\pm 2^\circ\text{C}$ and $40\pm 2^\circ\text{C}$ in a conditioning room and at climatic chamber (Froilabo), respectively. For earth mortar plasters, this test was done only at $23\pm 2^\circ\text{C}$. The logistic conditions justify the size of the boxes.



Figure 4.3- Sorption isotherms setup (Left- procedure at 40°C and Right- procedure at 23°C)

Table 4.6- Substances for salt solution for each RH

RH (%)	Substance
23	Potassium acetate (KC ₂ H ₃ O ₂)
43	Potassium carbonate (K ₂ CO ₃)
59	Sodium Bromide (NaBr)
75	Sodium chloride (NaCl)
85	Potassium chloride (KCl)
97	Potassium Sulphate (K ₂ SO ₄)

The samples were weighed periodically (≈ 5 in 5 days) using a scale with an accuracy of 0.01g. The equilibrium moisture content for each RH level was reached if the change of mass between three consecutive measurements was less than 0.1% of the total mass.

In order to save time, for the sorption curve all RH levels were tested at the same time. The initial point of the desorption curve was taken from the samples at EMC at different high RH, as explained below, and then successively moved to lower levels. It was necessary a minimum of three samples of each formulation for each RH level in order to improve the precision of the test.

The desorption process normally starts at the highest level of RH; however in this experimental procedure different starting RH levels were implemented. For earth mortar plasters two different levels were used, one at 97% and another at 85%. For Hemp concrete desorption was started from 85% and 75% due to the growth of fungi at 97% of RH. Also these conditions of RH levels are closer to the range used in the other test (MBV test). The desorption curve could only be measured at $23 \pm 2^\circ\text{C}$ due to a technical breakdown of the used climate chamber.

The water content is given by the eq. 4, previously presented in this dissertation. This calculation was made for all RH levels, enabling the construction of the experimental sorption and desorption curves for all samples and for all boundary conditions.

4.2.2. Water vapour permeability

The water vapour permeability, also loosely called "breathability", is a property that characterizes the material ability to transport water vapour under a vapour pressure gradient once the steady state is reached (Rahim et al. 2015). In the standard EN ISO 12572 (CEN 2001) for vapour permeability of building products the experimental setup and the associated calculation can be found. The water vapour permeability, δ_p [Kg/(m.s.Pa)], is the "density of water vapour flow rate divided by the water vapour pressure difference between the two specimen faces" (CEN 2001).

The experimental test can be called "wet cup" when is used an aqueous saturated solution or "dry cup" when the test cup contain either a desiccant. In the chosen procedure, it was used the wet cup method with RH levels closed to the ones used during the moisture buffering test. The samples were placed on top of the container containing a salt solution of Potassium Chloride to maintain a RH level of 85%RH, see Figure 4.4.

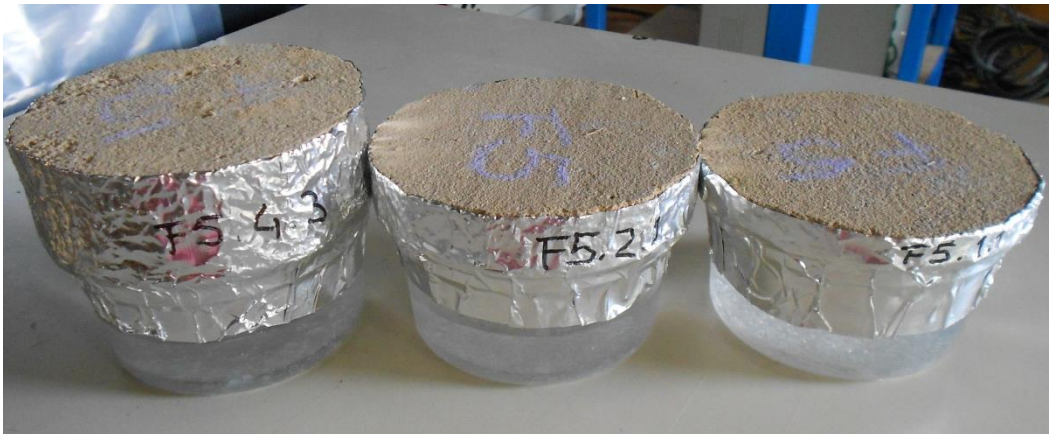


Figure 4.4- Example of setup for diffusion on water vapour permeability test (F5)

The samples with the cup were then stored in an Ineltec climatic chamber which was maintained at a RH level of 50% and 23°C for both materials. The cup design was according the procedure followed by McGregor (2014). Therefore, a thin bed of silicon was applied in order to seal the samples to the plastic cup. To seal the samples to the cup a vapour-tight aluminium tape was used. The use of aluminium tape is justified by its properties: completely water vapour impermeable and does not adsorb a significant quantity of moisture itself (McGregor 2014).

The investigation was carried out under varying boundary condition on round specimens of the previously referred material, where:

- Earth plaster: It was trimmed giving a circular shape with diameter equal 12cm and 1, 2 and 4cm of thicknesses;
- Hemp concrete: Diameter equal 16cm and only samples with 5cm of thickness.

According with EN ISO 12572 (CEN 2001) the air space between the salt solution and the bottom of the specimen shall be 15 ± 5 mm; however in order to reduce the risk of contact between the salt solution and the specimen this assumption was not met. This air layer was 30mm for all samples.

The environmental conditions (50% RH and 23°C) were constantly controlled by the climatic chamber Ineltec. Measurements were done periodically, on a scale outside of the chamber, until a constant decrease of mass for each test specimen was obtained.

During the water vapour permeability test the total of the mass of the set composed by plastic cup, salt solution and sample is monitored. The recording over the time presents a change in mass; this happens due to the water vapour moving through the sample. The mass variation was recorded until a linear relation be obtained between mass and time. In Figure 4.5 three different shapes for the graph were represented with the variation of the slope of the curve mass/time ($\rho_d(\partial u/\partial t)$). The initial non linear section (Equilibration stage) represents the phase when the samples balance the system, where the water vapour produced by the salt solution is dissipated in two processes: a part is adsorbed by the sample and another part is evaporated. The second phase (Permanent state) occurred when the water vapour transfer reaches a constant flow rate; in other words, the quantity of water vapour produced and evaporated is the same. The last phase only occurs when the water used in the salt solution is not sufficient to finish the test or the ventilation flow within the climatic chamber is reduced. When the amount of water within the cup is not sufficient, it promotes salt deposition and it increases the air layer in the cup, as well as the resistance to the flow of water vapour.

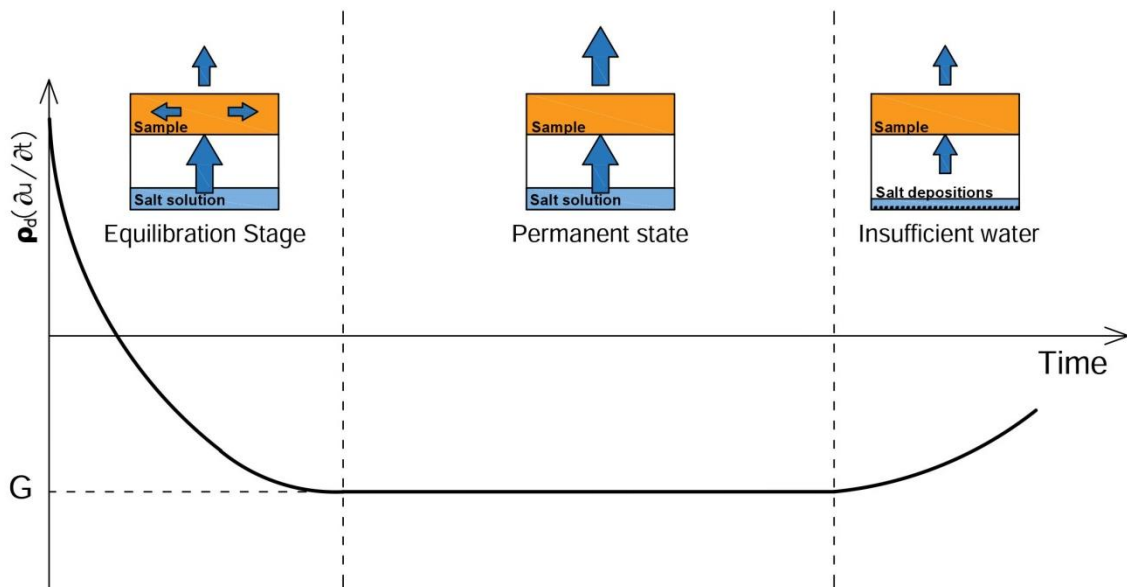


Figure 4.5- Three possible stages during the diffusion test

The calculations were performed following the Standard EN ISO 12572 (CEN 2001). After the linear relation was reached, as previously mentioned, the slope of the regression line $G = \rho_d(\partial u/\partial t)$ (kg/s)

can be determined. When the permanent state is reached, the vapour pressure gradient through the sample becomes homogeneous. Thus, the mass conservation equation (eq. 18) can be written in the form (eq. 30):

$$G = A \delta_p \frac{\Delta p_v}{d} \quad (30)$$

where A (m²) is the exposed surface of specimen, d is the thickness of the sample and Δp_v (Pa) is the water vapour pressure difference across the sample. Similarly to the heat transfer coefficient, a water vapour permeance coefficient, denoted by W (in Kg/(m².s.Pa)) and equal to δ_p/d is commonly used to quantify the ability of a mortar plaster to let the vapour to diffuse through its porous network. Using the previous equation, its expression is directly linked to the slope of the regression line, G , through (eq. 31):

$$W = \frac{G}{A \cdot \Delta p_v} \quad (31)$$

Finally, for convenient purpose, the vapour resistance factor is used rather than δ_p in order to quantify the water vapour permeability of the material. This latter is a dimensionless number defined as the ratio between the water vapour permeability of air (δ_a) and δ_p (eq. 32):

$$\mu = \frac{\delta_a}{\delta_p} \quad (32)$$

The value of δ_a can be estimated from the relation given by Künzel (1995) (eq. 33):

$$\delta_a \approx 2 \times 10^{-7} \frac{T^{0.81}}{p_0} \text{ [kg/(m s Pa)]} \quad (33)$$

where T is the ambient air temperature (K) and p_0 is its pressure (Pa). Thus, at 23°C and at atmospheric pressure (101325Pa), $\delta_a = 1.97 \cdot 10^{-10}$ kg/(m s Pa). The higher the value of water vapour resistance factor, the less is the value of permeability of the material and inversely a lower value of μ leads to a greater permeability.

The EN ISO 12572 (CEN 2001) proposes a correction, in Annex G, for the resistance of air layers in each side of the sample. In this correction, it is assumed that the layer of air between the specimen and the salt solution promotes some resistance to the flow of vapour, inducing a significant error in the case of very permeable materials. This correction is normally recommended when the water vapour diffusion-equivalent air layer thickness (s_d), calculated from eq 34, is lower than 0.2m. :

$$s_d = \mu \cdot d_a \quad (34)$$

The correction proposed by ISO 12572 (CEN 2001) is present in the equation (35), where d_a is the value of the height of the air layer (eq. 35).

$$W_c = \frac{1}{\frac{A \cdot \Delta P_V}{G} - \frac{d_a}{\delta_a}} \quad (35)$$

Where d_a is an estimated value using the test cup dimensions and the volume of used salt solution.

4.3. Test procedure: Dynamic test - Moisture buffering test

Results of this test provide information on dynamics of mass exchange between the air and the materials. It also characterizes the material contribution to the moderate variation of the RH in the indoor environment of Northern European countries. Therefore to obtain this results the moisture buffering test has been performed following the Nordtest protocol (Rode et al. 2005).

The samples that were made in large formworks were cut after the maturing period and the removing of mould. All earth mortar plaster samples, previously described, were cut in specimens with surface dimension equal to $15 \times 15 \text{ cm}^2$. Three samples of each thickness (1, 2 and 4cm) were prepared. In the cutting process the uniformity of the samples was taken into account because, in order to have a comparison of the hygrothermal behaviour, samples without cracks were necessary and some lack of homogeneity was induced by the mould. For hemp concrete, the cutting process was simplified. The big samples, previously described, were cut in three samples with different thicknesses (5, 10 and 15cm). Due to a lack of material, only one sample was made of each thickness for each formulation.

The specimens were sealed with aluminium tape in all surfaces except one (Figure 4.6) in order to have just one exposed surface in contact with the controlled environment.



Figure 4.6- Example of samples for Moisture buffering test (Left- Hemp concrete Calco; Right- Earth mortar plaster F3)

The boundary conditions applied in this test were the use of cycles of 33% to 75% with time steps of 8h at high RH and 16h at low RH. This test was realised at 23°C and 40°C for hemp concrete and only at 23°C for the earth mortar plasters.

The prepared samples, of each category of material, were placed at the same time in the climatic chamber Ineltec. The layout of the Moisture Buffering test can be seen in Figure 4.7. The mass was measured at set intervals at 0h, 1h, 3h, 5h, 7h, 8h, 9h and 24h for hemp concrete and 0h, 2h, 4h, 6h, 8h, 9h and 24h for earth mortar plasters using a scale with an accuracy of 0.01g placed outside of the chamber. This record was done outside in order to avoid the vibration promoted by the climatic chamber ventilation and to be able to measure all samples at the same time. After the placement of the samples in the chamber, it was necessary to wait until the stabilization in the alternating RH cycles was reached, which means that the weight amplitude must not vary by more than 5% from successive cycles. The conditions given by the climatic chamber (RH and temperature) were automatically recorded.

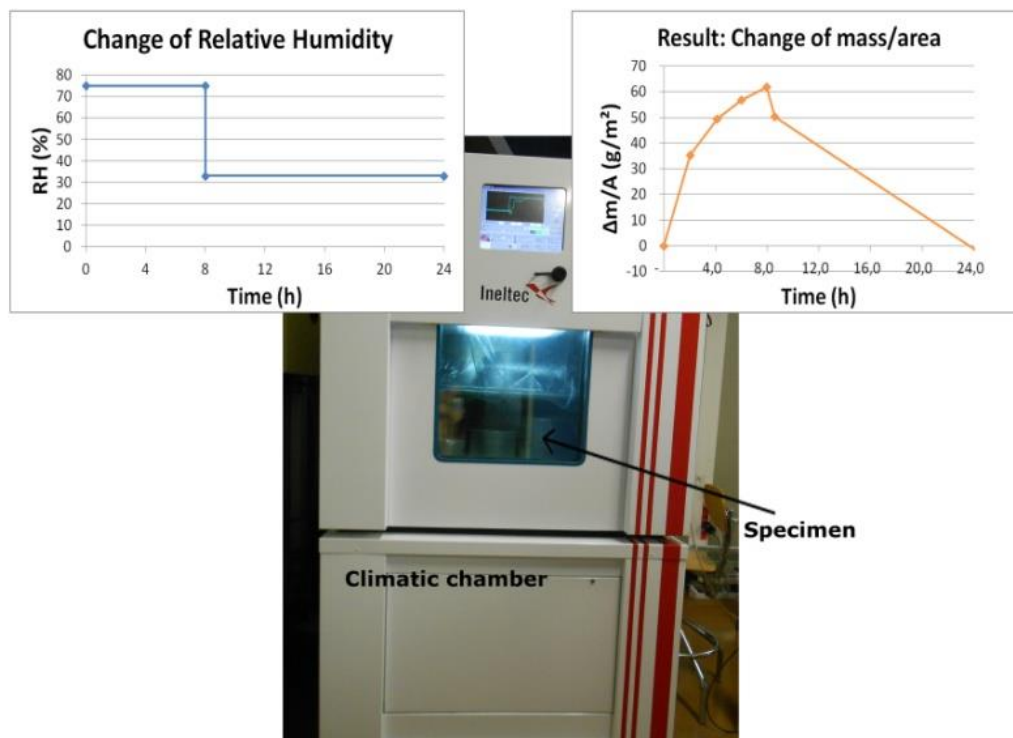


Figure 4.7- Moisture buffering test setup

Let us note that the initial results obtained for earth plasters when the samples of hemp concrete samples were placed at the same time in the chamber showed unusual behaviour (see Figure 4.8). This may be due to the interactions between the samples within the chamber. Therefore, to reduce these interactions, the use of the chamber was limited to the measurement of one type of material at the same time.

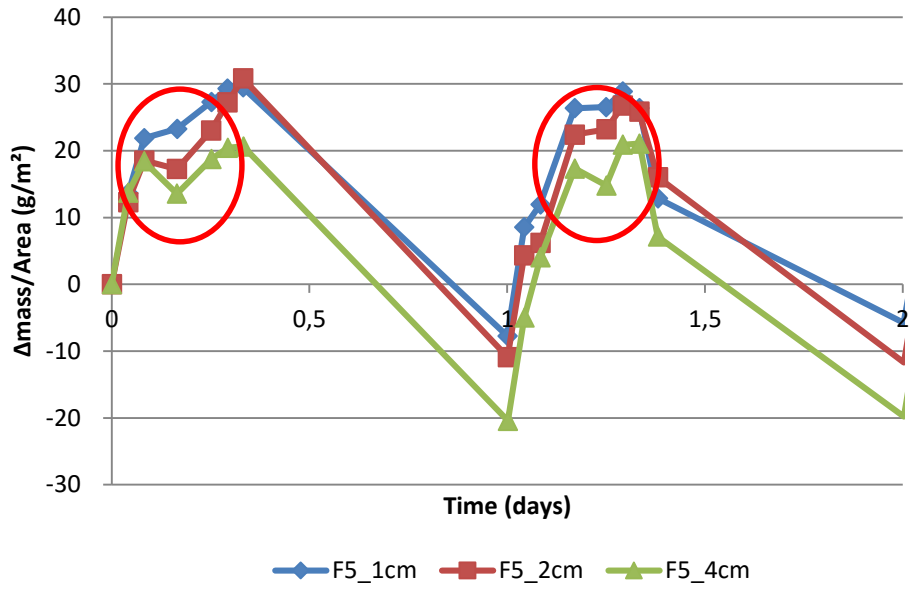


Figure 4.8- Earth plaster MBV test results when hemp concrete are in the same time in the climatic chamber. The unusual behaviours are highlighted with the red circles

5. Standard characterisation

5.1. Density

The dry density of hemp concrete formulations was obtained using the dry mass of the cylindrical samples of 16x32cm, referred previously, for PF70 and Calco. The value of dry density for NL was obtained using three dry little samples with a volume of $59 \pm 1 \times 10^{-3} \text{m}^3$. Table 5.1 gives the dry density, hemp/binder ratio and binder type of the hemp concrete formulations under study compared with results previously published. Nevertheless, the binder used in the previously study hemp concretes is Tradical PF70 while in the studied materials only a formulation have this type of binder but with different proportions.

Table 5.1- Dry density (ρ_d) of hemp concrete materials in function of their hemp/binder mass ratio and comparison with literature

	PF70	Calco	NL	Collet et al. (2008)	Collet et al. (2013)	Rahim et al. (2015)	Evrard (2006)
ρ_d (kg/m³)	509	502	407	664	430	482±15	400.66
Hemp/Binder (%w.)	0.33	0.33	0.42	0.50	0.50	-	0.50
Binder type	Tradical 70	Calco	-	Tradical 70	Tradical 70	Tradical 70	Tradical 70

The same study is made for earth mortar plasters. The values of dry density (Table 5.2) were assigned by CEREMA. In the same table a comparison with the physical properties tests for two types of commercial earth mortar plasters obtained by Mcgregor (2014) and the range of typical values of earth building materials provided by Röhlen & Ziegert (2011) are presented.

Table 5.2- Dry density of earth mortar plasters and comparison with literature

	F0	F3	F5	Mcgregor (2014)	Röhlen & Ziegert (2011)
ρ_d (kg/m³)	1596	1660	1720	1677-1725	600-2000
Clay content (%)	19.0	24.9	-	-	-
Clay type	Kaolinite	Ascal 10	-	Commercial plasters	-

The dry density of all earth mortar plasters is much higher than the values obtained for hemp concrete. These results are consistent because hemp concrete can be considered like a lightweight concrete.

5.2. Sorption isotherms

The EMC was determined using the eq. 4 when the wet mass of the samples reaches its equilibrium level.

In the representation of the sorption isotherms it is assumed that, after the drying process, the samples have 0% of moisture content and are exposed at 0% of RH. This assumption may not be valid as it is nearly impossible to be totally dry at 50°C oven temperature.

On the curves obtained in the sorption isotherms test at 23°C for hemp concrete (Figure 5.1) the point at 97% RH is not a precise value. All samples in this level of RH had growth of fungi, due to the longer time (49 days) exposed at highest RH, and consequently these samples were removed before stabilization. Therefore, the values presented for the 97% RH level would be higher because total equilibrium could not be reached in this level. However, this is not considered a problem as this high humidity level is unlikely to be achieved for a long period in a real building.

The sorption curves of the three formulations follow the same trend. A quite linear increase of water content from 0% RH to 60% RH is followed by a much more significant increase of water content until 97% RH. However, while sorption curves of Calco and NL are almost the same, PF70 presents lower values of moisture content. The values of all the samples are reported in Appendix C.1, where it is presented in red the samples not considered in the calculation (higher standard deviation compared with the other tested samples of the same formulation).

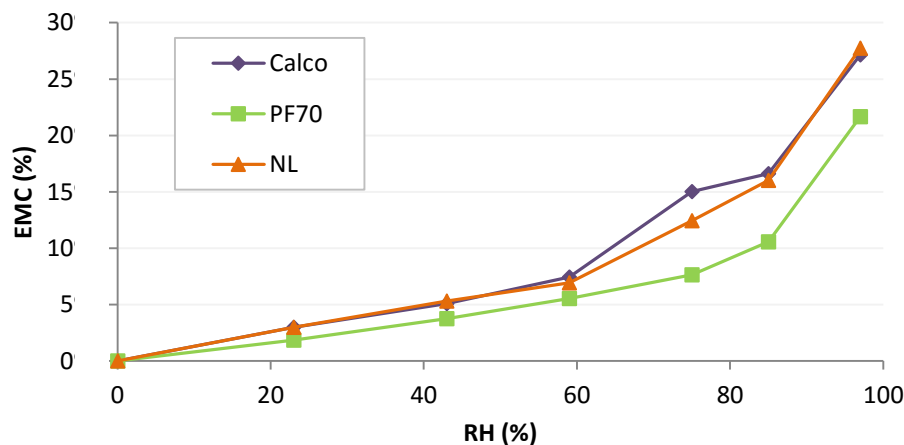


Figure 5.1- Sorption isotherms for hemp concrete at 23°C

Since the EMC was not reached for the 97% RH level and because the dynamic test was done between 33% and 75% RH, the desorption curves started at 85% and 75% RH level. This procedure was done in order to see the hysteresis between the desorption curves beginning at different states of RH, as well the difference of moisture capacity if these curves starts at distinct RH levels.

As it is possible to see in Figure 5.2, Figure 5.3 and Figure 5.4, a strong hysteresis was observed between the sorption and the desorption curves for all the tested hemp concretes. After the drying stage in an oven at 50°C, the remaining water content within the sample submitted to desorption is between 5% and 15%. The formulation which is more affected by this irreversibility is the Calco, while the less impacted is the PF70. These graphs emphasize that the moisture capacity estimated from the sorption curve may not be a good parameter to estimate the MBV_{ideal} and the penetration depth. In the following work, two values will be used: the one extracted from the sorption curve and the one from the desorption curve. The correct value should be between these two bounds.

The physical explanation of this irreversibility is not so clear. Indeed, one should think that it may be caused by water consumption due to carbonation of lime and/or hydration of hydraulic lime. But the tested samples were stored for at least 6 months at a RH of 50% before being tested. On the other side, some powder can be observed on the bottom of some samples after the MVB tests, which should indicate some hardening issues. Another explanation can be an irreversible uptake and release of water of the hemp particles due to the cellular structure of fibers. Nevertheless, some additional researches are needed to conclude on that point.

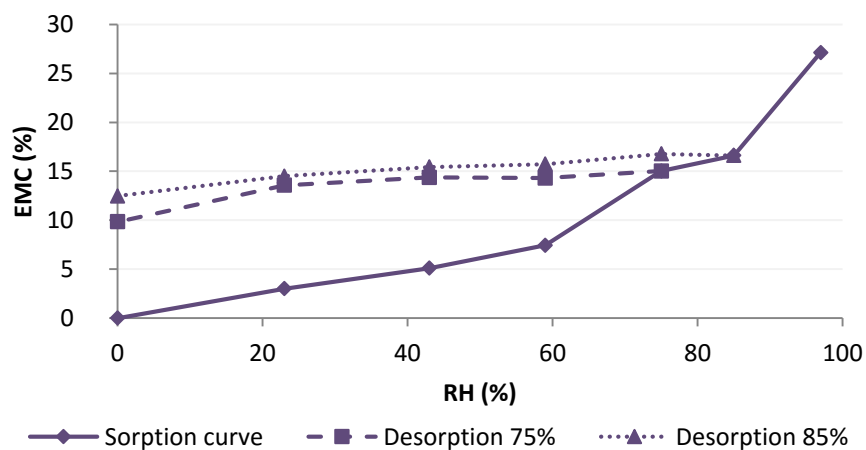


Figure 5.2- Sorption and desorption from 75% and 85%RH level for Calco

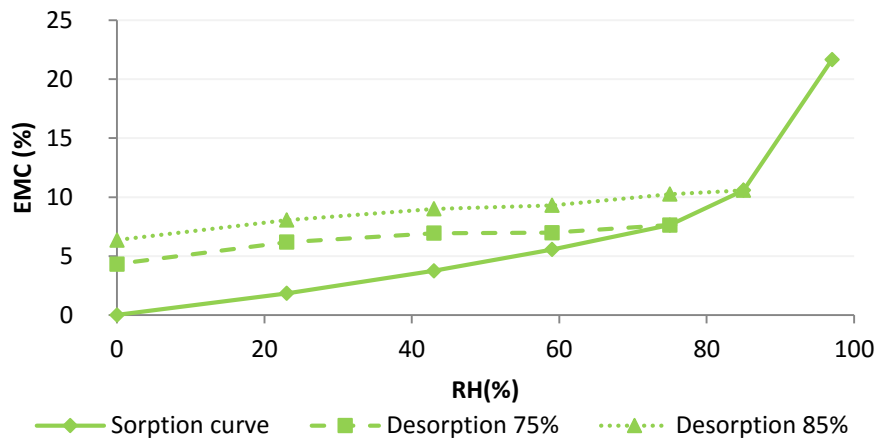


Figure 5.3- Sorption and desorption from 75% and 85%RH level for PF70

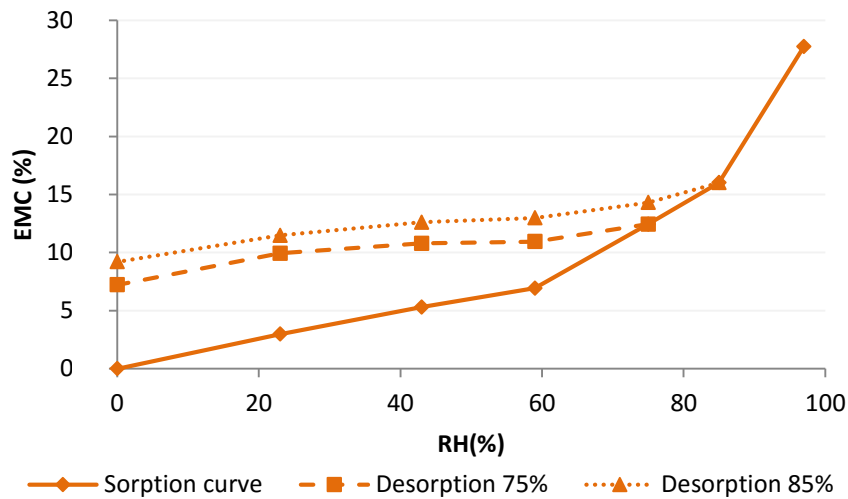


Figure 5.4- Sorption and desorption from 75% and 85%RH level for NL

The equilibration time of earth mortar plasters (Figure 5.5) is significantly lower than the equilibration time of hemp plasters. Therefore, contrary to the hemp concrete samples, the values obtained for the highest RH level are stabilized and it was not possible to detect mould growth during this process. All formulations presented the same shape in the sorption curves.

F0 is the formulation which has the higher moisture content in all RH levels with a water content of 2.7% at 97% RH. The lower EMC was obtained by F5 with a water content of 1.2% at 97%RH.

The water contents during the mixtures were 23.0%, 19.2% and 15.1% for F0, F3 and F5, respectively. This property can be a justification of the difference in EMC because more water content in the mixture leads to more porosity, which may increase the values of EMC. Another explanation can come from the composition of the clayey binder of these materials. Indeed, F0 is composed by pure kaolinite while the two other are composed by powders of unknown composition which are surely not composed only by clays.

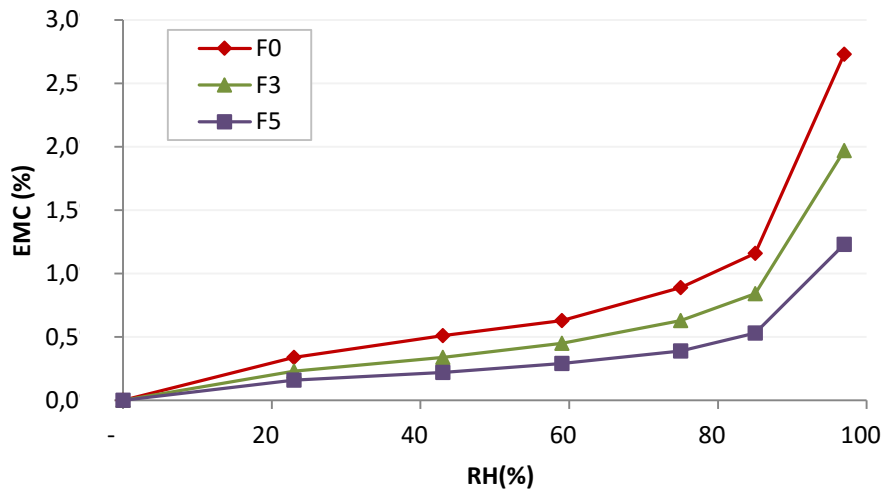


Figure 5.5- Sorption curve for each type of earth mortar plasters

Similarly to hemp concrete, desorption curves start at two different RH levels: 97%RH and 85%RH. They are represented in Figure 5.6 and Figure 5.7. In these figures it is possible to see that the difference between sorption and desorption curves is small, especially in the case of the curve starting at 85%. Nevertheless, in order to clarify this difference in Table 5.3 a resume of the hysteresis values obtained is made. It shows that the difference between the sorption and the desorption curves remains lower than 0.2% which is clearly negligible.

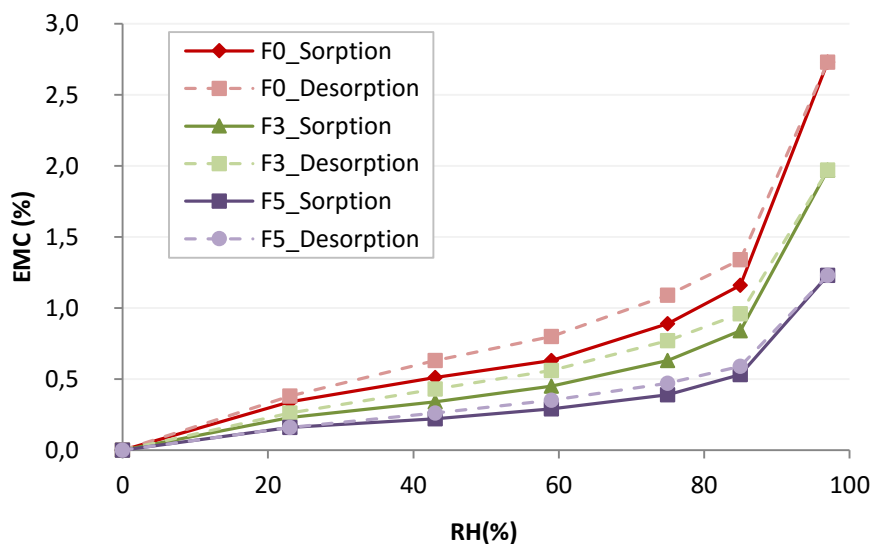


Figure 5.6- Sorption and desorption from 97%RH level for each type of earth mortar plasters

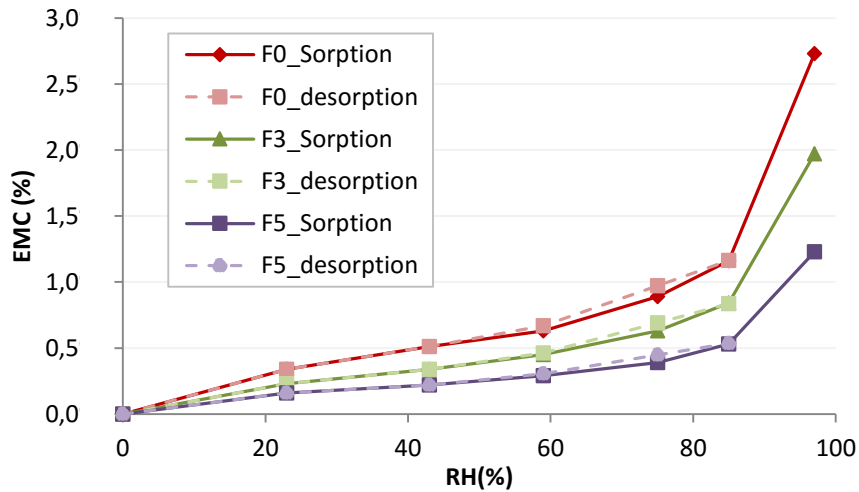


Figure 5.7- Sorption and desorption from 85%RH level for each type of earth mortar plasters

Table 5.3- Hysteresis values for two different RH levels (97% and 85%) for earth mortar plasters

RH (%)	F0 (%)		F3(%)		F5 (%)	
	97%	85%	97%	85%	97%	85%
0	0,00	0,00	0,00	0,00	0,00	0,00
23	0,04	0,00	0,03	0,00	0,00	0,00
43	0,12	0,00	0,09	0,00	0,04	0,00
59	0,17	0,04	0,11	0,01	0,06	0,02
75	0,20	0,08	0,14	0,06	0,08	0,06
85	0,18	0,00	0,12	0,00	0,06	0,00
97	0,00		0,00		0,00	

All results obtained for sorption and desorption curves for earth mortar plasters are presented in Appendix C.2.

It is possible to conclude that the hysteresis loop for earth mortar plasters can be considered negligible while for hemp concrete these values present an important range. This means that the hydric behaviour of hemp concrete seems to be much more complex. This complexity will lead to consider two moisture capacity values for hemp concrete (one from the sorption curve and one from the desorption curve) while only one value will be used for the earth mortar plasters.

The moisture capacity for each formulation was calculated using the eq. 12 taking into account the RH between 23% and 75%. This range is justified with the range used for MBV test. The results for all formulations (earth mortar plasters and hemp concrete) are in Table 5.4 where is clear the higher difference of water vapour adsorption between earth mortar plasters and hemp concrete. Due to the higher difference between sorption and desorption curves for hemp concrete the moisture capacity is very different in each

one. Therefore, an average value of moisture capacity between both was assumed. This average value was not necessary for earth mortar plasters once the hysteresis is negligible.

Table 5.4- Moisture capacity for all formulations

		ξ (kg/m ³) Sorption	ξ (kg/m ³) Desorption	ξ (kg/m ³) Average
Earth mortar plasters	F0	16,3	-	-
	F3	12,5	-	-
	F5	7,5	-	-
Hemp concrete	Calco	110,2	20.1	65.1
	PF70	56,5	20.4	38.4
	NL	70,3	20.9	45.6

Comparing earth mortar plasters with hemp concrete (Figure 5.8) and considering the EMC mass by volume, it was possible to see that the adsorption capacity of all of them was considerable lower compared with hemp concrete formulations. The highlight values in the graph were the equilibrium results for earth plasters. As explained previously, these values were not the EMC for hemp concrete at 97%. Such values should be higher if the equilibrium has been reached. However, hemp concrete has a retarded sorption phenomena compared with earth mortar plasters. In other words, the quantity of water vapour adsorbed by hemp concrete is higher but takes more time in order to reach the EMC.

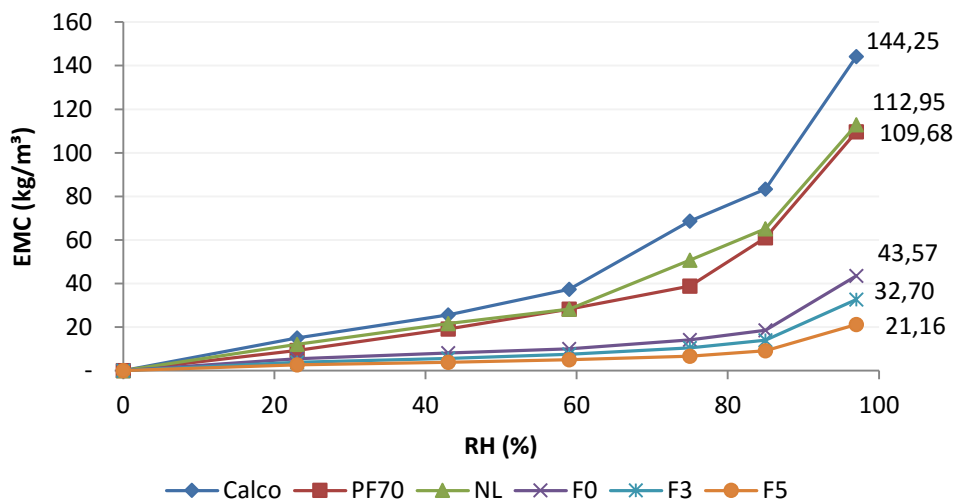


Figure 5.8- Comparison between earth mortar plasters and hemp concrete formulations using mass by volume

5.3. Water vapour permeability

The results of this mass variation were plotted as variation of mass versus time, see Figure 5.9, Figure 5.10 and Figure 5.11. The behaviour of all earth mortar plaster formulations was similar. During 5

days was visible the stabilization phase and afterwards the permanent stage with a higher variation of mass yet on the 15th day the variation decreased slightly. This late phenomenon is due to the modification of wind velocity within the climatic chamber (vertical line in the previously referred figures). It leads to conclude that a higher speed of the fans would artificially increase the measured value of the vapour permeability.

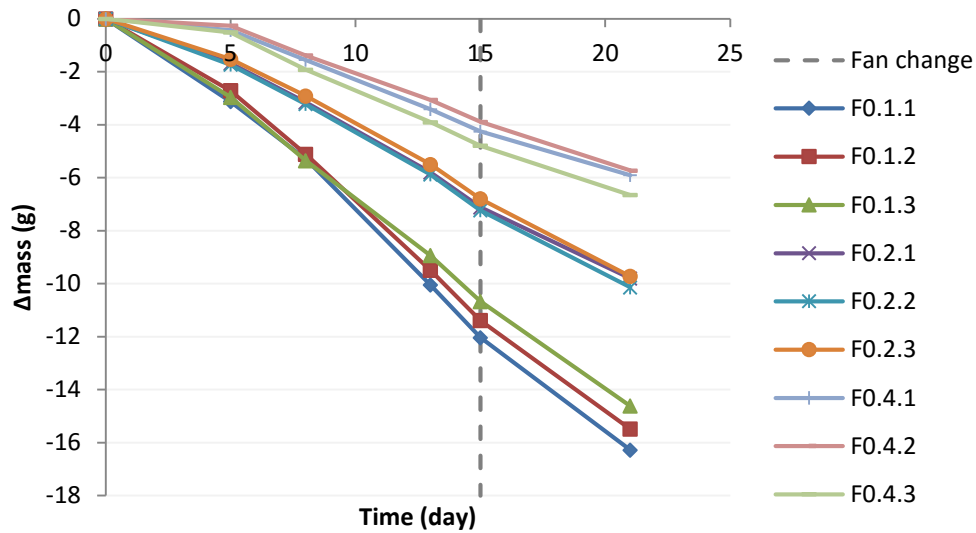


Figure 5.9- Variation of mass during the water vapour permeability test of earth mortar plaster F0 (the second number in the reference of the sample is the thickness)

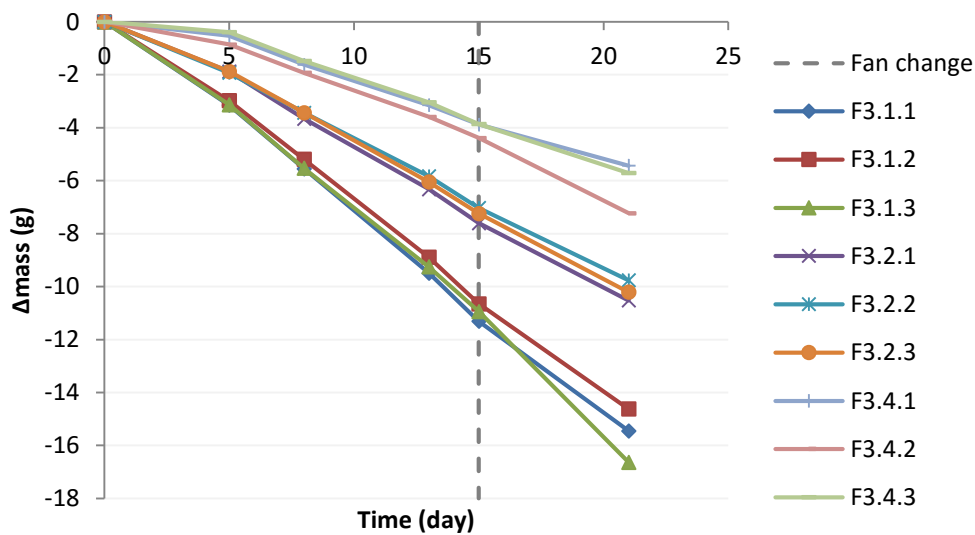


Figure 5.10- Variation of mass during the water vapour permeability test of earth mortar plaster F3 (the second number in the reference of the sample is the thickness)

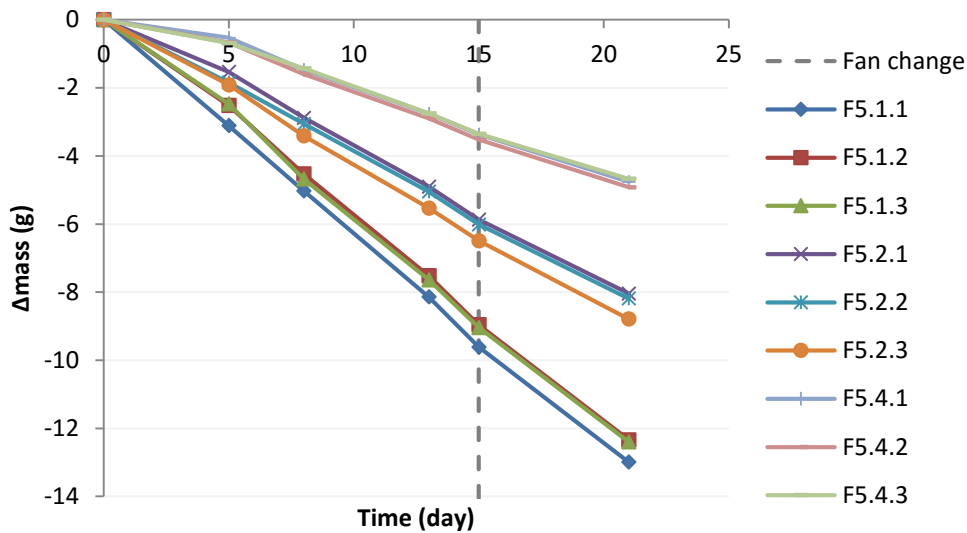


Figure 5.11- Variation of mass during the water vapour permeability test of earth mortar plaster F5 (the second number in the reference of the sample is the thickness)

The results obtained using the calculation procedure explained in the Chapter 4.2.2 are presented below.

In Table 5.5 can be seen the average values of each formulation, between different thicknesses, of water vapour permeability and vapour resistance factor as well as the standard deviation of this last value. These values are the original calculation, without correction. All formulations presented a standard deviation of vapour resistance factor high, this means that the different tested thicknesses obtained very different values. The highest thickness had the highest values while the lowest had a lowest value. However, the water resistance factor is an intrinsic value of the material. Therefore, two types of corrections were done, these are described below.

Table 5.5- Average values of water vapour permeability and water vapour resistance factor for each formulation of earth mortar plaster

	δ (kg/s.m.Pa)	μ (-)	
		Average	Standard deviation
F0	9.78E-12	20.15	5.99
F3	1.08E-11	18.24	5.53
F5	7.69E-12	25.63	6.53

The first correction starts with the calculation of water vapour diffusion-equivalent air layer thickness. For this the eq. 34 is applied the results were as follows in Table 5.6. Although the values are superior to the ones express in the ISO 12572 (CEN 2001) (0.2m) it was used this correction in order to compare between this proposal and the second correction, as explained before.

Table 5.6- Results of water vapour diffusion-equivalent air layer thickness for earth mortar plasters

Samples	d (m)	s _d (m)
F0.1	0.01	0.28
F0.2	0.02	0.40
F0.4	0.04	0.64
F3.1	0.01	0.25
F3.2	0.02	0.40
F3.4	0.04	0.55
F5.1	0.01	0.34
F5.2	0.02	0.51
F5.4	0.04	0.83

The average values of water vapour permeability and vapour resistance factor are in Table 5.7. In addition, the standard deviation of vapour resistance is represented and this value is lower compared to the original values.

Table 5.7- Average values of water vapour permeability and water vapour resistance factor for each formulation of earth mortar plaster with ISO correction

	δ (kg/s.m.Pa)	μ (-)	
		Average	Standard deviation
F0	1.07E-11	18.45	4.65
F3	1.19E-11	16.57	4.25
F5	8.24E-12	23.90	5.20

Even with the ISO correction, a significant difference can be observed on the vapour resistance values between the samples of different thicknesses. One may thus wonder if the ISO correction is sufficient. Indeed, as discussed previously, the modification of the fan velocity within the climatic chamber induces a significant variation of the results. But, this point is not taken into account in the ISO correction which assumes that the air velocity within the climatic chamber is sufficient to insure a good homogeneity within its volume. That is why, a new correction was proposed, called β correction, where the main principle is the partial pressure at each exposed surface of the sample (p_{v1}^* and p_{v2}^*) is compared with the environment partial pressure (p_{v1} and p_{v2}). A layout of the processes during the test is presented in Figure 5.12, where g is the density of water vapour flow rate, p is the partial vapour pressure, β is the apparent vapour transfer coefficient at the sample surface, s the exposed surface and d the thickness of the sample. All calculations are presented in the Appendix D.1.

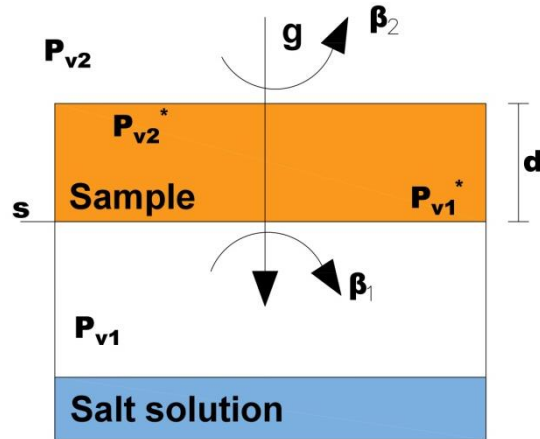


Figure 5.12- Layout of the processes during the test

With this second correction the expression of water vapour permeability is given by eq. 36:

$$\delta_p = \frac{G \cdot d}{s \cdot \Delta P_v - \frac{G}{\beta}} \quad (36)$$

where $\frac{1}{\beta} = \frac{1}{\beta_2} - \frac{1}{\beta_1}$ is estimated from an iterative calculation until a lower standard deviation between samples with same material but with different thicknesses is obtained. For this test, the β value is assumed 1.49×10^{-9} .

After this correction, the values between the different thicknesses are more similar with a standard deviation lower than the other correction and the original calculation (Table 5.8).

Table 5.8- Average values of water vapour permeability and water vapour resistance factor for each formulation of earth mortar plaster with β correction

	δ (kg/s.m.Pa)	μ (-)	
		Average	Standard deviation
F0	1.46E-11	13.45	0.94
F3	1.71E-11	11.53	1.41
F5	1.04E-11	18.86	1.51

The comparison between the obtained values of vapour resistance factor for all formulations with different thicknesses is in Figure 5.13. In a general visualisation of the values, the formulations F0 and F3 had similar water vapour resistance factor, while the value for F5 was higher. Therefore, the formulation with less permeability was F5. It is clearly visible in the Figure 5.13 that the difference obtained between thicknesses was higher in the original calculations as well in the results with ISO correction. While for the obtained results with β correction the values were similar between each tested thickness. Although, the

values of water vapour permeability obtained in this last correction for F0 and F3 were more closer to the results published in the literature for this type of material (Liuzzi et al. 2013; Mcgregor 2014), while the values obtained for F5 allow to conclude that this formulation have a discrepancy compared to the previously referred results. However, this difference might have resulted from the short time of stabilization, due to the lack of time.

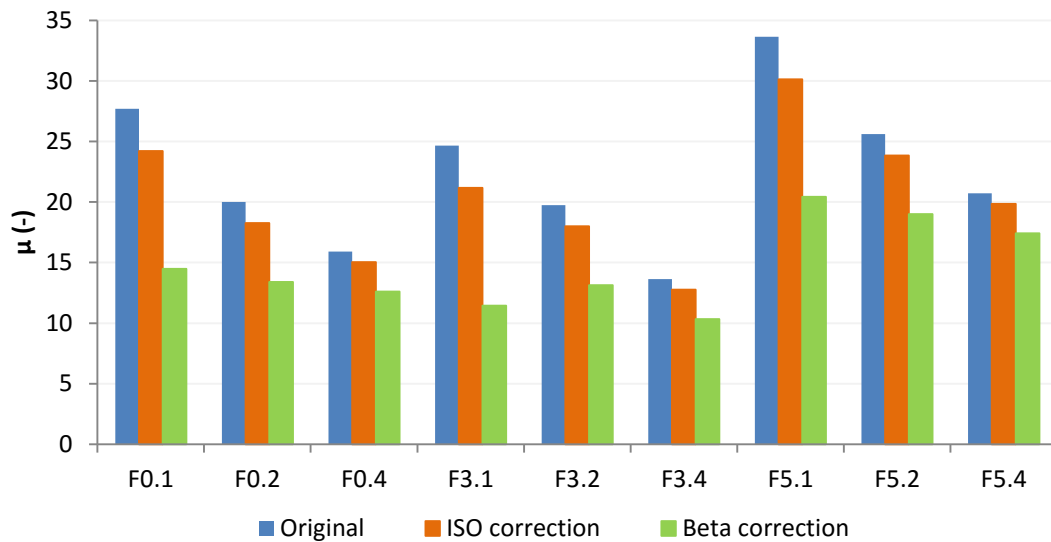


Figure 5.13- Comparison between the obtained values of water vapour resistance factor (μ) for Earth mortar plaster (with and without correction)

For hemp concrete, the test of water vapour permeability was done in two phases. Since this material adsorbs a big quantity of water vapour the quantity of water used for the salt solution was not sufficient to do the test in a single procedure. The variation of mass obtained in the first phase of the process can be seen in Appendix D.2 where in the 33.4 day it was possible to have the perception that the cup had insufficient water with salt depositions. Due to this fact, more water was added in the cups, an approximation of previously lost water. In this second phase, after the permanent stage was obtained the results below for water vapour permeability and vapour resistance factor without corrections (Table 5.9).

As explained for earth mortar plasters, the original calculation foreboded by EN ISO 12572 (CEN 2001) does not include the impact of the air layer in the cup. Therefore, it is used the ISO correction in order to obtain the values as close as possible to the real results due to the exposed conditions of test, even with s_d more than 0.20m. The results with this correction can be seen in Table 5.10.

However, the β correction was applied once in this correction is taken into account the air velocity. In the case of this material, the used parameter β was equal to the used for earth mortar plaster for simplification and due to this test has been carried out for samples with the same thickness. In this case, the standard deviation was not relevant for the choice of the correction. The obtained average results for water vapour permeability and resistance with β correction can be seen in Table 5.11.

Table 5.9- Average values of water vapour permeability and water vapour resistance factor for each formulation of hemp concrete

	δ (kg/s.m.Pa)	μ (-)	
		Average	Standard deviation
PF70	2.21E-11	8.63	0.43
NL	2.20E-11	8.64	0.39
Calco	2.80E-11	6.80	0.17

Table 5.10- Average values of water vapour permeability and water vapour resistance factor for each formulation of hemp concrete with ISO correction

	δ (kg/s.m.Pa)	μ (-)	
		Average	Standard deviation
PF70	2.36E-11	8.07	0.50
NL	2.38E-11	7.98	0.36
Calco	3.09E-11	6.15	0.15

Table 5.11- Average values of water vapour permeability and water vapour resistance factor for each formulation of hemp concrete with β correction

	δ (kg/s.m.Pa)	μ (-)	
		Average	Standard deviation
PF70	3.06E-11	6.25	0.75
NL	3.26E-11	5.84	0.27
Calco	4.68E-11	4.06	0.09

The comparison between all calculation procedures is presented in Figure 5.14. A significant difference is clearly visible between the sample PF70_2, NL_1 and C_2 compared with the other samples for the same formulations, it was not representative of the tested property. Therefore, these three previously referred samples were removed from the calculation of the average results in the Table 5.9, Table 5.10 and Table 5.11.

The observation of Figure 5.14 allows to verify that the NL and PF70 had similar behaviour, while Calco was slightly more permeable to the water vapour. The water vapour resistance factor for β correction was lower compared with the other calculations procedure.

Collet et al. (2013) had results of about 2.5×10^{-11} kg/(s m Pa) of water vapour permeability for hemp concrete composed by Tradical 70 and a higher quantity of fibres measured by the dry cup method. This value is close of the results obtained for the ISO correction. However, it is not sure that the β correction is the true results in reality, when used correction for another type of material. It will be probably required a specific correction factor for this type of material.

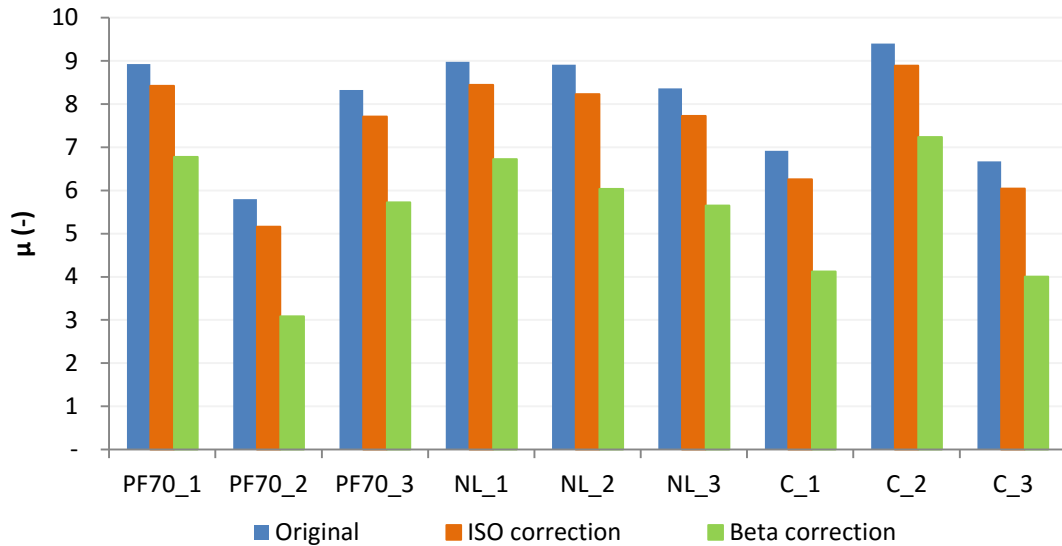


Figure 5.14- Comparison between the obtained values of water vapour resistance factor (μ) for hemp concrete (with and without correction)

Evrard (2006) did the dry cup test using Tradical 70 as binder with ratio hemp/binder equal 0.5 and several ways to do the mixture and pressure in mould. On this test, the author had values between 3.59 and 7.68 of vapour resistance factor and these extreme results correspond to the sample done with low pressure in mould and higher pressure, respectively. The results obtained for PF70, Calco and NL using the β correction can be inserted in this range while the manufacturing condition and mixture proportions were not the same. The values with this correction are similar to the one obtained by Collet et al. (2013) for sprayed hemp concrete using dry cup test.

Between October and December 2014 at the LGCB (ENTPE) were done water vapour permeability tests using dry cup with different RH (in cup and in the climatic chamber) for PF70 and Calco. In Table 5.12 are represented the boundary conditions of the procedure, as well the time until the stabilization, water vapour permeability and resistance factor for these materials. The comparison with other previously results (Table 5.9, Table 5.10 and Table 5.11) indicates that the formulations (Calco and PF70) are more permeable. However, this test had a different procedure (“dry cup” instead of “wet cup”) and was carried out only for one sample of each formulation in each boundary condition.

Table 5.12- Results of dry cup for Calco and PF70 (Chabriac 2014, personal communication)

		Calco			PF70		
Cup RH (%)	RH (%)	Test time (days)	δp (kg/s.m.Pa)	μ	Test time (days)	δp (kg/s.m.Pa)	μ
0	43.2	7.0	5.88E-11	3.40	6.9	4.91E-11	4.07
0	85	6.8	5.87E-11	3.41	6.8	4.71E-11	4.25
43	97	28.0	5.23E-11	3.83	6.8	9.07E-11	2.20

In order to understand the difference of results obtained from “wet cup” and “dry cup” methods, it is necessary to analyse the transport of water vapour during these tests (Figure 5.15). In the “wet cup” method, the produced water vapour in the cup is released, and the moisture flow is estimated from the mass decrease of the {wet cup, sample} system. On the opposite, in the “dry cup” method, the flux of vapour is in the opposite direction (from the climatic chamber to the dry cup). It follows that the moisture flow is estimated from the mass increase of the {dry cup, sample} system. But, whatever the method, the sample is initially equilibrated at the lower humidity level (i.e. dried sample for the “dry cup” method and 50%RH for the “wet cup” method). And thus, whatever the method, the mass of the sample increase during the equilibration stage.

In consequence, as it is illustrated in Figure 5.15, the error induced by an estimation of the vapour diffusion coefficient before the end of the equilibration stage modify the results in an opposite way for the two methods. It leads to an overestimation of the vapour flow (and thus an underestimation of μ) for the dry cup, and to an underestimation of the vapor flow (and thus an overestimation of μ) for the wet cup.

Once the example of dry cup given in Table 5.12 was done, in a time of approximately of 8 days, these samples may still be during the equilibration stage, with an apparent constant variation but an overestimated permeability.

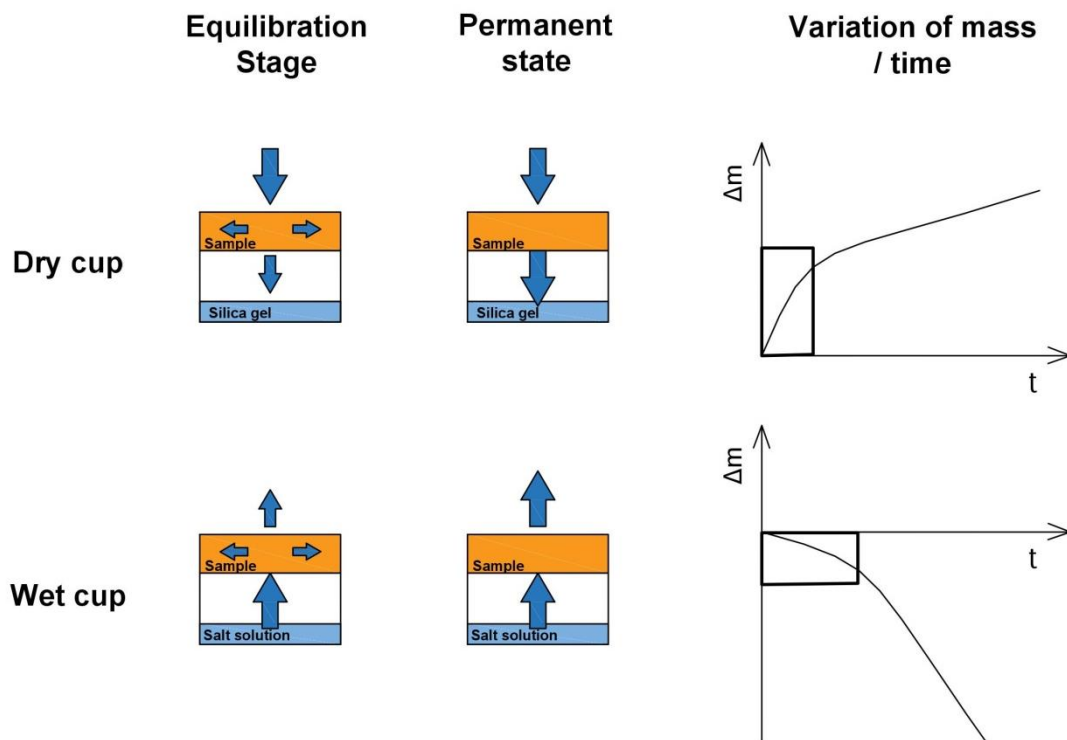


Figure 5.15- Transport of water vapour in the wet and dry cup test methods

6. Impact of thickness on hygroscopic capacity: Results and Discussion

6.1. On moisture buffering values

In this chapter has been taken as main reference the moisture buffering test at 23°C for earth mortar plasters and hemp concrete. However, the aim of this chapter is the comparison between the different thicknesses in order to observe the influence of this property on the moisture buffer effect.

All information about thickness and exposed surface for earth mortar plasters are available for consulting in Appendix E.1. For these formulations, the stabilization of the cycles is reached in 4-5 days and in order to save time it was done the complete register during the two last equilibrate cycles.

6.1.1. Results on earth mortar plasters

In Figure 6.1 is possible to see the variation of mass per exposed area ($\Delta m/A$) for F0 where the values for each thickness were similar. The lowest thickness had a moisture uptake range from 57.6g/m² to 61.8g/m², while for 2cm and 4cm the values were from 57.5g/m² to 60.5g/m² and from 55.0g/m² to 59.7g/m², respectively. The results for F3 are presented in Figure 6.2. This formulation also has similar results for all thicknesses, where the values of the moisture adsorption obtained for 1cm, 2cm and 4cm were in the range from 52.9g/m² to 54.0g/m², from 56.0g/m² to 56.8g/m² and from 53.5g/m² to 53.8g/m², respectively.

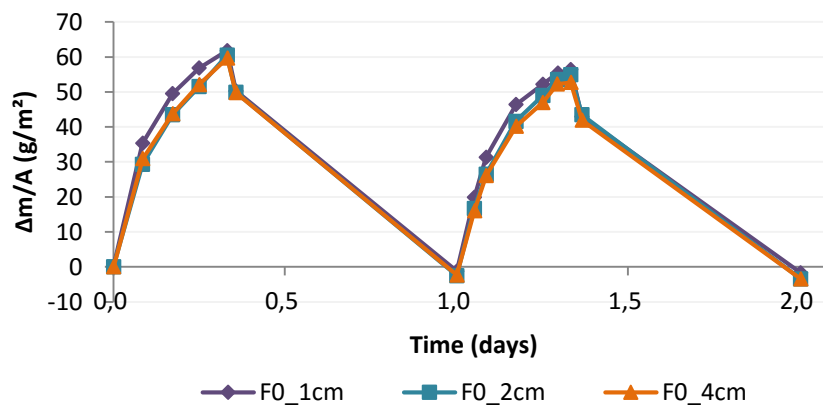


Figure 6.1- Moisture buffering test for F0 with 1, 2 and 4cm

The results for F5 are presented in Figure 6.3 where it is possible to see that the values obtained for 2cm and 4cm were similar, with moisture uptake in a range from 40.6 g/m² and 41.6 g/m² and from 43.5 g/m² and 44.3 g/m², respectively. However, the results for the lowest thickness in this formulation were different. It presented a maximum difference of 15% and 20% compared with the results obtained for 2cm and 4cm of thickness, respectively.

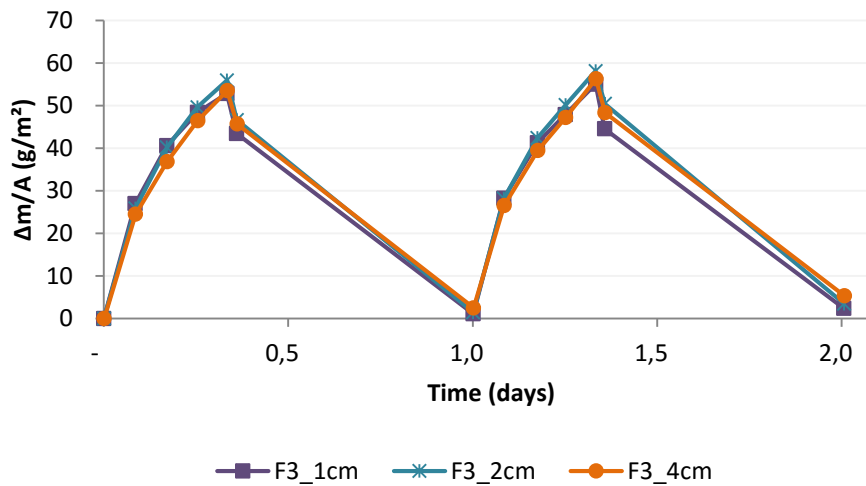


Figure 6.2- Moisture buffering test for F3 with 1, 2 and 4cm

Figure 6.4 shows the average values for all formulations with bar of the representation of the minimum and maximum values obtained for different thicknesses. However, F5 is a different case, because the samples with 1cm had moisture uptake (and release) lower compared with the other thicknesses for the same formulation. Therefore, in the graph is represented the average value of 2cm and 4cm for the F5 formulation, and the result for 1cm is shown separately. The observation of the Figure 6.4 allowed concluding that the formulations F0 and F3 had similar values of moisture uptake, while this property for F5 was lower.

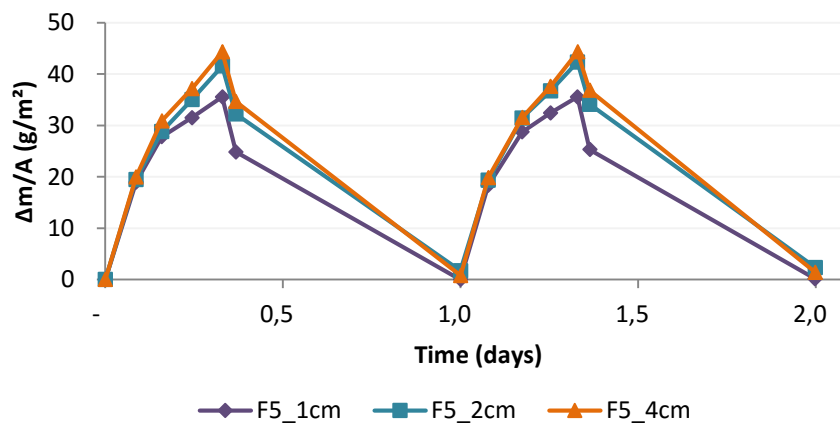


Figure 6.3- Moisture buffering test for F5 with 1, 2 and 4cm

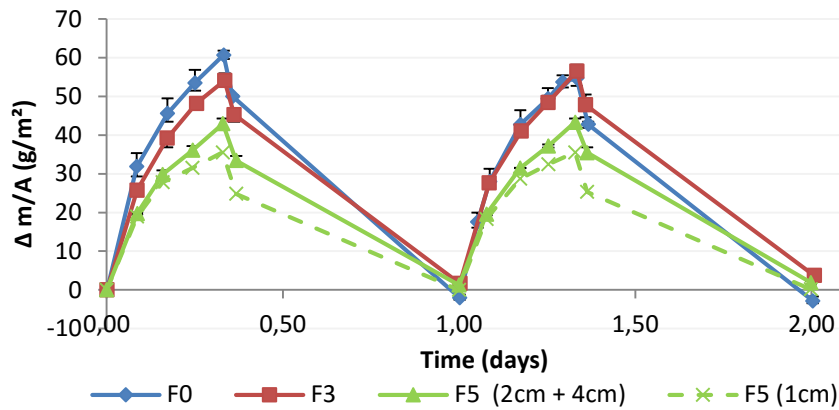


Figure 6.4- Moisture buffering test for all earth mortar plasters formulations, average values for different thicknesses

The average values of moisture buffering, called $MBV_{\text{practical}}$, for all formulation and thicknesses of earth plasters are presented in Figure 6.5. They were calculated from the experimental curves of the Figure 6.4 using the eq. 19 with the difference of mass adsorption during the two completed last cycles, exposed area equal 0.02m^2 and 42% of variation of RH. The standard deviation for these formulations was very low. As expected, F0 and F3 had similar results for $MBV_{\text{practical}}$ and higher compared with F5, even F5 with 1cm of thickness had lower $MBV_{\text{practical}}$ compared with the other thicknesses for the same formulation.

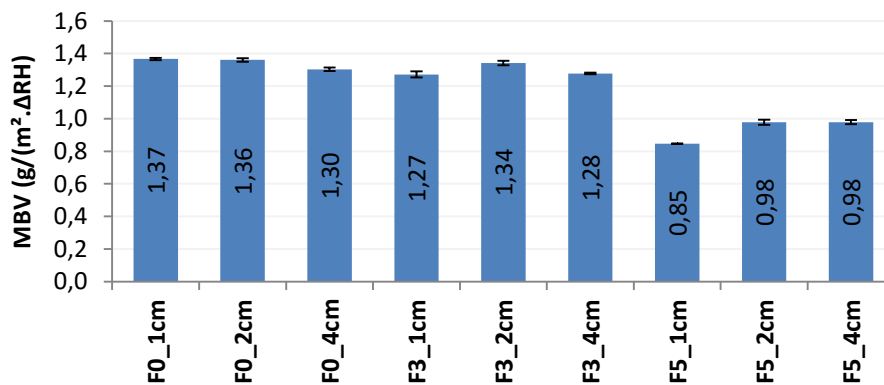


Figure 6.5- $MBV_{\text{practical}}$ for earth mortar plasters with different thicknesses

Taking into account the values exposed previously for the formulations F0 and F3, the values were not influenced by the thickness. However, F5 presents difference between the samples with 1cm and the other thicknesses. Therefore, it would be interesting to check the theoretical calculation of penetration depth (Chapter 6.2) in order to see if these results are consistent with the hygric parameter of the tested materials.

The $MBV_{\text{practical}}$ of earth plasters samples can be classified according to Nordtest project (Rode et al. 2005) using the Table 3.1. Therefore, F0 and F3 were classified as "Good" while F5 had the classification of "Moderate". And the results were similar to the $MBV_{\text{practical}}$ obtained for unfired clays (with quarry fines, kaolinite, quartzite grit sand and quartzite grit gravel) without fibers published by Liuzzi et al. (2013). It

seems that the quantity of fiber used is not sufficient in order to increase the moisture buffering of the tested material.

In parallel, the MBV_{ideal} was calculated using the values of vapour permeability obtained from the ISO correction and β correction. The eq. 24 was used in order to obtain the moisture effusivity (b_m) and the MBV_{ideal} was obtained by the eq. 25. For comparison, the value of $MBV_{practical}$ used for F5 is an average of the $MBV_{practical}$ for the samples with 2cm and 4cm due to the high deviation of the other tested thickness. In Table 6.1 is presented the values obtained for two types of corrections for all earth plaster formulation, where it was observed a good correlation between ideal and practical values mainly using β correction, except for F5. The difference between the obtained results with β and ISO correction were similar for all formulations.

Table 6.1- MBV_{ideal} for all earth mortar plasters formulations with different corrections and compared with the value of $MBV_{practical}$

	F0		F3		F5	
	β correction	ISO correction	β correction	ISO correction	β correction	ISO correction
MBV_{ideal} (g/(m².%RH))	1.37	1.17	1.29	1.08	0.78	0.70
$MBV_{practical}$ (g/(m².%RH))	1.34		1.31		0.98	
Relative difference (%)	2.28	-12.52	-1.16	-17.38	-19.92	-28.77
β vs ISO correction (%)	14.47		16.41		11.05	

6.1.2. Results on hemp concrete

In the Figure 6.6, Figure 6.7 and Figure 6.8 were the results of moisture buffering test obtained for the three kind of hemp concrete under analysis, NL, PF70 and Calco, respectively. In these figures are presented the values obtained during three stabilized cycles, at 23°C for different thicknesses (5, 10 and 15cm). The results at 40°C are presented in Appendix E.2. In the Figure 6.6 is possible to see a slightly difference between NL with 15cm and the two other thickness. However, the maximum difference, happens in the last cycle between 15cm and 10cm (8%, approximately). The results of moisture buffering test obtained for PF70 are presented in the Figure 6.7. Taking into account the values of moisture uptake, for each thickness, the maximum difference occurs in the last cycle and it was 13%, approximately, between 5cm and 15cm.

The results between thicknesses obtained for NL and PF70 at superior temperature (Appendix E.2) presents higher differences. However, this difference can be explained with the short time used for the equilibration at this temperature compared with the lower one, as it is further explained in the Chapter 7.2.

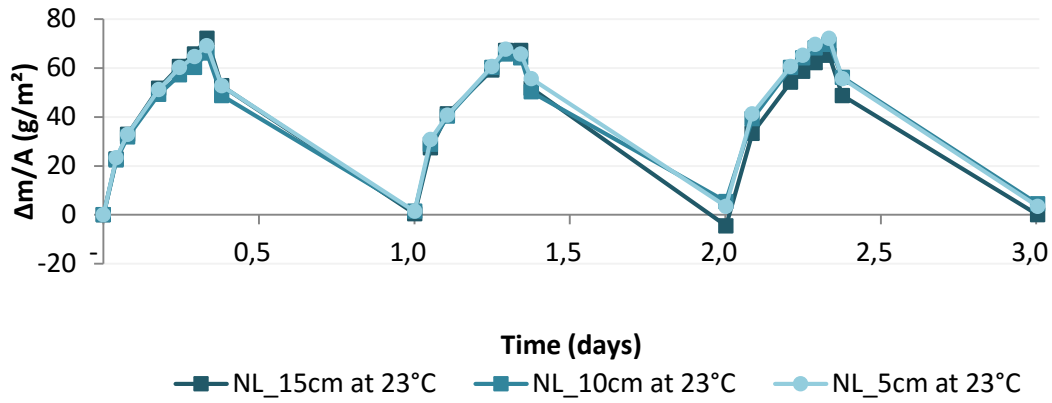


Figure 6.6- Moisture buffering test for NL with 5, 10 and 15cm at 23°C

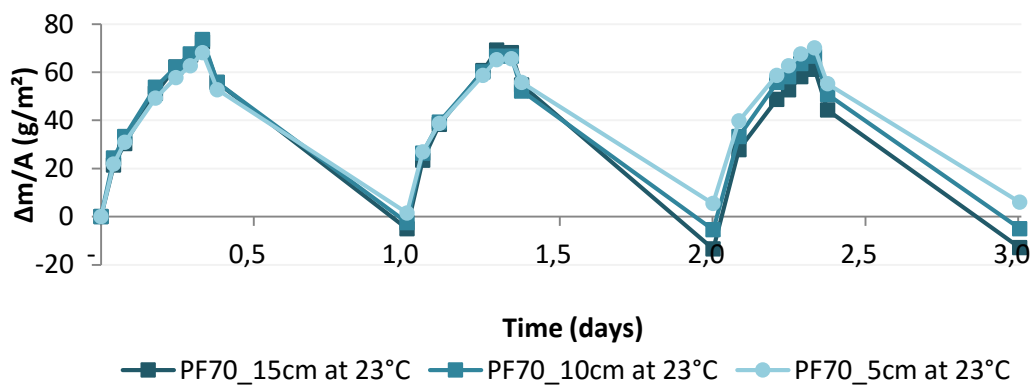


Figure 6.7- Moisture buffering test for PF70 with 5, 10 and 15cm at 23°C

In the literature, taking into account the test at 23°C, the obtained results are: about 2.15g/(m²%RH) (Collet & Pretot 2012) and about 1.46g/(m²%RH) (Mazhoud et al. 2015) with ratio hemp/binder equal 0.5 and 0.15, respectively. Since the ratio hemp/binder is equal to 0.42 and 0.33 for NL and PF70 formulations, respectively. These results may suggest that higher hemp content would lead to a higher MBV_{practical}. However, more tests are necessary to conclude on this correlation.

All samples of Calco present different behaviour in the moisture buffering test. It is possible to see (Figure 6.8) different values of moisture uptake and release between each thickness. For this formulation when the sample of 15cm were exposed at 23°C the values of moisture uptake were between 118.9g/m² and 146.2g/m². A similar tendency is observed for the other two thicknesses. The results obtained, at the same temperature, vary between 85.1g/m² to 100.0g/m² and from 79.0g/m² to 87.0g/m² for 10cm and 5cm, respectively. From these results it can be concluded that Calco had a higher difference between each thickness at 23°C, as well when the procedure was done at 40°C (Table 6.2).

It notices that the results of MBV obtained for Calco were different between each thickness under the same temperature and all samples of this formulation had superior values compared with the two other formulations. The thickness that had higher MBV was the highest, values were decreasing with the reduction of thickness. As shown in Table 6.2, the standard deviations of the MBV for Calco were superior for 40°C

than at 23°C, in the majority of cases. This table does a summary of all values of MBV obtained for all formulations of hemp concrete for each thickness and it can be seen that NL and PF70 did not present any impact of the thickness.

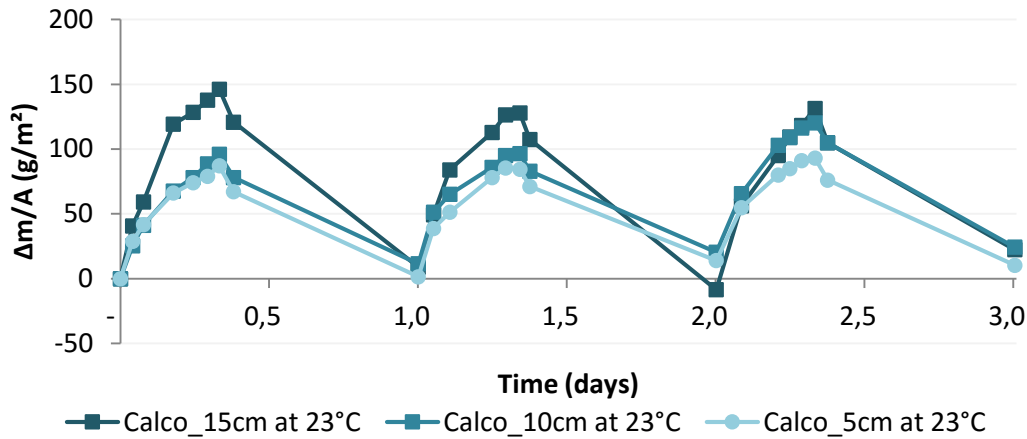


Figure 6.8- Moisture buffering test for Calco with 5, 10 and 15cm at several temperatures

Table 6.2- MBV for hemp concrete at 40°C and 23°C with different thicknesses

Samples	Thickness	MBV_40°C (g/(m²%RH))		MBV_23°C (g/(m²%RH))	
		Average	Stand. Dev.	Average	Stand. Dev.
Calco	15	6.08	0.31	3.21	0.34
	10	4.59	0.33	2.23	0.18
	5	3.73	0.71	1.98	0.09
NL	15	2.59	0.07	1.65	0.07
	10	2.52	0.03	1.53	0.04
	5	2.69	0.04	1.60	0.07
PF70	15	2.91	0.18	1.75	0.02
	10	2.80	0.05	1.71	0.05
	5	2.68	0.02	1.56	0.05

The MBV_{ideal} was determined using the results of permeability with corrections as explained previously for earth mortar plasters (Table 6.3). The presented values of $MBV_{practical}$ are an average between the results of several thicknesses. Calco had difference between each thickness, but this average number is just used as a reference. The obtained MBV_{ideal} was superior compared with the $MBV_{practical}$, in the majority of cases it was more than two times higher. Comparing the values obtained for both corrections, the difference was higher for Calco.

Nonetheless, the MBV_{ideal} is an approximated value and it depends on the obtained values of moisture capacity and water vapour permeability of each formulation. In addition, it can have a source of error associated with the background tests, as well modelling problems associated to this material.

Table 6.3- MBV_{ideal} for all hemp concrete formulations with different corrections and compared with the value of $MBV_{practical}$

	Calco		NL		PF70	
	β correction	ISO correction	β correction	ISO correction	β correction	ISO correction
MBV_{ideal} (g/(m ² .%RH))	4.88	3.97	3.41	2.92	3.04	2.66
$MBV_{practical}$ (g/(m ² .%RH))	2.53		1.59		1.66	
Relative difference (%)	92.82	32.13	113.73	82.87	83.19	60.83
β vs ISO correction (%)	18.74		12.21		14.44	

6.2. On penetration depth practical and theoretical

The penetration depth is the thickness needed to benefit from moisture buffer effect of uncoated hemp concrete and earth mortar plasters. During this chapter will be described practical and analytical ways to obtain an approximation of penetration depth.

An original procedure was developed to understand the moisture penetration depth during a moisture buffering test. Hygrometers were placed at different depths in order to understand the real penetration depth in the samples of hemp concrete. For this procedure, the specimens of hemp concrete with 15cm of thickness, described in the previous chapter, was used (Calco, PF70 and NL with 15cm).

The preparation of the cover with aluminium tape was the same as described in the Chapter 4.3. In these samples along the side was made three holes at different depths: 2, 4 and 8cm. These holes were done misaligned, see Figure 6.9. In each hole has been placed a Rotronic HC2-C04 (hygrometer/temperature sensor), insulated with aluminium tape, connected to the Rotronic HygroLog HL-NT. After preparation of the specimens they were placed in the climatic chamber and exposed to the same boundary conditions than what were described for the moisture buffering test (cycles of 33%RH and 75%RH during 16h and 8h, respectively, and test procedure at 23°C and 40°C).

After the experimental procedure it is possible to draw graphs with the variation of RH recorded by the sensors, placed at different depths, during the time. When it is visible variation of RH during the time, in the exposed samples at daily cycles, this depth is called active. Thus the definition of this active depth remains quite subjective. To objectivise it, the same criteria as the one used to estimate the theoretic penetration depth is considered. In other word, a depth is active if its variation of RH remains lower than 1% of the RH variation in the chamber (called the “ $d_{p,1\%}$ definition” in the following) or if it remains lower than $1/e \approx 37\%$ of the RH variation in the chamber (called the “ $d_{1/e}$ definition” in the following). The penetration depth is thus the higher depth that remains active.



Figure 6.9- Prepared sample of NL in the climatic chamber

The results obtained on each sensor (2, 4 and 8cm of depth) for a measurement during 24h for all hemp concrete formulations are presented in Figure 6.10, Figure 6.11 and Figure 6.12. The boundaries which correspond to the “ $d_{1\%}$ definition” and “ $d_{1/e}$ definition” are respectively represented by the dotted black and grey lines in these figures. At first, it can be see that the use of the “ $d_{p,1\%}$ definition” leads to a penetration depth higher than 8cm whatever the formulation. This definition seems thus to be too drastic, and the “ $d_{1/e}$ definition” is used in the following. In Figure 6.10, the formulation NL on the sensor at 4cm of depth seems to have low activity, in other words, the penetration depth within the material was between 2cm and 4cm. However, for the same material when the temperature increases (Figure F.1 in Appendix F) these measurement lead to a penetration depth slightly higher than 4cm. The tendency previously described for NL at 40°C was the same for PF70 for both temperatures (Figure 6.11 and Figure F.2 in Appendix F).

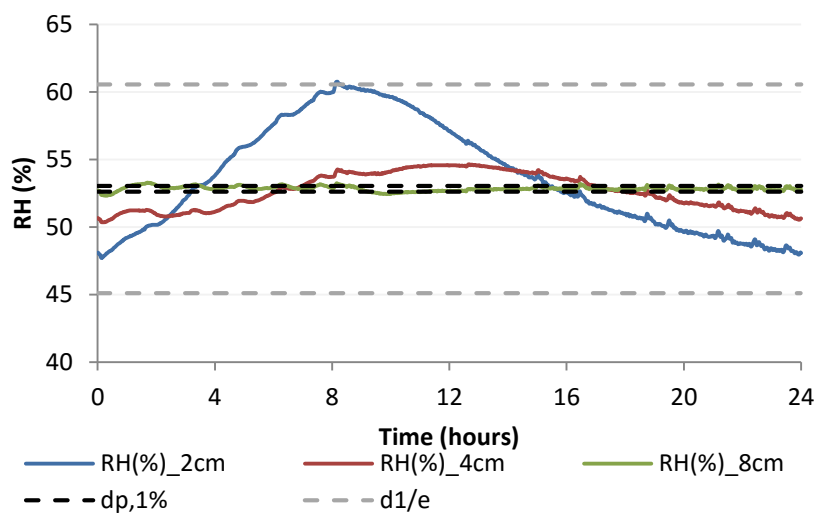


Figure 6.10- Real penetration depth for NL at 23°C

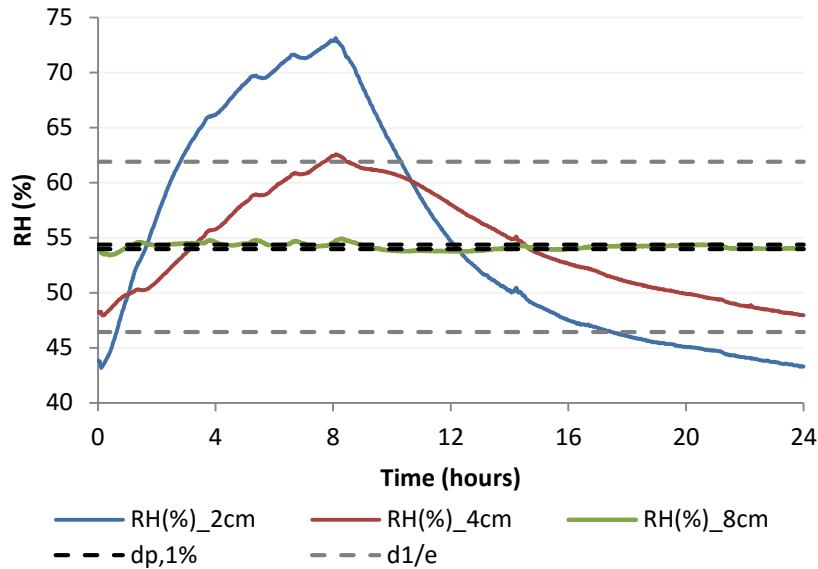


Figure 6.11- Real penetration depth for PF70 at 23°C

For Calco the behaviour was completely different compared with NL and PF70. At 23°C (Figure 6.12) the penetration depth was between 4cm and 8cm, because at this depth the sensor exhibits a slight variation of RH at 8cm. At 40°C (Figure F.3 in Appendix F), this material showed variation of its activity at all depths, this means that the penetration depth was greater than 8cm. This behaviour may be explained by the presence of two vertical holes that bore the whole thickness of the sample. These were caused by a test previously carried out. These holes are of small dimension and they were filled with hemp shives in order to avoid any impact on the thermal conductivity. These holes could be responsible of a greater penetration depth which therefore may also significantly modify the moisture buffering capacity.

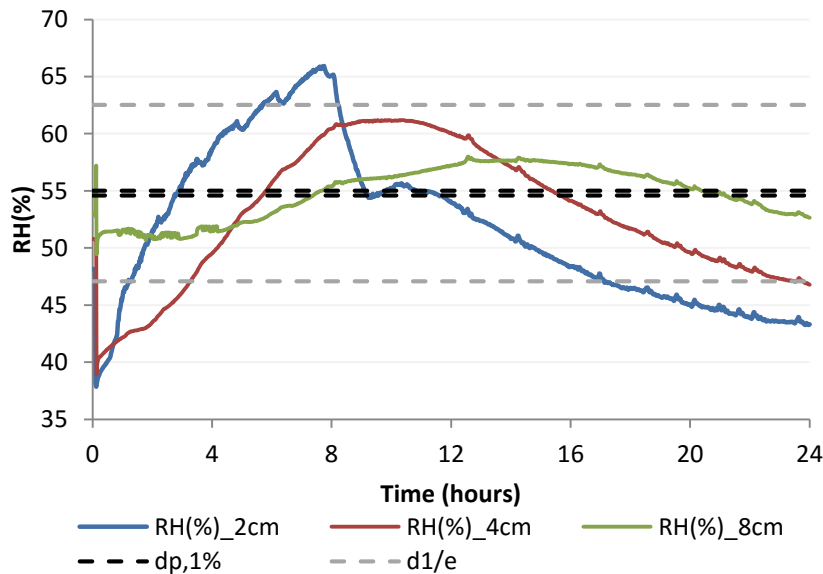


Figure 6.12- Real penetration depth for Calco at 23°C

These experimental observations are then compared to the theoretical estimation of the penetration depth, using the two expressions, called $d_{p,1\%}$ and $d_{1/e}$ which are reported in the Chapter 3 of this dissertation.

For the calculated penetration depth eqs. 28 and 29 were used with different values obtained for the water vapour permeability (with and without correction) and the average moisture capacity results from the sorption isotherms. The calculated results of penetrations depth of hemp concrete with three approximations of water vapour permeability are in Table 6.4. None of the calculation approaches were coherent with the practical values obtained through the sensors in the test. Table 6.5 shows the calculated results of penetrations depth of hemp concrete with three approximations of water vapour permeability, but using the moisture capacity given by the desorption curve. Even using this quite low value for the moisture storage capacity (which can be considered as a lower bound for this kind of material) the calculated penetration depth remains fairly lower than the practical one.

Actually, the theoretical penetration depth is estimated assuming a sinusoidal variation of the RH at the surface of the sample, which is clearly not the case in this test which follows the Nordtest's conditions. However, if this difference may partially be responsible of the differences between the calculated and the measured values, it cannot explain such a difference. Then, another explanation can come from the assumptions made to estimate this theoretical penetration depth (no liquid water migration, no hysteresis in the sorption-desorption curve, equilibrium between vapour and liquid water, etc...) which may not be valid for hemp concretes. However, additional studies are necessary in order to conclude on that point.

Table 6.4- Penetration depth for hemp concrete using the different approximation of water vapour permeability with the average moisture capacity

	Original		ISO correction		β correction	
	$d_{1/e}$ (mm)	$d_{p,1\%}$ (mm)	$d_{1/e}$ (mm)	$d_{p,1\%}$ (mm)	$d_{1/e}$ (mm)	$d_{p,1\%}$ (mm)
PF70	6.7	30.7	6.9	31.8	7.8	36.2
NL	6.1	28.2	6.4	29.3	7.4	34.2
Calco	5.8	26.6	6.1	27.9	7.4	34.3

Table 6.5- Penetration depth for hemp concrete using the different approximation of water vapour permeability with the moisture capacity in desorption

	Original		ISO correction		β correction	
	$d_{1/e}$ (mm)	$d_{p,1\%}$ (mm)	$d_{1/e}$ (mm)	$d_{p,1\%}$ (mm)	$d_{1/e}$ (mm)	$d_{p,1\%}$ (mm)
PF70	9.1	42.1	9.5	43.6	10.8	49.6
NL	9.0	41.6	9.4	43.3	11.0	50.6
Calco	10.4	47.8	10.9	50.2	13.4	61.8

According to Collet & Pretot (2012) the approximation of penetration depth of hemp concrete was 5.8cm using $d_{p,1\%}$ but its samples had more quantity of fibbers compared to the studded formulations.

In order to check the consistency of the experimental results obtained on hemp concrete an additional test is performed. It consists on measuring the water adsorption within samples of 5cm and 10cm

thick, when they are submitted to 75%RH at 40°C during 8 days (Figure 6.13). Although the penetration depth was slightly higher at this temperature, as observed in the Figure F.1 to Figure F.3 (in Appendix F), it is possible to observe that the ratio $\frac{\Delta m_{10}-\Delta m_5}{\Delta m_5}$ is very low for the formulations NL and PF70 on the first two tested days, while it is higher than 10% after only 3 hours for the Calco. In other words, the penetration depth of this RH increase remains lower than 5cm until two days for PF70 and NL and is higher than 5cm after 3hours for the Calco. Since the Nordtest impose an increase of humidity during only 8 hours, this results is consistent with the practical values of penetration depth measured in this study (higher than 5cm for Calco and between 2cm and 4cm for both NL and PF70). The results for Calco was expected, because the penetration depth according to the practical test was more than 8cm at 40°C (8cm, approximately, at 23°C). Thus, the thicker samples have more water vapour adsorption.

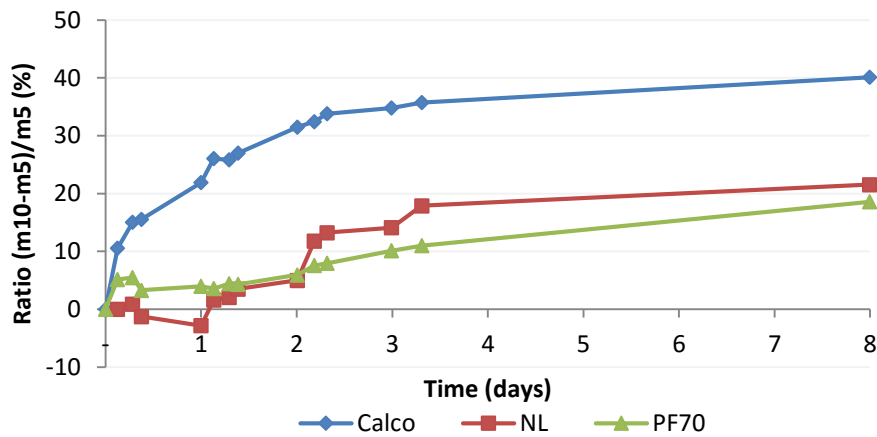


Figure 6.13- Hemp concrete adsorption for long time at 40°C and 75%RH

The penetration depth is a parameter linked to the moisture diffusivity, which in turn depends on the water vapour permeability, dry density, moisture capacity and saturation vapour pressure (constant for the same temperature). However, as expected, all formulations of hemp concrete had higher penetration depth than earth mortar plasters.

As such for the studied earth mortar plasters (except F5) samples with at least 1cm were sufficient in order to have a representative result. For F5 the minimum thickness is 2cm, while the samples of 1cm are not representative of the results. Concerning hemp concrete, the minimum recommended thickness is 5cm for PF70 and NL, but for Calco, it is not possible to have a conclusion because the tested samples lead to inconsistent results and therefore it would be necessary to make further tests using this formulation.

Table 6.6 gives the theoretical penetration depth obtained for the earth plasters formulations. Comparing the calculations using three kind of the approximation of water vapour permeability the difference was low, but between the two different ways to make the calculation ($d_{p,1\%}$ and $d_{1/e}$) this difference was high. When these results are compared to the $MBV_{practical}$ at different thicknesses, only $d_{1/e}$ has obtained

coherent values. Indeed, the $d_{p,1\%}$ values are higher than 2cm which should thus lead to significant difference in $MBV_{\text{practical}}$ results between the sample of 1cm, 2cm and 4cm thick, which is not the case.

The difference of mass uptake (and release) that has been observed for F5 can be explained with a difference of penetration depth relatively to the calculated value; only the calculated value is an approximation. Moreover, if the penetration depth is higher than 1cm within the sample the moisture uptake (and release) will be lower in a sample with 1cm of thickness.

The practical procedure to measure penetration depth was not considered appropriate to apply, since the maximum thickness of these samples were 4cm and to make the holes the samples could break.

Table 6.6- Penetration depth for earth mortar plasters using the different approximation of water vapour permeability

	Original		ISO correction		β correction	
	$d_{1/e}$ (mm)	$d_{p,1\%}$ (mm)	$d_{1/e}$ (mm)	$d_{p,1\%}$ (mm)	$d_{1/e}$ (mm)	$d_{p,1\%}$ (mm)
F0	6.8	31.4	7.1	32.8	8.3	38.4
F3	8.2	37.6	8.6	39.5	10.3	47.3
F5	8.9	40.9	9.2	42.4	10.3	47.7

Although the theoretical calculation presented similar results of penetration depth for hemp concrete and earth plasters, this fact is not in concordance with the practical values. Indeed, while $d_{1/e}$ values seem quite consistent with experimental observation for earth plasters, it is not the case for hemp concretes.

7. Influence of temperature on hygroscopic capacity: Results and Analysis

In this chapter, the tests were performed in order to observe the influence of temperature (23°C and 40°C) in hemp concrete materials. The higher temperature was chosen because of two main reasons: a practical one – the climatic chamber stabilisation was better at a higher temperature and 40°C is one of the highest temperatures that can be achieved easily on external building elements.

7.1. On sorption isotherms

In this chapter are presented the sorption curves for both temperatures up to 85% of RH. As previously explained in the Chapter 5.2, the masses of the samples in 97%RH at 23°C were not stabilized.

In Figure 7.1, Figure 7.2 and Figure 7.3 are presented the sorption isotherms at 23°C and 40°C for Calco, PF70 and NL, respectively. These results present the same tendency, revealing an EMC for the three formulations of hemp concrete that increase with the RH. However, the EMC decreases when the temperature increase. For Calco when the RH increases from 23%RH to 85%RH at 23°C the moisture uptake is 13.6% while at 40°C this difference of moisture content is 6.9%. The results obtained for NL was similar to the values obtained for Calco. The variation between 23%RH and 85%RH promotes a difference of 13.0% and 6.7% on the EMC at 23°C and 40°C, respectively. The same variation of RH for PF70 leads to a difference of 8.7% and 4.8% at 23°C and 40°C, these values are lower than the values obtained for the other formulations in each temperature.

For 40°C the adsorption process has taken less time compared with the lower temperature. At this temperature, the EMC for all RH levels lower or equal to 85% takes approximately 25days to be reached. The equilibrium for 97%, probably takes more time, but it was not possible to verify this fact as the climatic chamber (Froilabo), where this test was done, had a technical problem. This technical problem leads to the inability to make the desorption curve at 40°C.

In Appendix C.1 and C.3 are presented all results related with the sorption isotherms for the hemp concrete formulations at 23°C and 40°C, respectively (in red the samples not considered in the calculation).

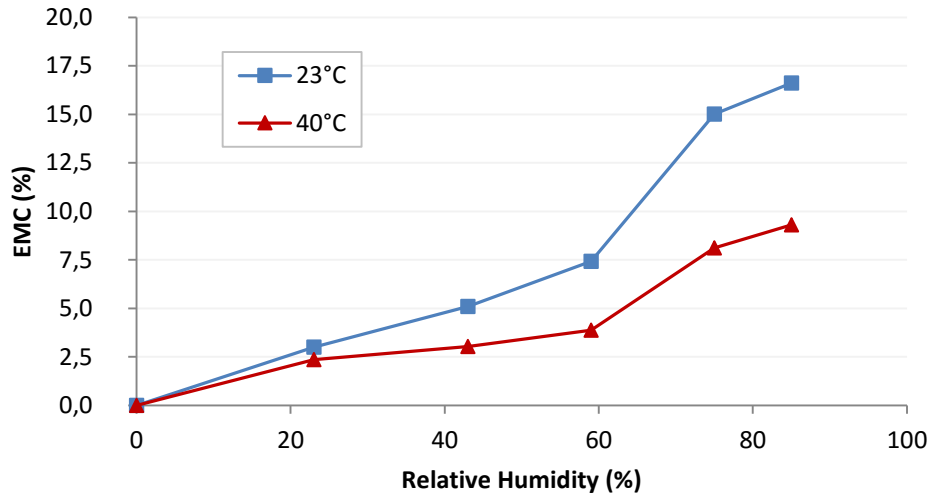


Figure 7.1- Temperature influence in the sorption curve of Calco

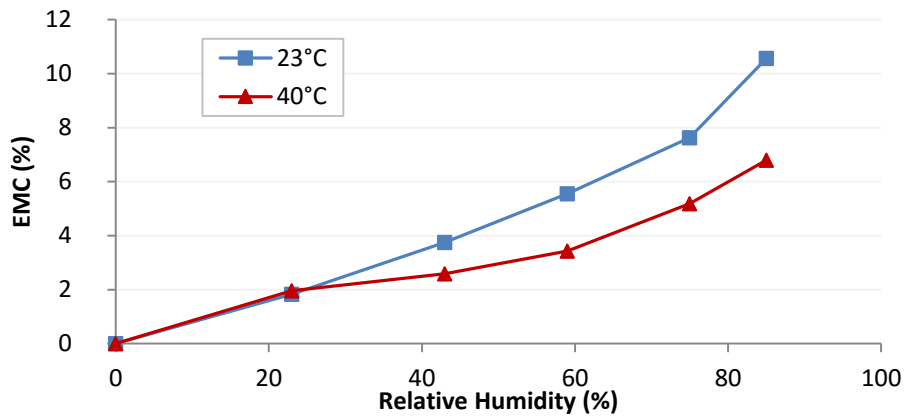


Figure 7.2- Temperature influence in the sorption curve of PF70

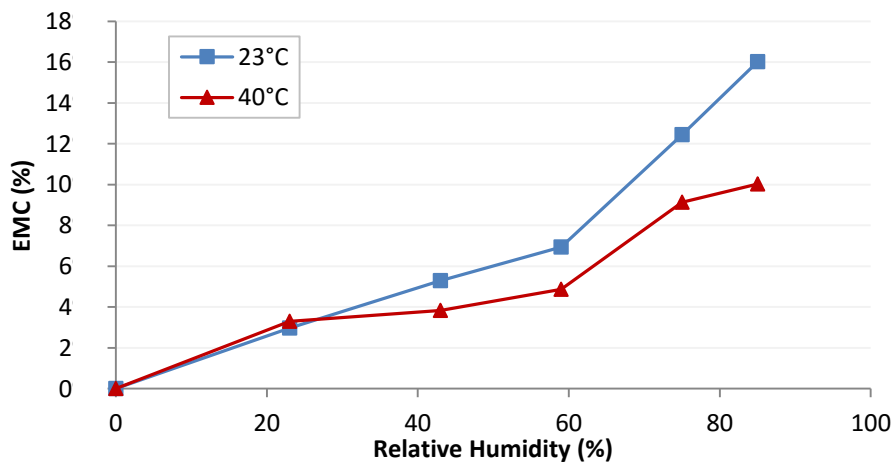


Figure 7.3- Temperature influence in the sorption curve of NL

At that stage, it is possible to question why the EMC decreases with the temperature, and generally, why the equilibrium RH is a function of moisture content and temperature: $\varphi = \varphi(u, T)$. For this, a first attempt of explanation can be furnished from the use of the Kelvin's Law (eq.10) and Jurin's Law (eq. 7). The starting point of this explanation is to assume that a direct relation exist between the radius of the liquid water – air interface (r_p in eq (7), denoted $r(u)$ in the following paragraph) and the water content. This relation is different for each tested material, but it is assumed to be intrinsic. In other words, it only depends of the material properties (porous network geometry, surface charge of the pore walls etc...) but is independent of the temperature. Under this assumption, and considering that the surface tension (γ) is dependent on the temperature, the wetting angle of the pore surface (θ) equal zero, the use of Kelvin's and Jurin's Law leads to (eq.37):

$$\frac{2\gamma(T)}{r(u)} = -\frac{\rho_w RT}{M_w} \ln(\varphi(u, T)) \quad (37)$$

As the $r(u)$ is independent of the temperature, the previous equation can be written as eq.38:

$$r(u) = -\frac{2\gamma(T_0)M_w}{RT_0\rho_w \ln(\varphi(u, T_0))} = -\frac{2\gamma(T_1)M_w}{RT_1\rho_w \ln(\varphi(u, T_1))} \quad (38)$$

where T_0 is a reference temperature, φ_0 the RH corresponding to the water content u at the temperature T_0 , while T_1 and $\varphi(u, T_1)$ are on other set of temperature and RH for which the water content is equal to u . Then, if $T_0=296.15\text{K}$ and $T_1 = 313.15\text{K}$, the relation (38) can be used in order to build the sorption curve at 40°C from the sorption curve at 23°C (eq.39):

$$\varphi(u, T_1) = \varphi(u, T_0) \frac{T_0\gamma(T_1)}{T_1\gamma(T_0)} \quad (39)$$

with $\gamma(T_0)=0.0715\text{N/m}$ and $\gamma(T_1)=0.0696\text{ N/m}$.

The comparison of results obtained for this theoretical model and the practical values for Calco, PF70 and NL are presented in Figure 7.4, Figure 7.5 and Figure 7.6, respectively. It was possible to see in all formulations that the simulated values at 40°C was inferior compared with practical values of 23°C but the difference remains slight. In contrast to the practical moisture content at the same temperature, that presents a high difference as previously referred. Therefore, this option does not explain such important decrease.

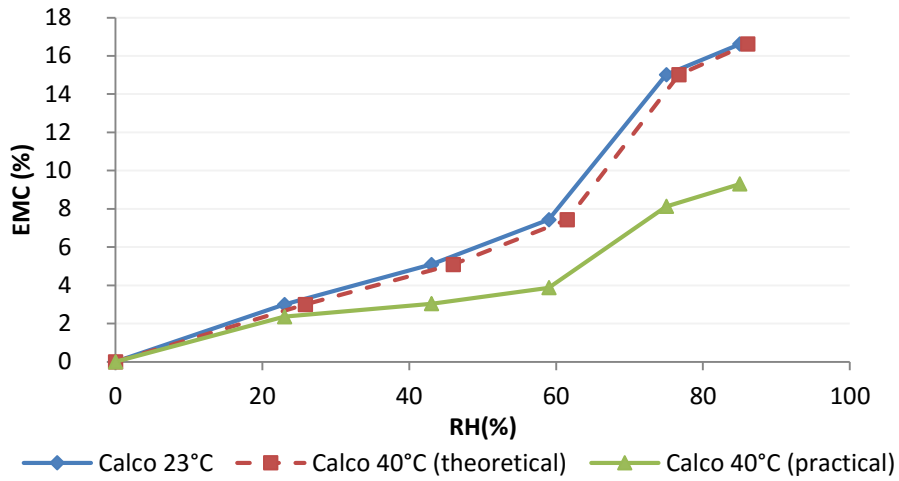


Figure 7.4- Practical and theoretical sorption isotherms for Calco

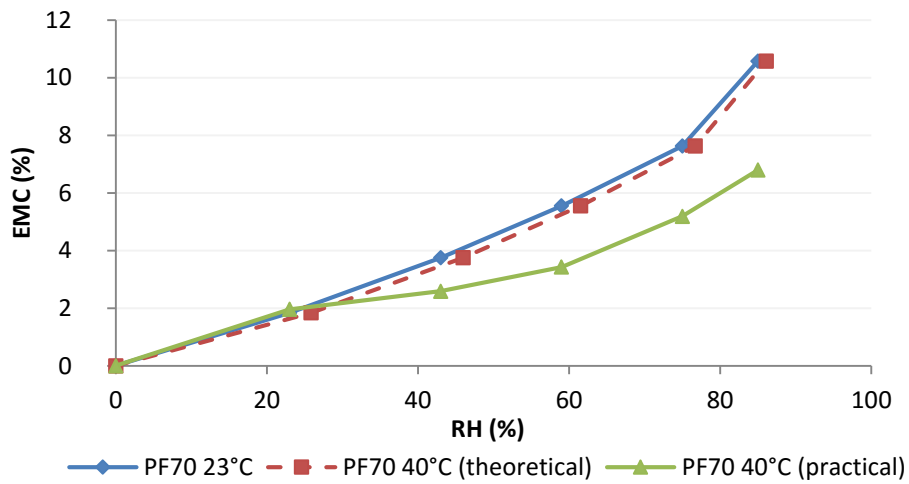


Figure 7.5- Practical and theoretical sorption isotherms for PF70

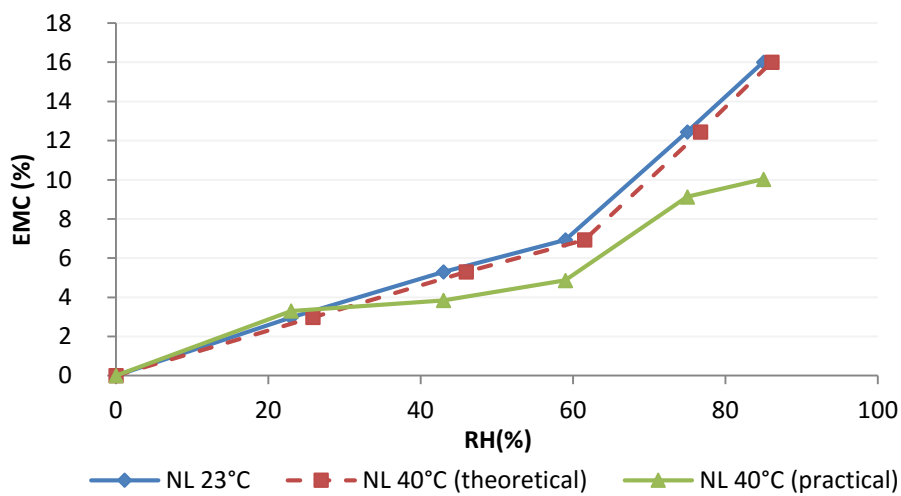


Figure 7.6- Practical and theoretical sorption isotherms for NL

Esteban et al. (2015) did the practical test of sorption (and desorption) at 15°C and 35°C using juvenile wood (between 10 and 20 years old) that is considered by the author as a "hygroscopic natural" material. Thus, it was decided to apply the theoretical model presented in eq. 39 was used in the juvenile wood in order to see if the model is coherent in this type of material (Figure 7.7). It was used $T_0 = 288.15K$ as the reference temperature, $\varphi(u, T_0)$ the practical RH used at T_0 and $T_1 = 308.15K$. Therefore, the surface tensions were $\gamma(T_0)=0.0735N/m$ and $\gamma(T_1)=0.07041 N/m$. In that case, the theoretical calculation appears to be quite consistent with the measured one. Indeed, the EMC is lower at higher temperature, but the difference remains quite small as predicted by the eq. (39). The bigger difference occurs between 15°C and 35°C for 71.5% RH level and is equal to 1.34%. This result tends to prove that the temperature dependence of the sorption curve of hemp concrete is quite unusual.

A possible explanation for the higher difference of the theoretical and practical values of the sorption isotherms, that can be seen in hemp concrete, can be related to the fact that the Kelvin's law considers free water and in the used range of RH only has adsorbed water. Therefore, it is supposed to consider the energy of adsorbed water instead of the free water. Let us note that this tendency (strong variations of sorption curves with temperature) was already observed in other construction materials like concrete (Poyet & Charles 2009).

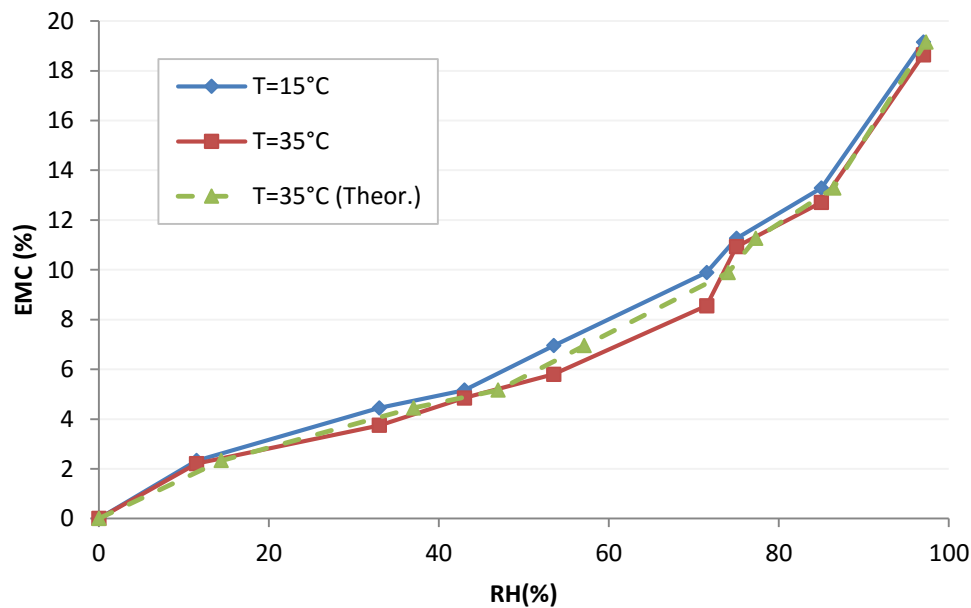


Figure 7.7- Results of sorption curves for juvenile wood at 15°C and 35°C by Esteban et al. (2015) and implementation of the theoretical model at 35°C

7.2. On moisture buffering values

The samples of hemp concrete were made in formworks so that the exposed surface remains the same in all cases. This exposed surface is equal to 0.02m², while the thickness changes slightly as it can be seen in Table 7.1.

The moisture buffering test described in Chapter 4.3 at 23°C and 40°C was used for all samples of hemp concrete. The procedure was first started with the lowest temperature, the samples were placed in the climate chamber undergoing successive cycles on the 10th of April 2015 in order to reach equilibrium. The recording of the variation of mass presented in the results was started on the 8th of June. While at 40°C the recording was started on the 15th of June. The samples took a long time to stabilize in the cycles at 23°C (less than 5% of difference between each cycle), at 40°C as they were already stabilised at 23°C the process was much faster.

Table 7.1- Thicknesses of the Hemp concrete samples used on MBV test

Samples	Thickness (cm)
Calco_15	15,0
Calco_10	10,0
Calco_5	6,2
NL_15	15,0
NL_10	10,0
NL_5	5,9
PF70_15	15,0
PF70_10	10,0
PF70_5	6,2

As explained in Chapter 6.2, the samples of Calco used for moisture buffering test (and water vapour permeability test) had a physical problem (with two vertical holes) that changes the results. Results for this formulation are not presented in this chapter, because of the random variation of these results they had to be excluded. However, these samples presented interesting results and the oversize results obtained would need to be investigated.

In the Figure 7.8 and Figure 7.9 are presented the average values of moisture uptake (and release) during the three last complete cycles of moisture buffering test for NL and PF70, respectively, as well as the changes of RH during the cycles. The average values are calculated between the values obtained in this test for the three different samples thicknesses (5, 10 and 15cm). Since the presented values are averages, the results include an error bar. This error bar represents the extreme values (minimum and maximum) obtained for each formulation. In the results of PF70 at 40°C (Figure 7.9) these error bars were considerably higher.

In the figure below, the NL at 40°C achieved higher moisture adsorption compared with the lower temperature (23°C): the mass uptake is in a range of 107.4 to 111.1g/m² at 40°C while it is in a range of 64.5 to 69.1g/m² at 23°C. The same tendency is seen for PF70 (Figure 7.9) where the range of moisture adsorbed is from 113.7 to 119.5g/m² for the procedure at 40°C while for 23°C it ranges from 68.8 to 71.5g/m².

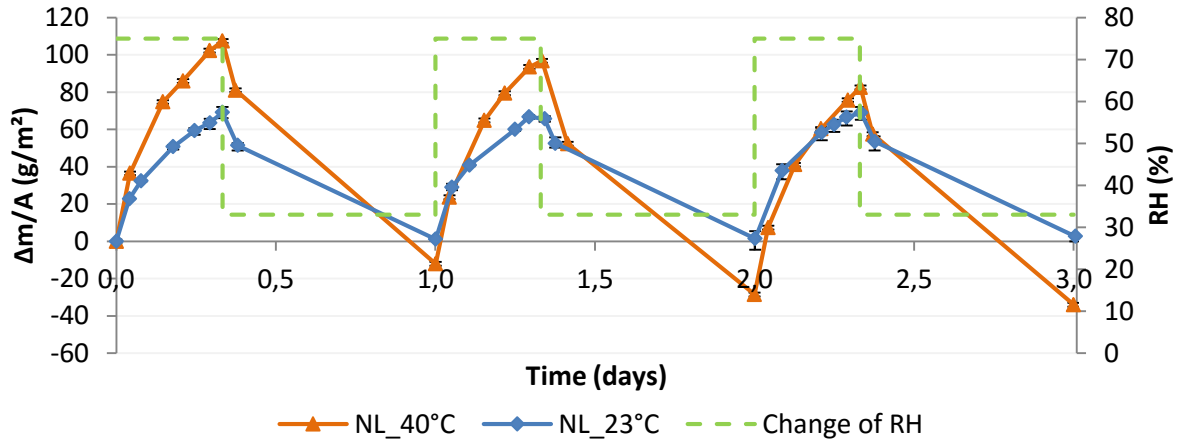


Figure 7.8- Average value from the moisture buffering test for NL at 40°C and 23°C

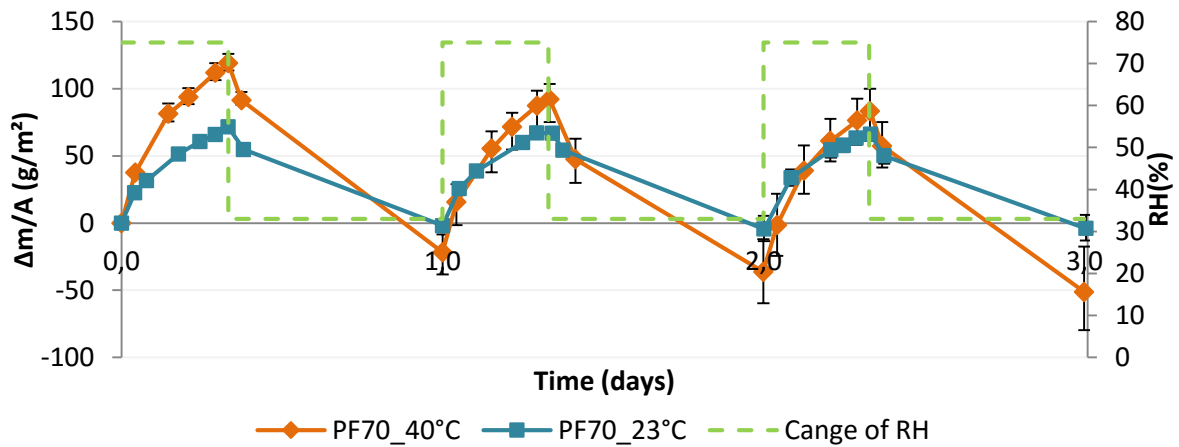


Figure 7.9- Average value from the moisture buffering test for PF70 at 40°C and 23°C

The values of $MBV_{practical}$ for hemp concrete was calculated as explained in the Chapter 6.1.1 using the average values obtained for three stabilized cycles.

It is possible to see in the Figure 7.10 that the MBV obtained for NL for all thicknesses is within the range from 2.52g/(m².%RH) to 2.69g/(m².%RH) at 40°C and from 1.53g/(m².%RH) to 1.65g/(m².%RH) at 23°C. The obtained values for PF70 were similar to the values of NL. For PF70 the moisture buffering values were between 1.56g/(m².%RH) to 1.75g/(m².%RH) and 2.68g/(m².%RH) to 2.91g/(m².%RH) for 23°C and 40°C, respectively. Both formulations presented a little standard deviation for the calculated MBV of the three considered cycles for each thickness (Table 6.2), except PF70 with 15cm at 40°C (standard

deviation of $0.18\text{g}/\text{m}^2\%RH$). This sample is the one that shows the largest error bars as presented previously (Figure 7.9).

Using the classification of moisture buffer ability published by Nordtest Project (Rode et al. 2005) both materials have different classification depending on the temperature. At 23°C these materials had "Good" performance, while for the same procedure at 40°C had "Excellent" moisture buffering ability. However, the reference temperature suggested on the Nordtest Project is 23°C , and the referred ranking is only valid for this temperature.

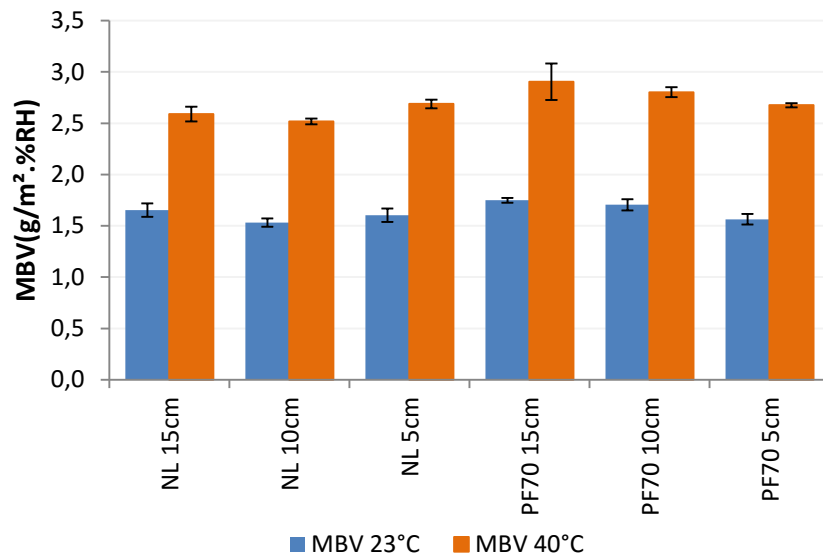


Figure 7.10- Comparison between moisture buffering value of NL and PF70 at 23 and 40°C

7.3.Discussion

This chapter will look into the results described in Chapter 5 and 7 relating them in order to characterise the hygrothermal behaviour considering temperature changes. The results obtained in the experimental procedure of moisture buffering test will be compared to the theoretical results using the steady-state hygrothermal properties (sorption isotherms and water vapour permeability) of the studied materials.

As expected, the sorption isotherms have a "S" shape, as explained in the Chapter 3.2.2 and can be classified with the type IIb according to Rouquerol et al. (1999). At given temperature, when occurs a rise of RH on the environment the EMC increases. This phenomenon was explained in Chapter 3.2.3, linked to the wetting characteristics that occur in the porous medium. According to Ashour et al. (2011), the increase in moisture content when rises the RH is due to the vapour pressure deficit (VPD), the difference between the moisture in the air and how much moisture the air can hold when it is saturated. For a given temperature with the rise of RH the VPD decreases and becomes close to the saturation state and increases the ability of the material to absorb more moisture from the environment. Nevertheless with the rise of temperature the

EMC decreases in all RH levels since the VPD increases promoting the moisture movements from or to the fibres (Ashour et al. 2011).

The calculation of the moisture capacity of the studied materials comes from the eq. 12. It is obtained from the sorption isotherms previously presented in Figure 7.1 to Figure 7.3, it is calculated with the slope of the sorption curves between 23% and 75%, and the dry density. Since the aim is to do a comparison between the steady-state and the dynamic properties, the range of RH defined for this calculation is comparable to the RH levels used in the moisture buffering test. The results of moisture capacity obtained for hemp concrete for two distinct temperatures are presented in Table 7.2. Since at 23°C was also done the desorption curve and as this one presents higher differences compared to the sorption curve, the values presented below for this temperature are the average of both moisture capacities. The majority of calculated slopes from the sorption isotherms do not present a large difference. However, Calco presents a higher moisture capacity, mainly at 23°C, compared with the other formulations, while PF70 has the lowest value with about 10kg/m³ of difference compared to NL. The values obtained when the procedure was carried out at 23°C were higher than at superior temperature.

Table 7.2- Moisture capacity using only sorption curves for hemp concrete at 23°C and 40°C

	ξ (kg/m ³)	
	T=23°C	T=40°C
Calco	65.1	51.7
PF70	38.4	30.7
NL	45.6	42.8

At higher temperature, the sorption isotherms decrease, as explained previously. However, the results of moisture buffering show a different tendency, when the temperature increases the MBV increases too.

In order to validate the experimental setup used in the moisture buffering test, the Figure 7.11 and Figure 7.12 show the monitored RH and temperature recorded by the climatic chamber, for the last three cycles of moisture buffering test at 23°C and 40°C, respectively. Nordtest project (Rode et al. 2005) refer that the step changes of RH should be realized up to 30minutes with $\pm 3\%$ RH and the temperature shall be maintained within $\pm 0.5^\circ\text{C}$.

At 23°C the climatic chamber had higher changes of RH and takes 40minutes, approximately, in order to reach the equilibrium at higher RH in the chamber environment and about 1h and 10min from high to low RH. The mean value of RH is slightly lower than $75\pm 3\%$ during adsorption (about 71.1%RH), during desorption the average value was in the range $33\pm 3\%$ (about 33.5%RH) and the temperature during all cycles was 22.9°C, approximately. At 40°C (Figure 7.12), the climatic chamber presents lower differences compared with the low temperature, the average RH during adsorption was about 73.7%RH, while during the desorption the average was 33.2%RH and the temperature was exactly 40°C. From low to higher RH the

equilibration was achieved within about 30min and within 40min from higher to low RH. At higher temperature, the climate chamber takes less time to equilibrate, yet the equilibration from higher to low RH was out of the range foreboded in the Nordtes project. Variation occurs when the chamber was open to weigh the samples but the stabilization was fast. This variation can be caused due to the temperature in the laboratory which was superior to the low testing temperature and closer to 40°C, since the RH stabilize within the chamber only after a stable temperature being reached. As for the time the climatic chamber takes to achieve equilibrated RH levels, Collet & Pretot (2012) citing the study carried out by Roels & Janssen (2005) that refers "that the time need to achieve the step in RH has a limited influence on the MBV (less than 5%) even if it takes 1h and a half to achieve the required RH".

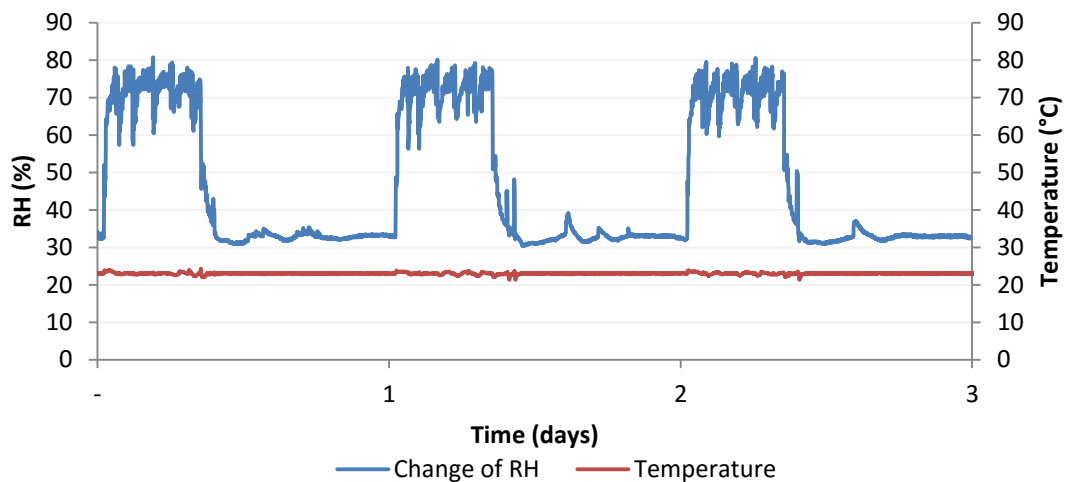


Figure 7.11-Monitored RH and temperature at 23°C

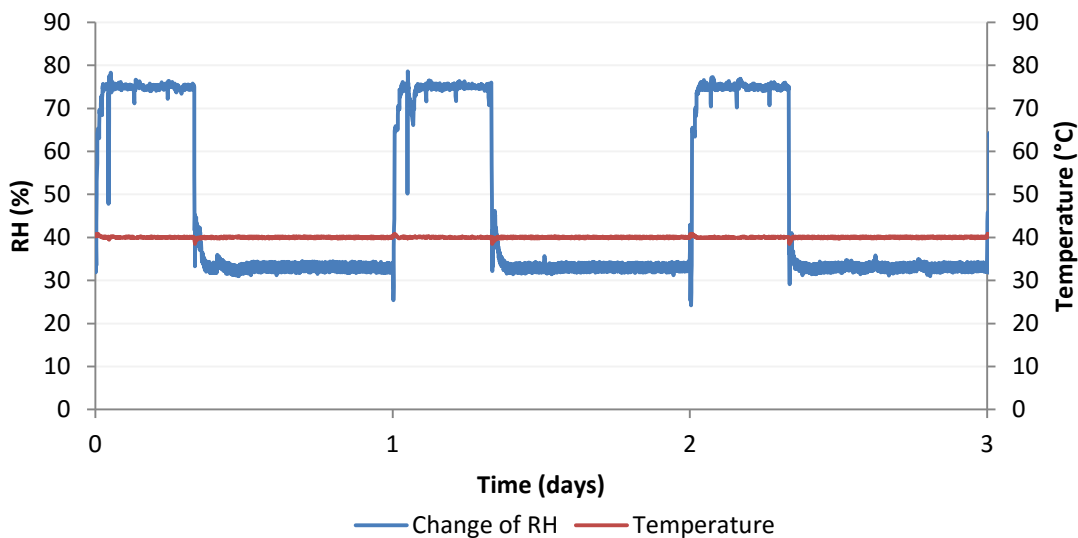


Figure 7.12- Monitored RH and temperature at 40°C

At 23°C the average of $MBV_{\text{practical}}$ obtained for NL was 1.60g/(m²%RH) while for 40°C was 2.60g/(m²%RH) (increase of 62.5%). The results for PF70 was similar, 1.67g/(m²%RH) at low temperature and 2.79g/(m²%RH) for the average value at higher temperature (increase of 67.1%).

The comparison between the steady state analysis and the dynamic measurements was done using the MBV_{ideal} . Table 6.3 and Table 7.3 show the values that were calculated taking into account the values of steady state at 23°C and 40°C, respectively. It was obtained the water vapour permeability with temperature using the eq. 33 and the relation given by eq. 32.

Table 7.3- MBV_{ideal} for NL and PF70 with different corrections of water vapour permeability and compared to the value of $MBV_{\text{practical}}$

	NL		PF70	
	β correction	ISO correction	β correction	ISO correction
$MBV_{\text{ideal}}(\text{g}/(\text{m}^2.\%\text{RH}))$	9.05	7.74	7.42	6.53
$MBV_{\text{practical}} (\text{g}/(\text{m}^2.\%\text{RH}))$	2.62		2.79	
Relative difference (%)	245.03	195.16	165.37	133.54
β vs ISO correction(%)	12.00		14.45	

For the calculation of MBV_{ideal} at 23°C was used the average values of moisture capacity, since the sorption and desorption curves present differences. However, the calculation of MBV_{ideal} when was done for both moisture capacities and both corrections of water vapour permeability (Figure 7.13) the better correlation appears when the moisture capacity of the desorption curve (lower value) was used and the ISO correction. These correlations were only done for NL and PF70, therefore the values of $MBV_{\text{practical}}$ for each set are similar. The difference between the calculated MBV would be expected while the moisture capacity of desorption is lower than the value obtained on sorption, consequently the moisture effusivity decreases providing a MBV_{ideal} less overestimated. Nevertheless, the values of moisture capacity of the desorption curve are very low taking into account the total moisture content in this formulations.

As for the $MBV_{\text{practical}}$, the results for MBV_{ideal} at 40°C were higher than the results obtained at 23°C. Nevertheless, the MBV_{ideal} results were oversized when compare with the obtained practical values for both temperatures.

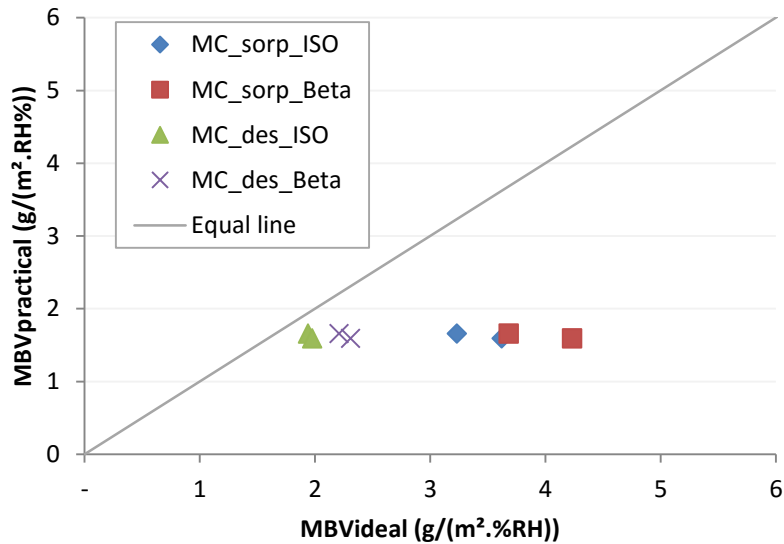


Figure 7.13- Correlation between measured and calculated MBV with different moisture capacities and corrections of water vapour permeability at 23°C (MC-Moisture Capacity; sorp- sorption curve; des- desorption curve)

In order to see where the difference between practical and analytical MBV comes it was done a comparison between the obtained values of moisture effusivity at several temperatures (Figure 7.14). The moisture effusivity calculated using the water vapour permeability with ISO and β correction and average moisture capacity at 23°C and the practical b_m using the values of moisture uptake during dynamic test at 23°C and 40°C, for samples with 5cm of thickness, applied on the eq. 25, called "practical". The moisture effusivity with higher difference between temperatures was the "practical" while for the other two approximations the values do not differ greatly. The calculated values obtained from the practical test lead to values of MBV similar to the ISO correction at 23°C. At 40°C since the b_m "practical" was lower, the MBV obtained with these values was lower compared to the MBV obtained using corrections. Nevertheless the "practical" moisture effusivity leads to a MBV higher than the $MBV_{practical}$ (for NL 2.84 g/(m²%RH) at 23°C and 4.64 g/(m²%RH) at 40°C; for PF70 2.78 g/(m²%RH) at 23°C and 4.66 g/(m²%RH) at 40°C). A possible explanation for the difference observed between analytical and practical comes from the non adequacy of the method to the studied material, because the "practical" moisture effusivity is obtained from the values of the MBV test but using a transformation of the analytical model (MBV_{ideal}). The reason is that the MBV_{ideal} is calculated using intrinsic material properties and this is "valid only for homogeneous material layer" (Rode et al. 2005).

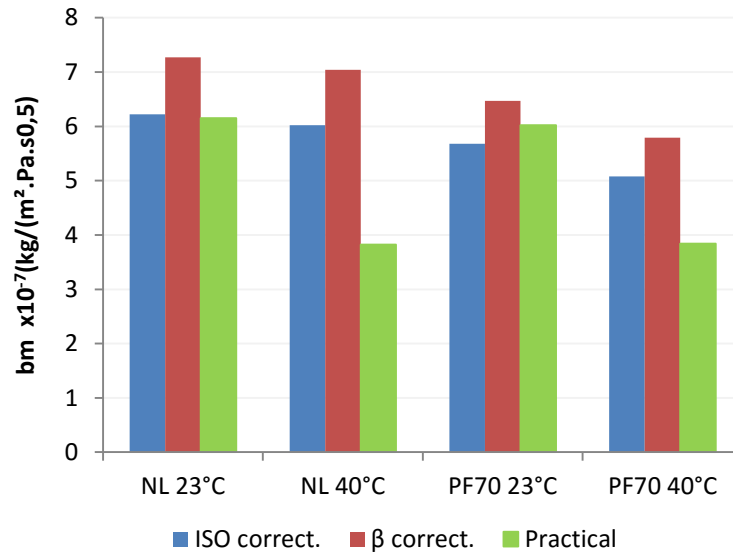


Figure 7.14- Moisture effusivity using ISO and β corrections (23°C and 40°C) and moisture effusivity value calculated from MBV at 23°C and 40°C for hemp concrete with 5cm of thickness

When the impact of each parameter on the calculation of MBV_{ideal} was analysed, assuming a water resistance factor equal for both temperatures, the water vapour permeability had more impact than the saturation vapour pressure which did not have a strong impact. Since the water vapour permeability is given by the steady state test, the difference between practical and theoretical can possibly result from the error associated to these tests. Therefore, changes to the analytical models would be needed for non-homogeneous materials, and the conditions affecting the water vapour permeability would need to be investigated

8. Conclusion

8.1. Concluding remarks

This study starts with a bibliographic study on the use of hygroscopic eco-building material and their advantages on different levels (ecological, in-door air quality, energy efficiency). After this brief general introduction, this dissertation focuses on the dynamic water vapour adsorption, in order to have a passive regulation of RH. To understand the physical origin of this phenomenon, several interactions between the water molecules and the hygroscopic material are presented. In particular, adsorption/desorption mechanisms and mass transfer equations of water are described in detail.

Two types of hygroscopic coating materials are studied: earth mortar plasters and hemp concretes. The first step was to characterise properly these materials (density, sorption-desorption curves, vapour permeability).

The obtained results of sorption isotherms curves are close for two of the three hemp formulations: NL and Calco. The sorption curve of the PF70 leads to low EMCs for each RH. For earth mortar plasters the EMC was strongly lower than the results for the other material, but this storage capacity takes more time to reach for hemp concrete. After sorption and desorption processes, the three hemp concretes show a strong irreversibility between these two processes (hysteresis), while earth mortar plasters had a negligible hysteresis loop.

During the measurement of water vapour permeability using the "wet cup" test, it was visible that an increase of the air velocity in the climatic chamber leads to an increase of the water vapour flow through the samples. It was then developed a correction, based on the analysis of the flow through three samples of the same formulation that consider this phenomenon and provides coherent results. The results using this correction varied between 1.04×10^{-11} kg/(m.s.Pa) and 1.71×10^{-11} kg/(m.s.Pa) for earth plasters while for hemp concrete the water vapour permeability was higher (3.06×10^{-11} kg/(m.s.Pa) to 4.68×10^{-11} kg/(m.s.Pa)).

The second stage was to study the impact of samples thicknesses on the MBV of the earth plasters and hemp concrete.

The MBV of earth plasters presents similar results for F0 and F3 for all tested thicknesses (1cm, 2cm and 4cm), about $1.30 \text{g}/(\text{m}^2 \cdot \% \text{RH})$, while F5 with 1cm of thickness had low MBV compared with the other thicknesses (about 30% lower). The $\text{MBV}_{\text{practical}}$ of PF70 and NL present similar values for all samples thicknesses (between $2.52 \text{g}/(\text{m}^2 \cdot \% \text{RH})$ and $2.91 \text{g}/(\text{m}^2 \cdot \% \text{RH})$ at 40°C). The $\text{MBV}_{\text{practical}}$ could be compared to the $\text{MBV}_{\text{ideal}}$ calculated from the steady state properties. For earth plaster, a good accuracy is obtained between the two values (except for the plaster F5), while for hemp concrete the $\text{MBV}_{\text{ideal}}$ values were overestimated. In conclusion, the simple equation of the $\text{MBV}_{\text{ideal}}$, which links the static and dynamic adsorption properties, can be used for earth plasters, but some additional research is needed for hemp concretes.

From the analysis of the results of practical MBV and penetration depths (only on hemp concrete), it was possible to conclude that the thickness has impact on the MBV when this geometrical property is lower than the penetration depth which is estimated upon the “ $d_{1/e}$ definition” (penetration depth = minimum depth at which the RH variation remains lower than $1/e=37\%$ of the RH variation within the climatic chamber). For earth mortar plasters, it was not possible to measure the practical penetration depth. Thus, this latter was estimated from the analytical solution reported by Rodes et al. (2005). If it is assumed that the penetration depth, denoted by $d_{1/e}$, is the minimum depth at which the RH variation remains lower than $1/e=37\%$ of the RH variation at the material surface, this calculation leads to $d_{1/e} \approx 1\text{cm}$ for each formulation. This result is consistent with $\text{MBV}_{\text{practical}}$ results on earth plaster (except for the formulation F5) since no significant variation is observed between the samples of 1cm, 2cm and 4cm thick.

In conclusion, for the tested formulations, a thickness of 1cm of earth plaster seems to be sufficient in order to benefit from their moisture buffering capability (Mcgregor et al. submitted) while a thickness of 5cm is necessary for hemp concretes of formulations NL and PF70. For the third hemp concrete formulation (Calco) the conclusion of minimum thickness was not valid due to some problems on the tested samples. This analysis was valid for hemp concrete and earth mortar plasters without finish coatings. In the case where finish coatings are applied results of moisture buffering would probably be different.

The last phase of this study consisted of understanding the influence of the temperature (23°C and 40°C) on the hygroscopic capacity of the hemp concrete formulations.

This analysis starts with the results of sorption isotherm for the studied temperatures, which lead to a decrease of water content with temperature at constant RH. It follows that the water content is a function of two parameters, which increase with the increase of RH and decrease with rise in temperature. Moreover, the samples take less time to reach the EMC because the quantity of water is less and the quantity of vapour with the air is higher (the vapour pressure at saturation significantly increase with temperature). The origin of this important difference was investigated with a developed theoretical solution based on the Kelvin's Law and Jurin's Law. However, for hemp concretes this model do not present good correlation between the practical and theoretical values. This difference can be explained by the fact that the Kelvin's Law do not consider adsorbed water, but only free water.

Unlike the results of sorption isotherms, the MBV test had higher dynamic adsorption with the rise of temperature. It was showed that PF70 and NL had good moisture buffering capacity at 23°C and this performance was excellent at higher temperature. When the $\text{MBV}_{\text{ideal}}$ was compared with $\text{MBV}_{\text{practical}}$ at 40°C this values presented more difference than at 23°C. The impact of each parameter on the $\text{MBV}_{\text{ideal}}$ leads to understand that the measured value of the water vapour permeability is the main one responsible for this variation.

The earth mortar plasters show hygroscopic capacities lower than hemp concrete. However, the selection of the material should depend of the desired application.

8.2. Future work

In order to continue the work developed in this dissertation, some future work is suggest. This suggested future work will be to confirm results obtained in the theoretical and practical analysis developed in this dissertation, as well as complementary studies for the comprehension of performance of the hygrothermal capacity, experimental and in-situ.

A repetition of the measure of the sorption isotherms using an automatic Dynamic Vapour Sorption device (DVS) is suggested, in order to increase the accuracy of the results in a shorter time. With this kind of apparatus, it would be possible to do the sorption-desorption tests for more temperatures. This equipment use samples with small dimensions, which may be a problem due to the representability of the material; yet it would be possible to verify the influence by comparing the results obtained through this method with the ones measured during the present study.

Since these materials can work like a passively regulator of the indoor RH, it is required the verification of thermal conductivity with an increase of the RH levels. This parameter is important to predict the power requirements of a building.

Due to a complex matrix in hemp concrete, more investigation could be done on the relation between the pore size distribution and the influence of this parameter in the dynamic adsorption properties. The adsorption and desorption on the hemp shives could be done to study the impact of this component on the hysteresis loop and on the delayed sorption behaviour observed in hemp concrete.

The dynamic adsorption and vapour permeability of Calco presented interesting results (higher MBV and water vapour permeability) that could be due to the presence of two vertical holes in these samples. Therefore, it would be necessary to investigate the influence of such holes on dynamic sorption.

In terms of application, it is necessary to investigate the behaviour of these materials in relation to a support (for example, internal condensation). That would clarify the interactions between hygroscopic materials and variable supports.

References

- Albers, B., 2014. Modeling the hysteretic behavior of the capillary pressure in partially saturated porous media: A review. *Acta Mech*, 225(8), pp.2163–2189.
- Allinson, D. & Hall, M., 2010. Hygrothermal analysis of a stabilised rammed earth test building in the UK. *Energy and Buildings*, 42(6), pp.845–852.
- ANAH, 2004. *Fiche technique Humidité Connaître Eau solide , eau liquide et eau vapeur*.
- Arundel, A. et al., 1986. Indirect health effects of RH in indoor environments. *Environmental Health Perspectives*, 65(3), pp.351–361.
- Ashour, T., Georg, H. & Wu, W., 2011. An experimental investigation on EMC of earth plaster with natural reinforcement fibres for straw bale buildings. *Applied Thermal Engineering*, 31(2-3), pp.293–303.
- Bruno, P. & Faria, P., 2010. Earth mortars from pre-historic habitat settlements in south Portugal Case studies. *Journal of Iberian Archeology*, 13, pp.51–67.
- BSI, 1989. BS 5250 - Code of practice for control of condensation in buildings.
- CEN, 2000. ISO 12571- Hygrothermal performance of building materials and products Determination of hygroscopic sorption properties.
- CEN, 2001. ISO 12572 - Hygrothermal performance of building materials and products - Determination of hygroscopic sorption properties.
- Chabriac, P.-A., 2014. *Mesure du comportement hygrothermique du pise, PhD thesis*. Ecole Nationale des Travaux Publics de l'Etat.
- Choudhury, T. & Misra, A.K., 2013. Minimizing changing climate impact on buildings using easily and economically feasible earth to air heat exchanger technique. *Mitigation and Adaptation Strategies for Global Change*, 19, pp.947–954.
- Collet, F. et al., 2013. Comparison of the hygric behaviour of three hemp concretes. *Energy and Buildings*, 62, pp.294–303.
- Collet, F. et al., 2008. Porous structure and water vapour sorption of hemp-based materials. *Construction and Building Materials*, 22(6), pp.1271–1280.
- Collet, F. & Pretot, S., 2014. Experimental highlight of hygrothermal phenomena in hemp concrete wall. *Building and Environment*, 82, pp.459–466.
- Collet, F. & Pretot, S., 2012. Experimental investigation of moisture buffering capacity of sprayed hemp concrete. *Construction and Building Materials*, 36, pp.58–65.

- Correia, J., 2013. *Avaliação da higroscopicidade de materiais correntes*, Master thesis. Faculdade de Ciência e Tecnologias da Universidade Nova de Lisboa.
- Coussy, O., 2004. *Poromechanics* 1st ed. L. John Wiley & Sons, ed., England.
- Dixit, M.K. et al., 2010. Identification of parameters for embodied energy measurement: A literature review. *Energy and Buildings*, 42(8), pp.1238–1247.
- Dubois, S., 2014. *Modelling the hygrothermal behaviour of crop-based construction materials*, PhD thesis. Université de Liège- Gembloux Agro-Bio Tech.
- Dubois, S., Evrard, A. & Lebeau, F., 2014. Modeling the hygrothermal behavior of biobased construction materials. *Journal of Building Physics*, 38(3), pp.191–213.
- Esteban, L.G. et al., 2015. Juvenile and mature wood of *Abies pinsapo* Boissier: sorption and thermodynamic properties. *Wood Science and Technology*, 49(4), pp.725–738.
- Evrard, A., 2006. Sorption behaviour of Lime-Hemp Concrete and its relation to indoor comfort and energy demand. In *23rd International Conference on Passive and Low Energy Architecture*. Geneva, Switzerland, pp. I553–I557.
- Faria, P., Santos, T. & Aubert, J.-E., 2015. Experimental characterization of an earth eco-efficient plastering mortar. *Journal of Materials in Civil Engineering*, 0401508-1-9. Doi: 10.1061/(ASCE)MT.1943-5533.0001363
- Gomes, M.I., Gonçalves, T.D. & Faria, P., 2013. The compatibility of earth-based repair mortars with rammed earth substrates. In *3rd Historic Mortars Conference*. Glasgow, Scotland, pp. 1–9. (CD).
- Gomes, M.I., Gonçalves, T.D. & Faria, P., 2014. Unstabilized Rammed Earth: Characterization of Material Collected from Old Constructions in South Portugal and Comparison to Normative Requirements. *International Journal of Architectural Heritage*, 8(2), pp.185–212.
- Gonçalves, H. et al., 2014. The influence of porogene additives on the properties of mortars used to control the ambient moisture. *Energy and Buildings*, 74, pp.61–68.
- Hamard, E. et al., 2013. A procedure to assess the suitability of plaster to protect vernacular earthen architecture. *Journal of Cultural Heritage*, 14(2), pp.109–115.
- Heath, A. et al., 2009. Compressive strength of extruded unfired clay masonry units. *Proceedings of the Institute of Civil Engineers: Construction Materials*, 162 (3), pp.105–112.
- Henriques, F.M.A., 2011. *Comportamento Higrotérmico de Edifícios*. Universidade Nova de Lisboa.
- Hens, H., 2011. *Applied Building Physics*, Belgium: Ernst & Sohn.

- Jaquin, P., 2008. *Analysis of historic rammed earth construction, PhD thesis*. Durham University.
- Krus, M. & Kiej, K., 1998. Determination of the moisture storage characteristics of porous capillary active materials. *Materials and Structures*, 31(10), pp.522–529.
- Künzel, H.M., 1995. *Simultaneous Heat and Moisture Transport in Building Components One- and two-dimensional calculation using simple parameters, PhD thesis*.
- Lai, B.T. et al., 2015. Poroelastic behaviour of fine compacted soils in the unsaturated to saturated transition zone. *Computers and Geotechnics*, 69, pp.627–640.
- Le, A.T. et al., 2014. Experimental investigation on the mechanical performance of starch–hemp composite materials. *Construction and Building Materials*, 61, pp.106–113.
- Lide, D.R., 2001. *Handbook of Chemistry and Physics* 82nd ed. C. Press, ed.
- Lima, J. & Faria, P., 2014. Earthen plasters : the potential of the clayey soils of barrocal region in Algarve. In *40th IAHS World Congress on Housing*. pp. 1–10 (CD).
- Lima, J. & Faria, P., 2015. ECO-EFFICIENT EARTHEN PLASTERS . THE INFLUENCE OF THE ADDITION OF NATURAL FIBERS. In *ICNF - 2nd International Conference on Natural Fibers*. S. Miguel, Azores, Portugal, pp. 27–29.
- Liuzzi, S. et al., 2013. Hygrothermal behaviour and RH buffering of unfired and hydrated lime-stabilised clay composites in a Mediterranean climate. *Building and Environment*, 61, pp.82–92.
- Maalouf, C. et al., 2013. Numerical and experimental study of the hygric inertia of a hemp-lime concrete. *International Journal of Mathematical Models and Methods in Applied Sciences*, 7(2), pp.149–156.
- Maniatidis, V. & Walker, P., 2003. *A Review of Rammed Earth Construction*.
- Mazhoud, B., Collet, F. & Pretot, S., 2015. Effect of temperature on thermal and hygric properties of hemp-lime plasters. In *1st International Conference on Bio-based Building Materials*. Clermont-Ferrand, France, pp. 567–574.
- Mcgregor, F., 2014. *Moisture buffering capacity of unfired clay masonry, PhD thesis*. University of Bath.
- Mcgregor, F., Simões, T., Fabbri, A., Faria, P., Morel, J-C. A method to assess the penetration depth of daily moisture loads in earth plasters. *Building and Environment* (submitted).
- Melià, P. et al., 2014. Environmental impacts of natural and conventional building materials: A case study on earth plasters. *Journal of Cleaner Production*, 80, pp.179–186.
- Minke, G., 2006. *Building With Earth-Design and Technology of a Sustainable Architecture*, Birkhäuser.

- Osanyintola, O.F. & Simonson, C.J., 2006. Moisture buffering capacity of hygroscopic building materials: Experimental facilities and energy impact. *Energy and Buildings*, 38, pp.1270–1282.
- Peuhkuri, R., 2003. *Moisture Dynamics in Building Envelops, PhD thesis*. Denmark Technical University.
- Pires, A.L.G., 2013. *Avaliação do comportamento higroscópico de argamassas de reboco, Master thesis*. Faculdade de Ciência e Tecnologias da Universidade Nova de Lisboa.
- Poyet, S. & Charles, S., 2009. Temperature dependence of the sorption isotherms of cement-based materials: Heat of sorption and Clausius-Clapeyron formula. *Cement and Concrete Research*, 39(11), pp.1060–1067.
- Radu, A. et al., 2012. *Heat , Air and Moisture Transfer Terminology Parameters and Concepts* V. P. de Freitas & E. Barreira, eds., International Council for Research and Innovation in Building and Construction.
- Rahim, M. et al., 2015. Characterization of flax lime and hemp lime concretes: Hygric properties and moisture buffer capacity. *Energy and Buildings*, 88, pp.91–99.
- Ramos, N., 2007. *A importância de inércia higroscópica no comportamento higrotérmico dos edifícios, PhD thesis*. Porto: Faculdade de engenharia da Universidade do Porto.
- Rode, C. et al., 2007. Moisture Buffer Value of Building Materials. *Journal of ASTM International*, 4(1), p.8.
- Rode, C. et al., 2005. Moisture buffering of building materials. Department of Civil Engineering, Technical University of Denmark.
- Roels, S. & Janssen, H., 2006. A comparison of the Nordtest and de japanese test methods for the moisture buffering performance of building materials. *Jornal of buildings physics*, 30, pp.137–161.
- Röhlen, U. & Ziegert, C., 2011. *Earth Building Practice - Planning, Design, Building* 1st ed., Berlin: Bauwerk Beuth.
- Rouquerol, F., Rouquerol, J. & Sing, K.S.W., 1999. *Adsorption by powders and porous solids* Academic Press, ed., London.
- Rouquerol, J. et al., 1994. Recommendations for the characterization of porous solids. *Pure & Appl. Chem.*, 66(8), pp.1739–1758.
- Salentijn, E.M.J. et al., 2015. New developments in fiber hemp (*Cannabis sativa* L.) breeding. *Industrial Crops and Products*, 68, pp.32–41.
- Sanya, T., 2007. *Living earth. The sustainability of earth architecture in Uganda*. Oslo School of Architecture and Design, Norway.

- Sassoni, E. et al., 2014. Novel sustainable hemp-based composites for application in the building industry: Physical, thermal and mechanical characterization. *Energy and Buildings*, 77, pp.219–226.
- Sing, K.S.W. et al., 1985. Reporting physisorption data for gas / solid systems, with special reference to the determination of surface area and porosity. *Pure & Appl. Chem.*, 57(4), pp.603–619.
- Straube, J.F., 2006. Moisture and Materials. *Building Science*, 138(10), pp.1–7.
- Torraca, G., 2009. *Lectures on Materials Science for Architectural Conservation*, Los Angeles: The Getty Conservation Institute.

Appendix

A. Proof of the Kelvin's law

The chemical potential of a liquid body chemical grade (ϕ_l) is the relation between the liquid and gas pressures and the bulk density of liquid. But in this analysis the liquid is water and the gas is air ($p_w - p_a$).

$$\phi_l = \frac{p_l - p_g}{\rho_l} = \frac{p_w - p_a}{\rho_w}$$

The potential of vapour (ϕ_v), is taken to be a perfect gas, it is possible to express the expression bellow. Where M is the molar mass and is express in Kg.mol^{-1} .

$$\phi_v = \frac{RT}{M} \ln\left(\frac{p_v}{p_{v,sat}}\right)$$

When the equality between the chemical potential of liquid and gas phase is expressed, it gives the relationship between RH and matric suction. That can be represented though the Kelvin's Law, used in unsaturated soils, where ($p_a - p_w$) is the difference between the air and water pressures, called the matric suction [Pa], ρ_w is the density of water [Kg.m^{-3}], M_w its molar mass of water [g.mol^{-1}] and the ϕ is expressed in decimal (and not in percentage).

$$(P_a - P_w) = -\frac{\rho_w RT}{M_w} \ln\left(\frac{p_v}{p_{v,sat}}\right) = -\frac{\rho_w RT}{M_w} \ln(\phi)$$

B. Materials information

B.1. Technical sheet of PF70



Fiche technique

Juillet 2006

Tradical® PF70

Liant chaux aérienne préformulé pour maçonner et dégrossir
Conforme aux DTU 26.1 et DTU 20.1

Définition et Domaine d'emploi

Tradical® PF70 est un liant préformulé à base de chaux aérienne (75 %), de liants hydrauliques (15 %) et pouzzolanique (10 %), destiné après mélange avec des agrégats (sable) et gâché à l'eau, à réaliser des mortiers de pose pour pierre naturelle, moellons de tout type (sauf pierre très tendre), briques creuses ou pleines, briquettes ainsi que des gobetis, dégrossis et sous-enduit traditionnels, en conformité avec les DTU 20.1 chap. 2.2, 4.2 et 4.3, et DTU 26.1.

Stockage

Selon d'origine (22 kg) et stocké à l'abri, le liant Tradical® PF70 peut être conservé 6 mois.

Conception des ouvrages et Mise en œuvre

Selon le type d'ouvrage, se reporter aux DTU correspondants :
 - maçonnerie : DTU 20.1 chap. 2.2, 4.2 et 4.3
 - enduit : DTU 26.1

Supports

Pour les enduits : mouiller le support à refus la veille, réhumidifier le cas échéant et laisser réessuyer.
 Ne pas appliquer sur des supports gelés ou en cours de dégel, surchauffés ou ruisselants.
 Sur les supports modernes à base de ciment (parpaing, béton, etc.), prévoir un gobetis conforme au chap. 5.11 du DTU 26.1

Préparation

Mélanger le sable suivant les proportions indiquées dans la brochure technique correspondante, sans ajout de liants hydrauliques. Puis gâcher à consistance par adjonction d'eau propre.
 Malaxer 3 à 5 minutes en bétonnière.

Mise en œuvre

Température à respecter de +5° à +35°C, protéger du soleil, du vent violent et de la pluie battante.
 Mise en œuvre en projection pneumatique ou mécanique :
 → consulter le fabricant du matériel en fonction du sable utilisé.
 → procéder comme pour un mortier traditionnel.

Dosages

Le dosage en liant par rapport au sable varie en fonction :
 a/ du type d'ouvrage à réaliser et
 b/ du sable utilisé (granulométrie, nature et taux d'humidité)
 En règle générale, le liant se dose à raison de :
 → 200 à 350 kg par m³ de sable (humidité inférieure ou égale à 5%).
 → ou en volume : 1 volume de liant pour 2 à 3,5 volumes de sable

Utilisable en coulis, en pâte pure

Divers

- Contrôle
 Chaque fabrication est contrôlée en laboratoire. Un prélèvement est archivé avec la référence portée sur chaque sac.


- Garantie décennale et/ou de bon fonctionnement
 Dans le cadre de la PIB de l'entreprise. RC fabricant, contrat SMABTP N°043-088L.

Performance	
Coeff de conductivité thermique λ	$\leq 0,20$
Densité	$= 0,62 \pm 0,02$
Silice soluble (hydraulicité)	$\leq 10 \%$
Teneur en CO2	$\leq 8 \%$
Adjuvants (colloïdes végétaux et surfactants)	$\leq 0,5 \%$
Rétention d'eau	$\geq 75 \%$
Granulométrie	$\leq 90 \text{ mm}$
Traction/Flexion	$\geq 1,4 \text{ N/mm}^2$
Compression	$\geq 4,3 \text{ N/mm}^2$



BCB
 Zac de Valentin - BP 3011
 25045 Besançon cedex - France
 Tél. 33 (0)3 81 47 40 10
 Fax 33 (0)3 81 47 40 19
 contact@bcb-tradical.com
 www.bcb-tradical.com

B.2. Technical sheet of Calco



CALCOBLANC

1/2
PATRIMOINE - BÂTI ANCIEN

FAÇADES PATRIMOINE - BÂTI ANCIEN

LES «PLUS» PRODUIT

- Chaux hydraulique naturelle
- A mélanger avec des sables locaux
- Améliore la courbe granulométrique du mortier
- Application manuelle et mécanique

LIANT BLANC À LA CHAUX HYDRAULIQUE NATURELLE HL 3,5

DÉFINITION

- **CALCOBLANC** est un liant à base de chaux hydraulique naturelle que l'on mélange à des sables du terroir directement sur chantier, pour la réalisation de gobetis, corps d'enduit, finition et rejointolement.
- Mélange de tradition et de modernité, **CALCOBLANC** est destiné à la rénovation.
- La blancheur de **CALCOBLANC**, allié aux sables du terroir, vous permettront de donner à vos façades ce caractère d'authenticité recherché suivant les aspects choisis (taloché, gratté, brossé, lissé, ferré, arraché, ...) et évite ainsi toute adjuvantation supplémentaire.
- La formulation du **CALCOBLANC** permet une application à la fois manuelle et mécanique.
- **CALCOBLANC** respecte la tradition tout en apportant la protection nécessaire à votre ouvrage.

SUPPORTS

Admissibles

- Maçonneries anciennes montées aux mortiers peu résistants (DTU 26.1 – Chap. 11).
- Maçonneries enduites aux mortiers traditionnels conformes au DTU 26.1.
- Enduits monocouches d'imperméabilisation.
- Maçonneries et murs en :
 - blocs de béton (NF P 14-301 et 14-304).
 - briques et blocs de terre cuite (NF P 13-301 et 13-305).
 - béton de granulats courants.
 - béton d'argile ou de schiste expansé conforme aux DTU les concernant, notamment DTU 20.1 et 23.1.

Exclus

- Enduits exclusivement à la chaux aérienne ou au plâtre, peintures, revêtements et plastiques épais.
- Supports à base de terre (torchis, pisé, adobe).
- Maçonneries en blocs de béton cellulaire.
- Enduits hydrauliques allégés de résistance mécanique inférieure au mélange.
- Supports exposés inclinés de plus de 10° par rapport à la verticale.

CARACTÉRISTIQUES

Composition

- Chaux hydraulique
- Charge calcaire
- Adjuvant hydrofuge
- Adjuvant rhéologie.

Performances

(selon les sables utilisés)

- Masse Volumique Apparente du liant : 700 à 860 g/L.
- Masse Volumique Apparente du mortier : 1700 à 1800 g/L.
- Masse Volumique Apparente du mortier durci : 1500 à 1600 g/L.
- Module d'élasticité du mortier : 4 600 à 5 800 Mpa.
- Résistance à la compression du mortier : 2,5 à 4 Mpa.
- Résistance à la traction du mortier : 1,2 à 1,8 Mpa.
- Rétention d'eau du mortier : 96 à 98 %.
- Capillarité du mortier : 3 à 5.
- Clarté : L=86+/-1.
- Perméance à la vapeur d'eau : très élevée.

Toutes les valeurs indiquées sont des moyennes calculées sur des résultats obtenus, suivant des procédures normalisées, en laboratoire.

MISE EN OEUVRE

Préparation des supports

- Sains, propres, dépoussiérés.
- Traiter les remontées capillaires (efflorescences et salpêtre).
- Sonder, éliminer toutes les parties non adhérentes, les peintures, les revêtements organiques et les plâtres.
- Dégarnir les joints de 2 à 3 cm.
- Toutes les réparations doivent être effectuées au minimum 2 jours avant l'enduction.
- Pour les préparations particulières, se reporter au cahier des charges et au DTU 26.1.
- Sur béton et supports peu absorbants, l'application doit être faite en 2 passes, dont la première adjuvantée de 1 L de 751 LANKOLATEX ou FIXOPIERRE par sac de 25 kg.
- La planimétrie et l'aplomb des supports neufs seront conformes aux exigences des DTU 20.1.

Matériel

Truelle

- Application manuelle.

Pot de projection

- Pression d'air 2,5 à 4 bars.

Machine à projeter

- Pression pompe 6 à 8 bars.
- Débit d'air 60 m³/heure minimum.

ASSISTANCE TECHNIQUE : La Société ParexGroup S.A. assure l'information et l'aide aux entreprises qui en font la demande pour le démarrage d'un chantier afin de préciser les dispositions de mise en œuvre du produit (ou procédé). Cette assistance ne peut être assimilée ni à la conception de l'ouvrage, ni à la réception des supports, ni à un contrôle des règles de mise en œuvre.

Documentation Technique 2013 - La présente fiche technique a pour but d'informer sur les propriétés du produit. Les renseignements qui y figurent sont basés sur nos connaissances actuelles. Il est l'utilisateur de s'informer sur l'adaptation du produit à l'usage désiré et de vérifier si cette fiche n'a pas été remplacée par une édition plus récente - Mise à jour consultable sur www.parexlanko.com

92446 Issy les Moulineaux Cedex

PAREXLAN

B.3. Drying of earth mortar plasters

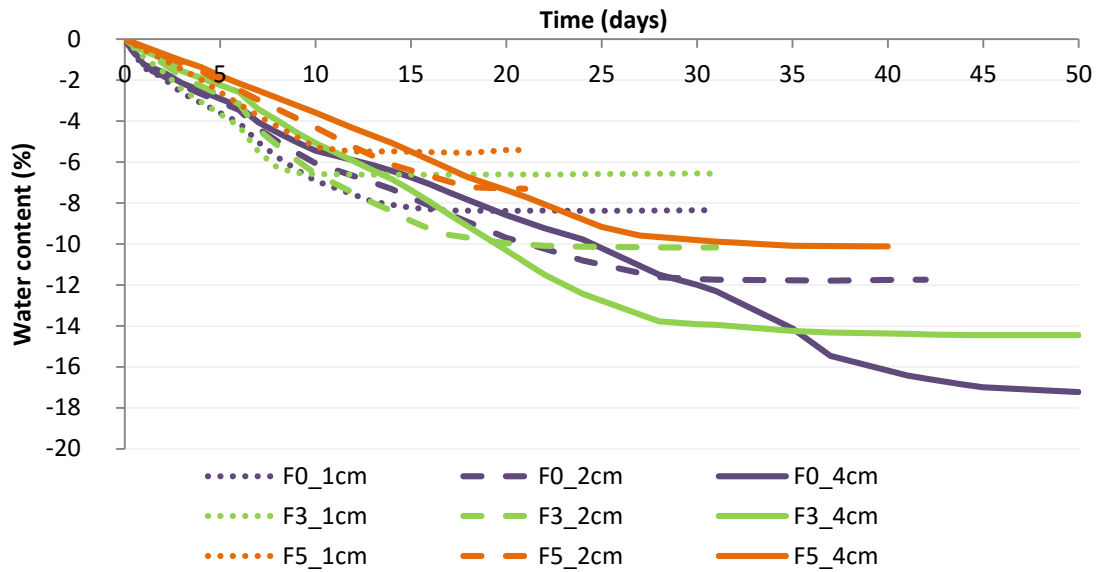


Figure B.1- Drying curves for all samples of earth mortar plasters

C. Sorption Isotherms

C.1. Hemp concrete at 23°C

Calco	RH (%)	Dry mass (g)	Equilibrium mass (g)	EMC (%)	EMC Average (%)
C-1	23	18,39	18,87	2,99	3,00
C-2		18,71	19,20	3,00	
C-3		18,66	19,15	3,01	
C-4	43	23,51	24,61	5,17	5,09
C-5		19,30	20,19	5,20	
C-6		19,07	19,90	4,91	
C-7	59	18,04	19,17	7,13	7,43
C-8		16,70	17,77	7,40	
C-9		20,96	22,41	7,76	
C-10	75	20,29	23,12	15,70	15,02
C-11		22,43	24,64	10,96	
C-12		16,54	18,59	14,34	
C-13	85	17,11	19,82	18,20	16,61
C-14		23,65	26,91	15,24	
C-15		27,34	31,45	16,39	
C-16	97	22,09	28,43	31,94	27,13
C-17		17,53	21,65	26,97	
C-18		15,65	19,31	27,29	

PF70	RH (%)	Dry mass (g)	Equilibrium mass (g)	EMC (%)	EMC Average (%)
PF70-1	23	19,18	19,5	1,89	1,84
PF70-2		23,90	24,29	1,82	
PF70-3		24,99	25,4	1,80	
PF70-16	43	31,49	32,71	4,18	3,75
PF70-17		19,07	19,69	3,70	
PF70-18		27,74	28,6	3,36	
PF70-13	59	23,39	24,5	5,23	5,55
PF70-14		27,43	28,83	5,57	
PF70-15		24,43	25,73	5,84	
PF70-10	75	17,87	18,77	5,78	7,60
PF70-11		24,54	26,25	7,68	
PF70-12		27,26	29,62	9,42	
PF70-7	85	25,58	28,07	10,67	10,57
PF70-8		18,80	21,25	14,82	
PF70-9		21,20	23,19	10,48	
PF70-4	97	18,85	22,39	21,34	21,65
PF70-5		18,92	22,46	21,20	
PF70-6		26,60	31,99	22,11	

NL	RH (%)	Dry mass (g)	Equilibrium mass (g)	EMC (%)	EMC Average (%)
NL-1	23	19,79	20,31	2,98	2,98
NL-2		27,46	28,22	3,01	
NL-3		27,26	27,99	2,93	
NL-4	43	19,64	20,31	3,85	5,30
NL-5		23,00	24,21	5,81	
NL-6		23,04	24,34	6,23	
NL-7	59	20,63	21,87	6,76	6,94
NL-8		23,50	24,87	6,43	
NL-9		24,56	26,26	7,62	
NL-10	75	25,92	28,79	12,12	12,45
NL-11		22,37	25,07	13,39	
NL-12		27,57	30,57	11,83	
NL-13	85	25,50	29,13	15,62	16,01
NL-14		20,65	23,47	15,30	
NL-15		24,97	28,86	17,11	
NL-16	97	24,02	30,22	28,49	27,75
NL-17		26,78	33,62	27,86	
NL-18		23,38	29,07	26,92	

C.2. Earth mortar plasters

F0	RH (%)	Dry mass (g)	Equilibrium mass (g)	EMC (%)	EMC Average (%)
F0-1	23	44,43	44,57	0,32	0,34
F0-2		50,94	51,13	0,37	
F0-3		47,73	47,89	0,34	
F0-4	43	48,02	48,27	0,52	0,51
F0-5		49,63	49,88	0,50	
F0-6		52,33	52,60	0,52	
F0-7	59	53,48	53,82	0,64	0,63
F0-8		39,59	39,84	0,63	
F0-9		51,49	51,81	0,62	
F0-10	75	47,43	47,84	0,86	0,89
F0-11		59,47	60,00	0,89	
F0-12		35,15	35,47	0,91	
F0-13	85	57,96	58,64	1,17	1,16
F0-14		45,21	45,72	1,13	
F0-15		52,00	52,62	1,19	
F0-16	97	48,23	49,56	2,76	2,73
F0-17		48,98	50,31	2,72	
F0-18		61,80	63,48	2,72	

F3	RH (%)	Dry mass (g)	Equilibrium mass (g)	EMC (%)	EMC Average (%)
F3-1	23	56,89	57,03	0,25	0,23
F3-2		52,86	52,98	0,23	
F3-3		53,39	53,51	0,22	
F3-4	43	36,23	36,35	0,33	0,34
F3-5		51,07	51,25	0,35	
F3-6		55,59	55,78	0,34	
F3-7	59	52,00	52,23	0,44	0,45
F3-8		48,14	48,35	0,44	
F3-9		49,61	49,84	0,46	
F3-10	75	52,02	52,35	0,63	0,63
F3-11		49,07	49,38	0,63	
F3-12		54,95	55,30	0,64	
F3-13	85	58,84	59,16	0,54	0,84
F3-14		59,87	60,38	0,85	
F3-15		52,38	52,81	0,82	
F3-16	97	38,80	39,56	1,96	1,97
F3-17		61,08	62,29	1,98	
F3-18		57,08	58,21	1,98	

F5	RH (%)	Dry mass (g)	Equilibrium mass (g)	EMC (%)	EMC Average (%)
F5-1	23	91,43	91,58	0,16	0,16
F5-2		59,31	59,40	0,15	
F5-3		61,91	62,01	0,16	
F5-4	43	47,49	47,59	0,21	0,22
F5-5		58,90	59,03	0,22	
F5-6		48,31	48,42	0,23	
F5-7	59	43,61	43,74	0,30	0,29
F5-8		44,33	44,46	0,29	
F5-9		54,50	54,65	0,28	
F5-10	75	42,28	42,46	0,43	0,39
F5-11		54,27	54,48	0,39	
F5-12		61,85	62,08	0,37	
F5-13	85	55,52	55,82	0,54	0,53
F5-14		43,15	43,39	0,56	
F5-15		49,17	49,42	0,51	
F5-16	97	57,78	58,51	1,26	1,23
F5-17		58,42	59,14	1,23	
F5-18		46,10	46,65	1,19	

Table C.1- EMC for sorption and desorption curve from 97%

RH %	F0 (%)		F3 (%)		F5 (%)	
	Sorption	Desorption	Sorption	Desorption	Sorption	Desorption
0	0,00	0,00	0,00	0,00	0,00	0,00
23	0,34	0,38	0,23	0,26	0,16	0,16
43	0,51	0,63	0,34	0,43	0,22	0,26
59	0,63	0,80	0,45	0,56	0,29	0,35
75	0,89	1,09	0,63	0,77	0,39	0,47
85	1,16	1,34	0,84	0,96	0,53	0,59
97	2,73	2,73	1,97	1,97	1,23	1,23

Table C.2- EMC for sorption and desorption from 85% processes for earth mortar plasters

RH %	F0 (%)		F3 (%)		F5 (%)	
	Sorption	Desorption	Sorption	Desorption	Sorption	Desorption
0	0,00	0	0,00	0,00	0,00	0
23	0,34	0,34	0,23	0,23	0,16	0,16
43	0,51	0,51	0,34	0,34	0,22	0,22
59	0,63	0,67	0,45	0,46	0,29	0,31
75	0,89	0,97	0,63	0,69	0,39	0,45
85	1,16	1,16	0,84	0,84	0,53	0,53
97	2,73	-	1,97	-	1,23	-

C.3. Hemp concrete at 40°C

Calco	RH (%)	Dry mass (g)	Equilibrium mass (g)	EMC (%)	EMC Average (%)
C-19		23,65	24,14	2,29	
C-20	23	21,04	21,49	2,41	2,36
C-21		21,08	21,53	2,39	
C-22		21,62	22,21	3,06	
C-23	43	20,32	20,87	3,04	3,04
C-24		20,32	20,86	3,01	
C-25		22,76	23,55	3,83	
C-26	59	25,70	26,62	3,92	3,87
C-27		17,61	18,2	3,86	
C-4		23,53	25,27	8,17	
C-5	75	19,31	20,73	8,32	8,12
C-6		19,08	20,44	8,08	
C-7		18,06	19,48	8,98	
C-8	85	16,71	18,05	9,26	9,30
C-9		20,97	22,78	9,66	
C-1		18,40	21,91	21,72	
C-2	97	18,71	22,47	22,83	21,04
C-3		18,66	21,82	19,24	

PF70	RH (%)	Dry mass (g)	Equilibrium mass (g)	EMC (%)	EMC Average (%)
PF70-19		26,30	26,77	1,95	
PF70-20	23	20,75	21,12	1,98	1,96
PF70-21		22,80	23,20	1,95	
PF70-22		23,69	24,27	2,69	
PF70-23	43	21,85	22,35	2,53	2,59
PF70-24		23,67	24,22	2,55	
PF70-25		20,28	20,89	3,38	
PF70-26	59	23,60	24,32	3,35	3,43
PF70-27		20,25	20,89	3,55	
PF70-16		31,49	33,07	5,40	
PF70-17	75	19,07	19,97	5,35	5,19
PF70-18		27,75	28,98	4,82	
PF70-13		23,40	24,79	6,57	
PF70-14	85	27,43	29,12	6,71	6,80
PF70-15		24,44	26,00	7,03	
PF70-1		19,18	23,03	22,73	
PF70-2	97	23,90	27,95	18,70	18,23
PF70-3		24,99	29,03	17,76	

NL	RH (%)	Dry mass (g)	Equilibrium mass (g)	EMC (%)	EMC Average (%)
NL-19		16,69	17,15	3,16	
NL-20	23	18,98	19,55	3,41	3,30
NL-21		26,74	27,56	3,35	
NL-22		17,22	17,78	3,74	
NL-23	43	17,16	17,75	3,93	3,84
NL-24		17,57	18,16	3,85	
NL-25		16,57	17,27	4,88	
NL-26	59	15,22	15,85	4,88	4,86
NL-27		18,89	19,69	4,83	
NL-4		19,63	20,97	7,71	
NL-5	75	23,00	24,99	9,59	9,13
NL-6		23,05	25,15	10,09	
NL-7		20,62	22,42	9,79	
NL-8	85	23,50	25,52	9,50	10,03
NL-9		24,55	26,96	10,80	
NL-1		19,78	24,42	26,45	
NL-2	97	27,45	33,66	24,63	24,99
NL-3		27,25	33,22	23,87	

D. Diffusion test

D.1. β correction

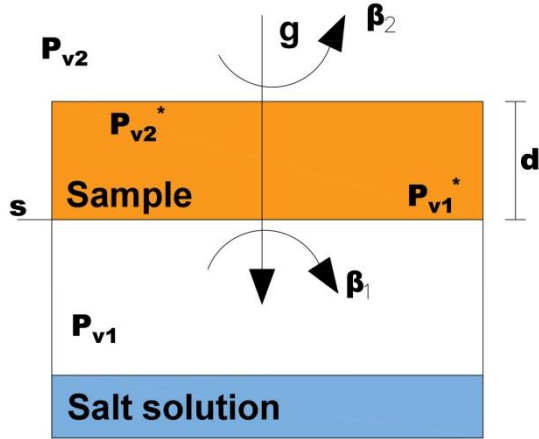


Figure D.1- Layout of the processes during the test

g is the density of water vapour flow rate;

p is the partial vapour pressure;

β is the apparent vapour transfer coefficient at the sample surface;

s the exposed surface;

d the thickness of the sample.

It is assumed that the density of water vapour flow rate descendent, therefore $P_{v2} > P_{v1}$.

$$\frac{\Delta m}{\Delta t} = G = s \cdot g = s \cdot \delta_p \cdot \frac{P_{v2}^* - P_{v1}^*}{d} \Leftrightarrow s \cdot \delta_p \cdot \frac{\Delta P_v^*}{d} = G$$

$$g = \beta_2(P_{v2} - P_{v2}^*) = \beta_1(P_{v1}^* - P_{v1})$$

$$\frac{G}{s} = \beta_2(P_{v2} - P_{v2}^*) = \beta_1(P_{v1}^* - P_{v1})$$

$$\begin{cases} \frac{G}{s} = \beta_2(P_{v2} - P_{v2}^*) \\ \frac{G}{s} = \beta_1(P_{v1}^* - P_{v1}) \end{cases} \Leftrightarrow \begin{cases} P_{v2}^* = P_{v2} - \frac{G}{s \cdot \beta_2} \\ P_{v1}^* = P_{v1} + \frac{G}{s \cdot \beta_1} \end{cases} \Rightarrow \Delta P_v^* = \Delta P_v - \frac{G}{s \cdot \beta_2} - \frac{G}{s \cdot \beta_1}$$

$$G = s \cdot \delta_p \frac{\Delta P_v - \frac{G}{s \cdot \beta_2} - \frac{G}{s \cdot \beta_1}}{d} \Leftrightarrow G = s \cdot \delta_p \left(\frac{\Delta P_v}{d} - \frac{G}{s \cdot d \cdot \beta_2} - \frac{G}{s \cdot d \cdot \beta_1} \right) \Leftrightarrow$$

$$\Leftrightarrow G = \frac{\delta_p}{d} \left(s \cdot \Delta P_v - \frac{G}{\beta_2} - \frac{G}{\beta_1} \right) \Leftrightarrow \delta_p = \frac{G \cdot d}{s \cdot \Delta P_v - G \left(\frac{1}{\beta_2} - \frac{1}{\beta_1} \right)}$$

$\frac{1}{\beta_2} - \frac{1}{\beta_1}$ is the correction factor, however in order to simplify the calculation it is assumed that $\frac{1}{\beta_2} - \frac{1}{\beta_1} = \frac{1}{\beta}$ and the β factor is finding using an iterative process. Therefore, the expression of water vapour permeability is given by:

$$\delta_p = \frac{G \cdot d}{s \cdot \Delta P_v - \frac{G}{\beta}}$$

D.2. Variation of mass in the diffusion test for hemp concrete- 1st phase

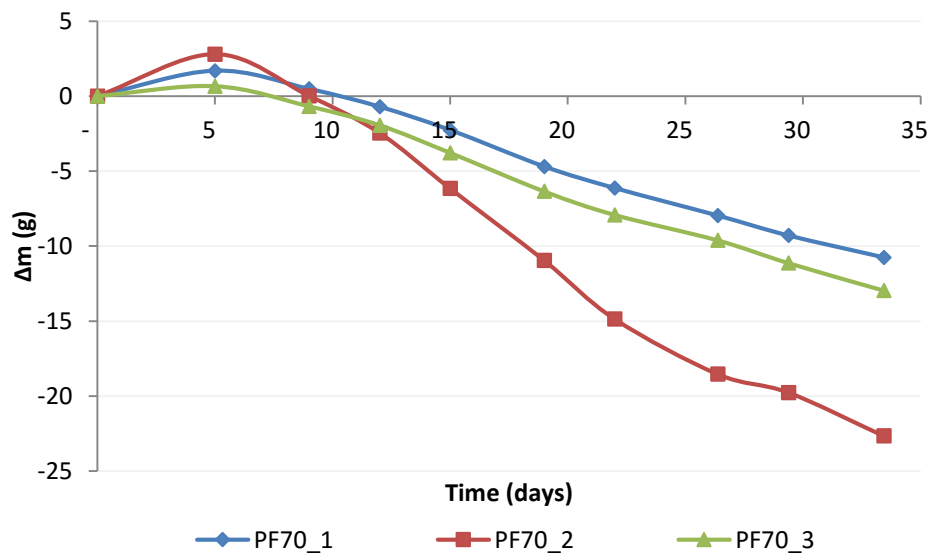


Figure D.2- Variation of mass during the first phase of the penetration depth of PF70

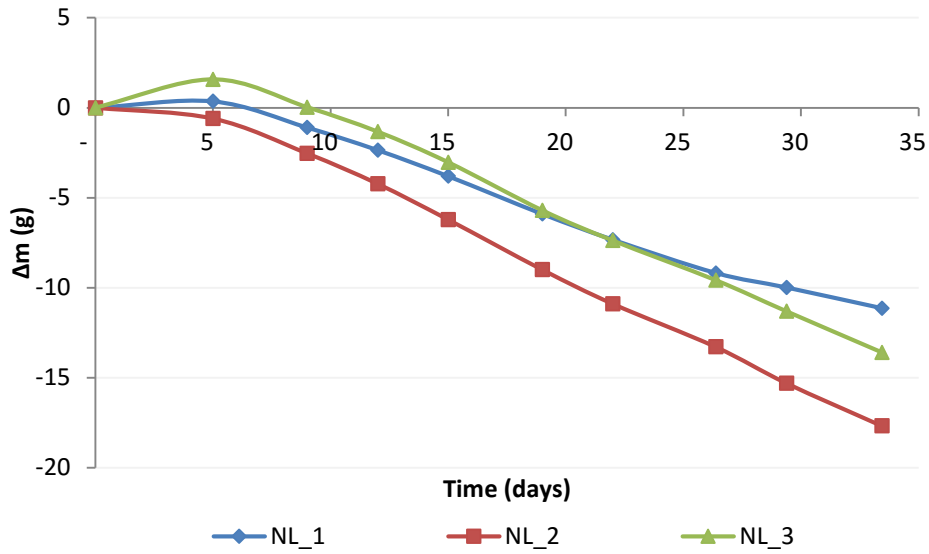


Figure D.3- Variation of mass during the first phase of the penetration depth of NL

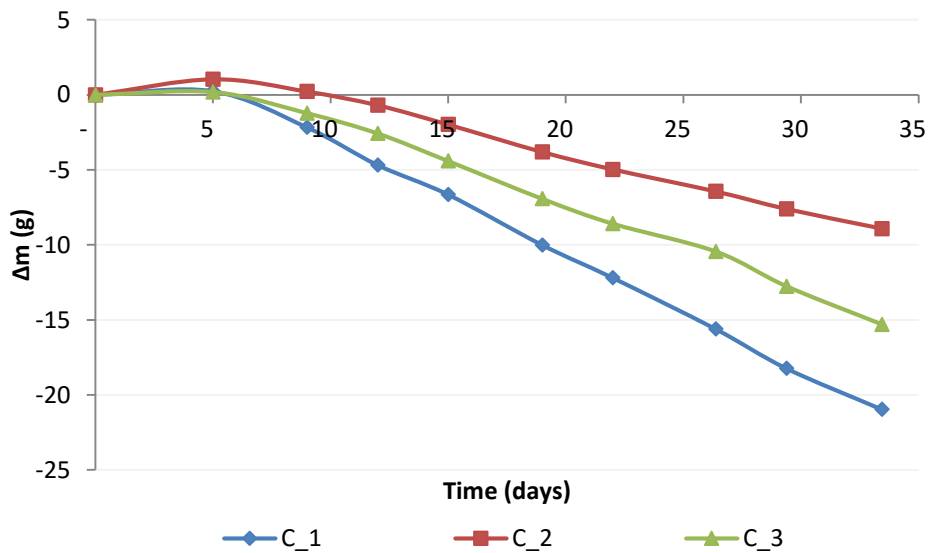


Figure D.4- Variation of mass during the first phase of the penetration depth of Calco

E. MBV

E.1. Earth mortar plasters

Table E.1- General information of earth mortar plasters samples

Samples	Thickness (cm)	Dimensions (cm)		Surface (cm²)	Exposed surface (cm²)
F0.11	1,2	15,0	15,1	226,5	214,6
F0.12	1,3	15,0	15,0	225,0	213,2
F0.13	1,3	15,1	15,0	226,5	214,6
F0.21	2,2	15,0	14,8	222,0	210,2
F0.22	2,3	15,0	15,1	226,5	214,6
F0.23	2,3	14,9	14,9	222,0	210,3
F0.41	4,2	15,1	15,1	228,0	216,1
F0.42	4,2	15,0	15,2	228,0	216,1
F0.43	4,1	15,0	15,1	226,5	214,6
F3.11	1,2	14,8	14,9	220,5	208,8
F3.12	1,3	15,0	15,0	225,0	213,2
F3.13	1,3	14,9	14,8	219,8	208,1
F3.21	2,3	14,8	14,9	220,5	208,8
F3.22	2,3	14,9	15,0	222,8	211,0
F3.23	2,3	14,9	15,2	226,5	214,6
F3.41	4,1	15,0	15,0	225,0	213,2
F3.42	4,1	15,0	15,0	225,0	213,2
F3.43	4,1	15,1	15,0	226,5	214,6
F5.11	1,2	15,1	15,0	226,5	214,6
F5.12	1,2	15,2	15,1	229,5	217,6
F5.13	1,1	14,8	15,2	224,2	212,4
F5.21	2,3	15,1	15,0	226,5	214,6
F5.22	2,2	14,9	15,1	225,0	213,2
F5.23	2,2	15,0	15,1	226,5	214,6
F5.41	4,1	15,0	15,0	225,0	213,2
F5.42	4,2	15,1	15,1	228,0	216,1
F5.43	4,1	14,9	15,0	223,5	211,7

E.2. Hemp concrete at 40°C

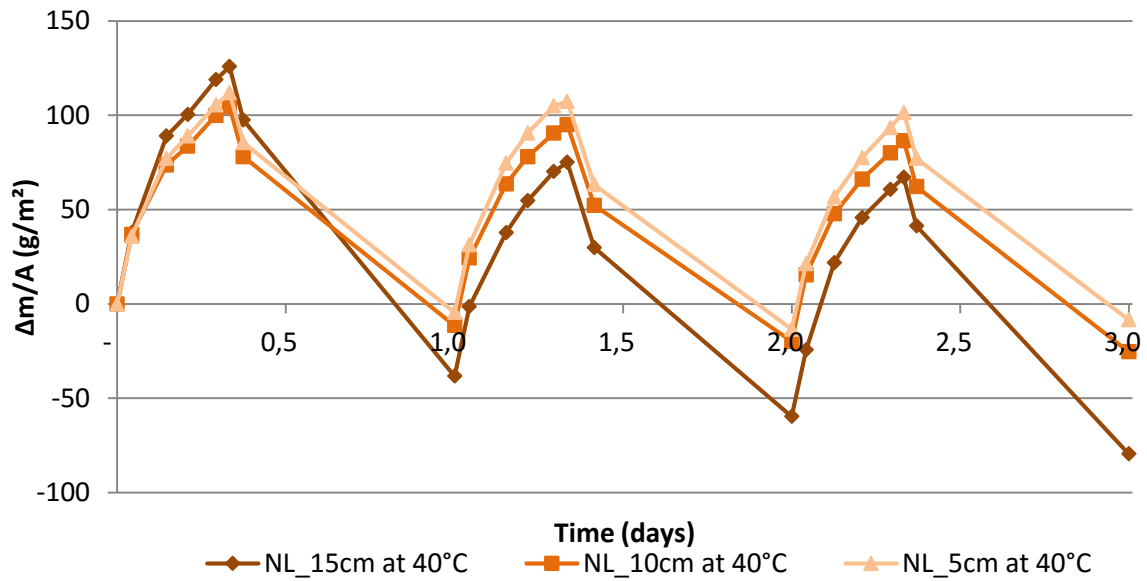


Figure E.1- Moisture buffering test for NL with 5, 10 and 15cm at 40°C

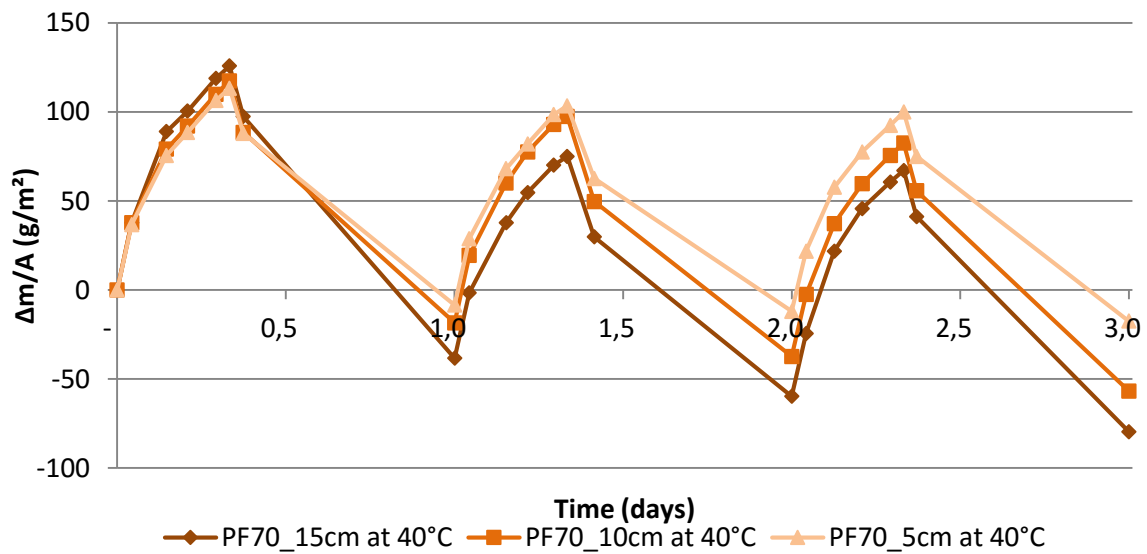


Figure E.2- Moisture buffering test for PF70 with 5, 10 and 15cm at 40°C

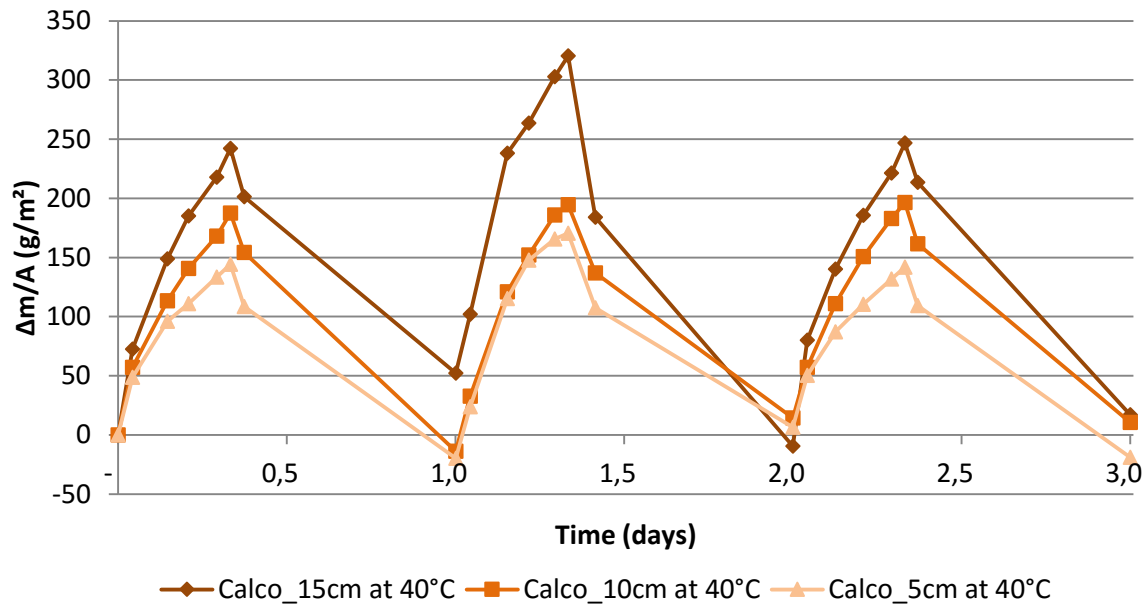


Figure E.3- Moisture buffering test for Calco with 5, 10 and 15cm at 40°C

F. Practical penetration depth

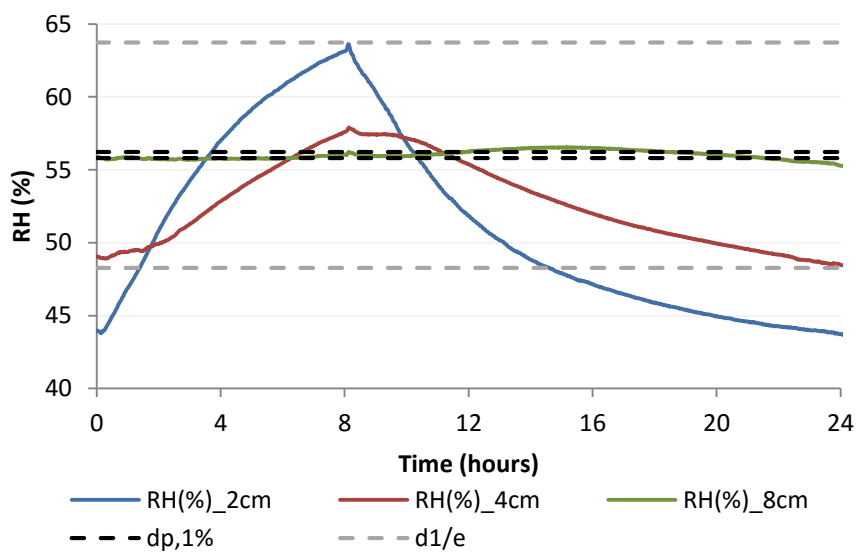


Figure F.1- Real penetration depth for NL at 40°C

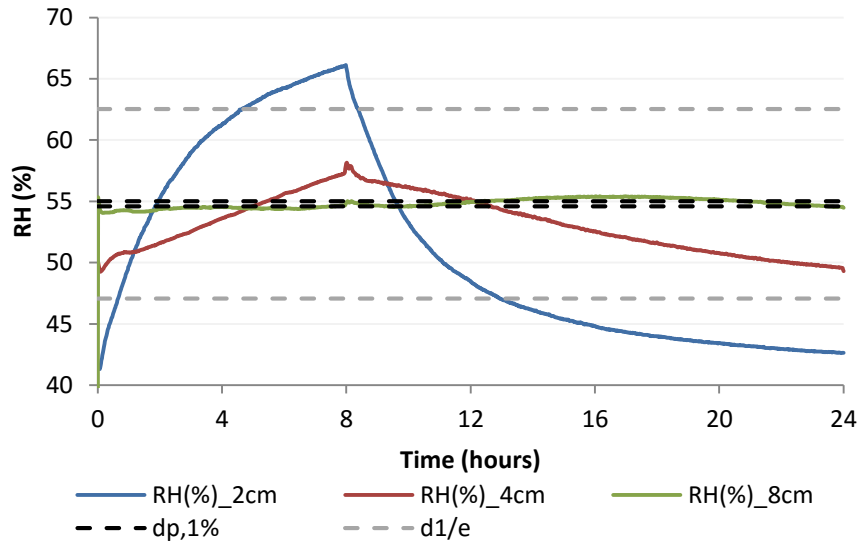


Figure F.2- Real penetration depth for PF70 at 40°C

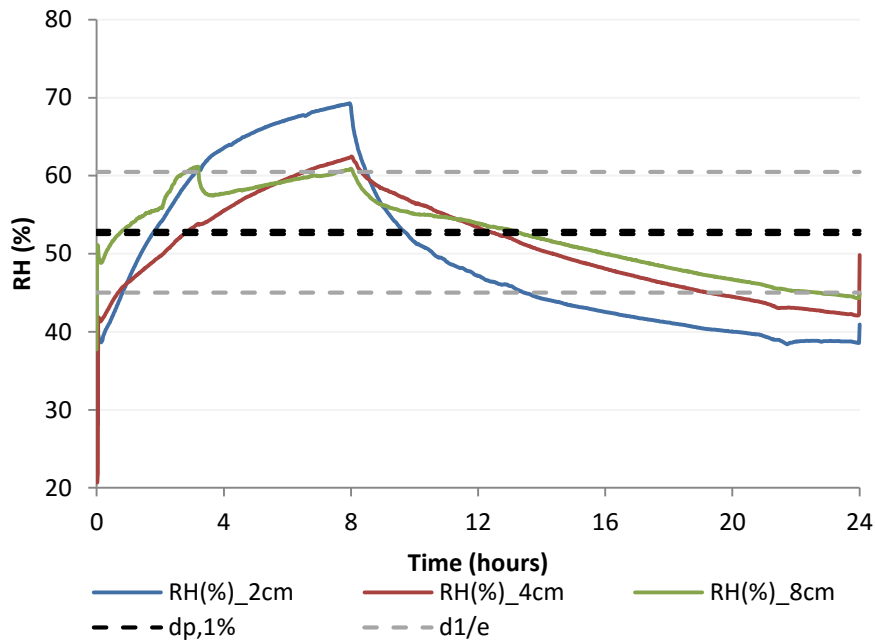


Figure F.3- Real penetration depth for Calco at 40°C